ENHANCING LOW VOLTAGE RIDE THROUGH CAPABILITY OF DFIG BASED WIND TURBINE: A CASE STUDY OF ADAMA-II WIND TURBINE

THESIS SUBMITTED

IN PARTIAL FULFILLMENT OF THE REQUIREMENTS

FOR THE DEGREE OF MASTER OF SCIENCE

IN

POWER SYSTEM AND ENERGY ENGINEERING

BY

FSAHA MEBRAHTU

ADVISOR: DR. BASEEM KHAN

CO-ADVISOR: MR. BERHANE DARSENE

DEPARTMENT OF ELECTRICAL AND COMPUTER ENGINEERING

HAWASSA UNIVERSITY INSTITUTE OF TECHNOLOGY

HAWASSA (ETHIOPIA)

MAY, 2019

DECLARATION

I hereby declare that the thesis "Enhancing Low Voltage Ride through Capability of DFIG Based Wind Turbine: A Case Study of Adama-II Wind Turbine" is my own work conducted under the guidance of Dr. Baseem Khan and Mr. Berhane Darsene, Department of Electrical and computer Engineering, Hawassa University Institute of Technology, SNNPRS, Hawassa, Ethiopia.

I further declare that to the best of my knowledge the thesis doesn't contain any part of that has been submitted for the award of any degree either in this university or any other university without proper citation.

Fsaha Mebrahtu _____
Name Signature

ID Nº: PGEng /012/ 09

This is to certify that the statement made above by the candidate is true to the best of my knowledge.

Date: 18/05/2019

Dr Baseem Khan _____
Advisor Name Signature

Mr. Berhane Darsene _____
Co-advisor Signature
Department of Electrical and computer Engineering

Hawassa University

Hawassa, SNNPRS, 05

HAWASSA UNIVERSITY
SCHOOL OF GRADUATE STUDIES

EXAMINERS' APPROVAL SHEET

As members of the Board of Examiners of the final Master's degree open defense, we certify that we have read and evaluated the thesis prepared by **Fsaha Mebrahtu** under the title **Enhancing Low Voltage Ride Through Capability of DFIG Based Wind Turbine** and recommend that it be accepted as fulfilling the thesis requirement for the Degree of Master of Science in Electrical Engineering with Specialization in Power System and Energy Engineering.

Name of the Chair Person	Signature	Date
Name of Internal Examiner	Signature	Date
Name of External Examiner	Signature	Date
Name of Principal Advisor	Signature	Date
Name of the Co-Advisor	Signature	Date

Final approval and acceptance of the thesis is contingent upon the submission of the final copy of the thesis to the SGS through the DGC/SGC of the candidate's department.

Thesis approved by

SGC	Signature	Date

ACKNOWLEDGEMENTS

First of all, I would take this opportunity to give glory to almighty God without his support the completion of this work would have been impossible. Next to that I would like to express my sincere gratitude to my advisor Dr. Baseem Khan for his expertise guidance, constructive comments, suggestions and encouragement. He has been a constant source of inspiration throughout this work. And also I would like to thank my co-advisory Mr. Berhane Darsene for his excellent guidance, certain supports. Also, I would like to extend my thanks to Mr. Damot Tesfaye faculty of electrical engineering and to Mr. Mesfin Fanuel head of electrical and computer engineering, and Electrical power coordinator for Mr. Mulualem and all the staffs of the Electrical and Computer Engineering of Hawassa university and to the Adama-II wind farm, for providing me all the invaluable materials and helpful pieces of advice for Mr. Ahmed Awel, Mr. Mesfin, Mr. Melaku and Mr. Leul from Adama wind farm-II for their support by providing the required data.

ABSTRACT

Doubly fed induction generators (DFIG) based wind turbines (WT) are major sources of energy generation around the world. One of such energy source is wind generation, which is very much popular now days. It utilizes doubly fed induction generator (DFIG) to generate electricity in generation mode. But sometimes wind turbines are disconnected from the power system in the event of grid faults. To avoid grid instability as well as to ensure the secure and reliable operation of the power systems, all wind turbines must stay connected with the grid during faults and capable to ensure the operation of the utility grid side during voltage sags in the event of a fault that is performed by analyzing the low voltage ride through (LVRT) capability of DFIG based wind turbines.. DFIG is very sensitive to any grid disturbances, if a severe voltage dip occurred due to grid fault, high currents will pass through stator and rotor windings and also a very high DC voltage would be induced in converter circuit, which may lead to damage the converter circuit and the DFIG windings. A crowbar protections system is essential to avoid the disconnection of the doubly fed induction wind generators from the network during faults and to protect the DFIG from the dangerous effects of the electrical fault. Accordingly, Ethiopia have been started to expand its energy generation by installing renewable energy source like wind farm. Presently, Ethiopia has installed wind farms like Ashegoda, Adama-I and Adama-II. The Adama-II wind farm project has 153 MW with 102 units, each of with generation capacity of 1.5 MW. This work focused on the improvement of low voltage ride through capability (LVRT) of Adama-II wind turbines. In this thesis a crowbar protection system is used to improve the power system fault ride through capability of DFIG of Adama-II. During the symmetrical fault using crowbar protection the value of crowbar current at time three 3 seconds is overshoot to 3000 A and it will reduce to the original condition after 100 ms. Also the value of stator voltage, stator flux during faulty and symmetrical conditions before the fault and after are the same, but during the voltage dip the stator flux is decreased and the stator voltage is also reduced. The dynamic behavior of DFIG under normal and various grid fault conditions are simulated and analyzed to provide the recommendations. MATLAB/Simulink software is utilized for the development of proposed system.

Key words: *DFIG, LVRT and Crowbar protection*

TABLE OF CONTENTS

DECLARATION i
EXAMINERS' APPROVAL SHEET ii
ACKNOWLEDGEMENTS iii
ABSTRACT iv
LIST OF FIGURE viii
LIST OF ABBREVIATION x
CERTIFICATE xii
CHAPTER ONE 1
1. INTRODUCTION 1
1.1. Back Ground 1
1.2. Statement of the Problem 3
1.3. Objective of This Thesis 4
1.3.1. General Objective of This Thesis 4
1.3.2. Specific Objective 4
1.4. Motivation of the Thesis 4
1.5. Scope of This Study 5
1.6. Contribution of This Thesis 5
1.7. Outline of the Thesis 6
CHAPTER TWO 7
2. THEORETICAL BACKGROUND AND LITERATURE REVIEW 7
2.1. Literature Review 7
2.2. Theoretical Background 11
2.3 Wind Energy Conversion Systems 11
2.3.1. Definition of Wind Turbine 12
2.4 Wind Turbine 14
2.5 Gearbox 14
2.6 Generators Used In the Wind Industry 15
2.6.1 Doubly Fed Induction Generator (DFIG) 15
2.6.2 Operation of Doubly Fed Induction Generator (DFIG) 17
2.6.3 Advantage of Doubly Fed Induction Generator (DFIG) 17
2.7. Low Voltage Ride through (LVRT) Capability 18

2.8 Crowbar Protection Scheme 19
2.9 Dc Chopper Protection Scheme 22
2.10. Analysis of the DFIG during Fault Time 24
2.10.1 Introduction 24
2.10.2 Electromagnetic Force Induced In the Rotor 24
2.10.3 During The Normal Operation of DFIG 25
2.10.4 Three Phase Voltage Dips 27
2.10.5 Single Phase Dip (Unsymmetrical Faults) 28
2.10.6 Equivalent Model during the different faults 31
2.11 Power Curve of Adama-II Wind Turbine Generation 32
CHAPTER THREE 35
3. METHODOLOGY AND MODELING OF DFIG BASED ON WIND TURBINE 35
3.1. Methodology 35
3.2. Modeling of DFIG Based Wind Turbine 35
3.2.1 Structure of the Machine and Electric Configuration 35
3.2.2 Aerodynamic Model 36
3.3 Dynamic Modeling of DFIG 38
3.3.1 α-β Model 38
3.3.2 dq- Model 41
3.4. Fault Detection and Control of DFIG Based Wind Turbine System 42
3.4.1. Maximum Power Point Tracking (MPPT) Control Methods 42
3.4.2 Pitch Angle Control 43
3.4.3 Protection of DFIG Using Crowbar Resistor 44
3.4.3.1 Control Strategy of Crowbar Protection Based DFIG 48
3.4.4. Vector Control of DFIG Using AC/DC/AC Converter 50
3.4.4.1 Vector Control of Rotor Side Converter (RSC) 50
3.4.4.2 Vector Control of Grid Side Converter (GSC) 51
3.5. Phase Locked LOOP (PLL) 53
3.6. Analysis of DFIG Based Of Adama-II Wind Farm Turbine and Power Converter 54
3.6.1 Reasons for Choosing Crowbar Protection 55
3.6.2 Super and Sub Synchronous Operation of DFIG 56
3.6.3. Analysis of Steady State Equivalent Circuit of DFIG with RSC 57

3.7. Analysis of Adama-II Wind Farm Turbine 59
3.7.1. Converter Equivalent Impedance at 2000 RPM (Slip is Less than Zero) 61
3.7.2. Converter Equivalent Impedance at 1500 RPM (Synchronous Speed) 63
3.7.3 Equivalent Impedance of Converters at 1000 RPM 64
3.7.4. Steady State of DFIG with Wind Energy Conversion System at Unity Pf 67
CHAPTER FOUR 68
4. SIMULATION RESULT AND DISCUSSION 68
4.1 Introduction 68
4.2. Activation and Deactivation of Crowbar Protection 69
4.2. Simulated Result of Existing System with the Help of Capacitor Bank 70
4.3 Asymmetrical Fault Analysis under Different Voltage Dip 72
4.4 Simulation Results of DFIG under Asymmetrical Fault on RSC 72
4.5 Simulation Results of DFIG under Asymmetrical Fault on GSC 75
4.6 Simulation Results of DFIG LVRT Capability under Symmetrical Fault 76
4.7 Simulation Results of DFIG LVRT Capability with Crowbar Protection on RSC 78
4.8. Simulation Results of DFIG LVRT with Crowbar Protection on GSC 80
4.9. Simulation Results of DFIG on RSC under Steady State Condition 81
4.10 Simulation Results of DFIG on GSC under Steady State Condition 84
CHAPTER FIVE 88
5. CONCLUSION AND RECOMMENDATIONS 88
5.1 Conclusion 88
5.2 Recommendation 89
5.3 Future Work 89
REFERENCE 90
APPENDIX A-1: ADAMA-II WPP DFIG PARAMETERS 93
APPENDIX A-2 95
APPENDIX A-3 96
APPENDIX A-4 96

LIST OF FIGURE

Figure 1-1 Global map of Adama wind farm..... 3
Figure 2-1 Adama-II wind plant 13
Figure 2-2 Simplified block diagram for DFIG wind energy conversion system 16
Figure 2-3. The grid code requirements that consist of (a) ride-through curve and (b) support curve of reactive current 19
Figure 2-4. System equipped with a crowbar 20
Figure 2-5 Equivalent circuit of the system when the crowbar is activated 21
Figure 2-6 Alternative implementation of a crowbar 21
Figure 2-7 Active crowbar with a set of various resistors 22
Figure 2-8 Schematic diagram of DC chopper protection circuit. 22
Figure 2-9 dc link system 23
Figure 2-10 Balanced system 25
Figure 2-11 Space vectors of the stator flux for an 80% single phase dip starting at t_0=0 29
Figure 2-12 Stator flux trajectory for an 80% single phase dip starting at t_0=0 30
Figure 2-13 Space vectors of the stator flux for an 80% single-phase dip starting at t_0 =T/4 31
Figure 2-14 Voltage across rotor phase for an 80% single phase dip starting at t_0=0 31
Figure 2-15 Equivalent circuit for normal operation 31
Figure 2-16 Equivalent circuit for three phase voltage dips 31
Figure 2-17 Equivalent circuit for asymmetrical voltage dips 32
Figure 2-18 Turbine mechanical power versus wind speed curve. 33
Figure 3-1 General supply of configuration of DFIG 36
Figure 3-2 Different reference frames to represent space vectors of the DFIG 38
Figure 3-3 Equivalent Model of the DFIG in the α-β reference frame 39
Figure 3-4 Equivalent Model of the DFIG in d-q reference frame 42
Figure 3-5 C_p as a function of pitch angle and tip speed ratio. 44
Figure 3-6 block diagram of crowbar protection 46
Figure 3-7 Positive sequence equivalent circuit of DFIG with crowbar 47
Figure 3-8 Negative sequence equivalent circuit of DFIG with crowbar 48
Figure 3-9 Synchronous rotating dq reference frame aligned with the stator flux space vector . 50
Figure 3-10 current control loops of DFIG 51
Figure 3-11 (a) Equivalent of DFIG for analysis of dip voltage and (b) space vector diagram at sub synchronism in a generator mode 52
Figure 3-12 Evolution of the space vector magnitudes from the first instant when the stator voltage is reduced until the steady state reached at the dip 52
Figure 3-13 Stator flux growth in p.u during 80% voltage dip 53
Figure 3-14 (a) System equipped with three phase DC crowbar protection 53
Figure 3-15 (b) one phase equivalent circuit of the system when the crowbar is activated 53
Figure 3-16 Grid voltage angle estimation with PLL 54
Figure 3-17 Power speed characteristics in a DFIG wind energy system with MPPT control . .. 56

Figure 3-18 Power flow in DFIG wind energy conversion system 57
Figure 3-19 equivalent circuit of steady state DFIG with RSC 57
Figure 3-20 equivalent circuit of DFIG at maximum torque 66
Figure 4-1 over all Simulink model of Adama-II wind farm with single turbine 68
Figure 4-2 Activation and deactivation time of crowbar protection 69
Figure 4-3 simulated result of stator voltage 70
Figure 4-4 simulation result of torque 70
Figure 4-5 simulated result of I_q 70
Figure 4-6 simulated result of current on d- axis 71
Figure 4-7 simulated result of stator current 71
Figure 4-8 simulated result of simulated result of v_{dr} 72
Figure 4-9 simulated result of grid current grid side 72
Figure 4-10 Modeling of RSC on asymmetrical fault 73
Figure 4-11 simulation result on the RSC 73
Figure 4-12 simulation result of current and voltage at q-component 74
Figure 4-13 simulation result of stator voltage at asymmetrical faults 74
Figure 4-14 modeling of GSC under asymmetrical faults 75
Figure 4-15 simulation result bus voltage and grid current on d-axis 76
Figure 4-16 Simulation of stator voltage and grid current 76
Figure 4-17 Stator voltage during fault analysis 77
Figure 4-18 (a) crowbar current during fault analysis (b) stator flux during fault analysis 77
Figure 4-19 modeling of rotor side control under LVRT 78
Figure 4-20 Speed and quadrature current Rotor Side Control 79
Figure 4-21 Voltage across d-axis and torque on rotor side control 79
Figure 4-22 Stator voltage on rotor side control 80
Figure 4-23 modeling of grid side control under LVRT 80
Figure 4-24 Bus voltage and reactive power at grid side control 81
Figure 4-25 Stator voltage of grid side control 81
Figure 4-26 Modeling of RSC under steady state 82
Figure 4-27 simulation result of speed and I_q on steady state condition 82
Figure 4-28 simulation result of torque and V_{dr} on steady state condition 82
Figure 4-29 simulation result of i_d and V_q on steady state condition 83
Figure 4-30 Simulation result of V_S on steady state condition 83
Figure 4-31 Stator and rotor current of rotor side on steady state analysis 84
Figure 4-32 Modeling of Grid side control under steady state 84
Figure 4-33 Bus voltage and I_d on steady state analysis 85
Figure 4-34 Grid voltage and grid side reference reactive power 85
Figure 4-35 Grid voltage and current on steady state analysis 86
Figure 4-36 Stator voltage on steady state analysis 86
Figure 4-37 Grid current on steady state analysis 87

LIST OF ABBREVIATION

$V_{\alpha r}$, $i_{\alpha r}$	α-axis rotor voltage and current
$V_{\alpha s}$, $i_{\alpha s}$	α-axis stator voltage and current
$V_{\beta r}$, $i_{\beta r}$	β-axis rotor voltage and current
$V_{\beta s}$, $i_{\beta s}$	β-axis stator voltage and current
AC	Alternative current
DC	Direct current
DFIG	Doubly Feed Induction Generator
DQ	Rotor Reference Frame
Dq	Synchronous Reference Frame
DVR	Dynamic voltage restorer
EEP	Ethiopian Electric Power
EMF	Electromagnetic Force
FRT	Fault ride through
FSWT	Fixed Speed Wind Turbine
GSC	Grid Side Converter
HAWT	Horizontal Axis Wind Turbine
IGBT	Insulated-gate bipolar transistor
ISC	Indirect Speed Controller
L_m	Mutual inductance (H)
L_{mr}	Rotor leakage inductance (H)
L_{ms}	Stator leakage inductance (H)
LVRT	Low Voltage Ride Through

MPPT	Maximum Power Point Tracking
MW	Mega watt
PLL	Phase Locked Loop
R_r	Rotor resistance (Ω)
R_s	Stator resistance((Ω))
RSC	Rotor Side Converter
RSPC	Rotor Side Power Converter
SCR	Silicon controlled rectifier
SNNPRS	South Nation, Nationalities and people region
SVC	Static VAR compensator
T_g	Electrical torque.
UVRT	Under Voltage Ride Through
VAWT	Vertical Axis Wind Turbine
VSC	Voltage Source Converter
VSWT	Variable Speed Control Of Wind Turbine
WECS	Wind Energy Converter System
WRING	Wound Rotor Induction Machine
WT	Wind Turbine
WTGS	Wind Turbine Generator System
α-β	Stator Reference Frame
$\psi_{\alpha r}$	α- axis rotor flux linkage
$\psi_{\alpha s}$	α-axis stator flux linkage
$\psi_{\beta r}$	β -axis rotor flux linkage
$\psi_{\beta s}$	β -axis stator flux linkage

CERTIFICATE

This is to certify that the work entitled "An Improved Low Voltage Ride through Capability of DFIG Based Wind Turbine: A Case Study of Adama-II Wind Turbine" submitted by Fsaha Mebrahtu (ID No. PGEng /012/09), Department of Electrical and computer Engineering, Hawassa University, Institute of Technology, Hawassa, Ethiopia is a record of beneficial research carried out by him under my supervision and guidance. The thesis work in my opinion, has reached the requisite fulfilling the requirement of Master of Science Degree. The results contained in the thesis have not been submitted in part or full to any other University or Institute for the award of any degree.

Date: 18/053/2019

Place: Hawassa, Ethiopia

Advisor Name: Dr Baseem Khan

Co-advisor: Mr. Berhane Darsene

Department of Electrical and computer Engineering

Hawassa University

Hawassa, SNNPRS, 05

CHAPTER ONE

1. INTRODUCTION

1.1. Back Ground

Electrical power is the most widely used source of energy for our homes, work places and industries. Population and industrial growth have led to significant increases in power consumption over the past three decades. Nowadays a day's electrical power is the most broadly used source of energy for the daily activity. Population and industrial growth have led to significant increases in power consumption day by day. Governments have been openly acknowledged that the use of conventional energy sources is unsustainable due to the environmental pollution and decreasing resources. With this recognition comes to search for better ways to implement alternative energy sources such as wind turbines, solar, hydroelectric and others. In addition to causing less environmental degradation, these alternative sources have several advantages. Moreover, there is an absence of waste products such as carbon dioxide, which occurs in coal fired power stations, and renewable energy sources may require less maintenance than conventional sources [1].

Wind energy is one of the fastest growing industries at present time and it will continue to grow worldwide, as many countries have plans for future development. The increased penetration of wind energy into power system over the last decade generates new challenges for the power system operators, who have to ensure a reliable and safe grid operation during the presence of faults at the grid [2].

The rise in level of wind penetration into the power grid is transforming the way wind farms are operated. The large penetration of wind power has made it is equivalent to conventional power plants and therefore it expected to present enhanced protection characteristic during grid voltage disturbances. They are also expected to support the grid during system faults and recover soon in order to maintain the grid stability. Comparing to other requirements in wind power, low voltage ride through (LVRT) is the most demanding and is given major focus due to the rising grid penetration of wind energy and the recent advances in grid codes. The wind farm connected to grid is mandatorily required to stay connected even during balanced or unbalanced voltage sags/dip during the system faults and support the grid through reactive power generation during fault period. Failing to support the grid or sudden disconnection of wind farms during faults may lead to severe consequences in grid and will make worse the problem. Hence, ride through

capability of wind turbines is being highlighted and the countries with largely growing wind energy capacity have started to mandate the LVRT capability in wind farms, which were installed without this LVRT provision [3].

Ethiopian electric power (EEP) grid system is highly dependent on electric power generation from hydropower, which is affected by the factors like weather and rainfall. To satisfy the end users, EEP installed wind farms for power generation with different capacities. Actually, in Ethiopia, wind farm is the second highest power generation source next to hydro generation. Wind generation is renewable and clean with short construction periods. It has the significant advantage of quick generation. Thus, EEP constructed wind power plants to solve the problem of deficiency of electric power supply. This will increased penetration of wind energy into EEP's grid and will have significant influence on the stability of the power system [4].

During grid voltage faults it is clear that grid codes recommend that wind turbines must stay connected to the grid and should support the grid by generating reactive power to support and restore quickly the grid voltage after the fault. Among the various wind turbines the doubly fed induction generator (DFIG) indicated in Figure 2.2 are dominant due to their variable speed operation, the separately controllable active and reactive power and their partially rated power converter. But, the reaction of DFIGs to grid voltage disturbances is sensitive for symmetrical and asymmetrical voltage dips, and it requires additional protection for the rotor side power electronic converter [5].

Doubly Fed Induction Generator (DFIG) becomes one of the most popular generators in a variable wind turbine systems. Adama wind farm-II utilizes DFIG and it has the advantages of low cost, low weight, and high efficiency. However, one of its main disadvantages is its sensitivity to the voltage dips and cut off from the national grid. Therefore, there are various techniques were developed to protect the DFIG and enhance its performance during the faults, so as to meet the grid codes requirements [6].

Adama-II wind farm is found in Ethiopia at the town of Nazreth at the latitude of 8° 18' 35.5", longitude: 38° 53' 4.2" and its Global map is shown below.

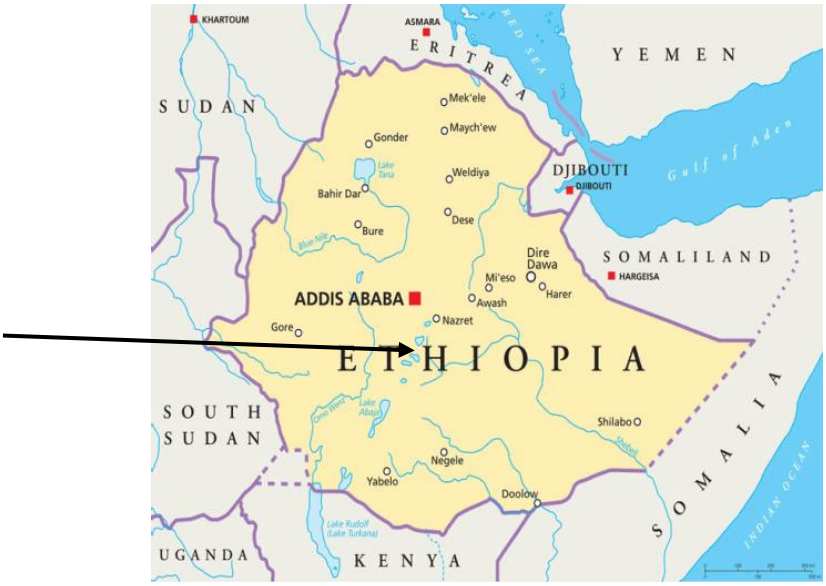

Figure 1-1 Global map of Adama wind farm [7]

The Ethiopian Electric Power Corporation is inaugurated the "Adama Wind Farm-I" project built at a cost of 117 million dollars. The Adama phase-I wind power project has an installed generation capacity of 51 MW. The wind farm has a total of 34 towers each with a generating capacity of 1.5 MW. The second Adama wind farm had installed generation capacity of 153 MW project will have 102 units (turbines) each with a generation capacity of 1.5 MW [Source: The Reporter Ethiopia].

1.2. Statement of the Problem

Doubly Fed Induction Generator (DFIG) becomes one of the most popular generators in variable speed wind turbine systems. DFIG has advantages of low cost, low weight, and high efficiency. However, one of its main disadvantages is sensitivity to the grid faults. The DFIG is very sensitive to any grid disturbances, if a severe voltage variation is occurred due to grid fault, high currents will pass through stator and rotor windings, stability problem and also a very high DC voltage would be induced in converter circuit. Due to the fault, power electronics converters and the DFIG winding will be damaged. Crowbar protection system is essential to avoid the disconnection of doubly fed induction wind generators from the system during faults and to keep away the DFIG from the hazardous effects of the faults. Adama phase-II wind farm is utilized DFIG for power generation and have been used capacitor bank for their systems but even though the problem under fault condition will there.

The ability of wind turbine, stay connected to the grid during grid fault condition is known as the low voltage ride through (LVRT) capability. Moreover, the studies on LVRT capability for DFIG based WT is a popular challenge for the scientists to propose a healthy system considering variable load and severe fault conditions. Furthermore, a proportional study is carried out between a crowbar and DC chopper protection schemes during severe asymmetrical fault condition resulting in reasonable LVRT capability of proposed system.

In order to overcome the above problems the concept of active crowbar protection is introduced in this work for Adama-II wind farm. The active crowbar protection is used to dissipate high current created during grid faults through its resistance, so winding of DFIG and the converters are protected from any damage and reactive power will be follow to the grid to compensate.

1.3. Objective of This Thesis

1.3.1. General Objective of This Thesis

The general objective of this thesis is to enhancing low voltage ride through capability of DFIG based wind turbine situated at Adama-II wind farm during the grid faults and model crowbar protection scheme.

1.3.2. Specific Objective

The specific objective of this thesis is as flows;

- To model DFIG circuit.
- To design controller circuit.
- To design crowbar protection
- To improving the fault ride through capability of wind turbine.
- To deliver controlled power to the grid.
- To protect the converter circuit against the overvoltage and overcurrent.

1.4. Motivation of the Thesis

According to the grid code requirements, wind turbines generators must remain connected to the grid during grid disturbances, but when DFIG is connected to the grid, many issues come into the picture, which may affect the working principle of the generator. The major issues faced during grid interconnection are severe voltage dip occurred due to grid fault, high currents will pass through stator and rotor windings, sudden wind gust, grid abnormalities (voltage sags and

swells), frequency variation and also very high DC voltage would be induced in converter circuit, it may lead to damage the converter circuit and the DFIG windings.

Crowbar protections systems is essential to avoid the disconnection of the doubly fed induction wind generators from the network during faults and to protect the DFIG from the dangerous effects of the electrical fault.

Wind is an irregular movement sometime high and sometime low. Due to the variation of wind many problems are presented, like voltage variation and short circuit at the grid side. This fault creates many hazardous conditions. Unbalanced voltage, over current, mismatch of reactive power and under voltage will faced at the grid side.

Different researcher are proposed different method to improve LVRT, but the most common method is to employ active crowbar protection in order to improve the LVRT capability of the DFIG based wind turbine (WT). In this thesis, a case study, about the behavior of 153-MW Adama-II wind farm is presented, which consist of 102 DFIG based wind turbine units each 1.5 MW connected to the grid.

1.5. Scope of This Study

By studied related tasks mentioned under the titles called literature review and it is mainly deals with the wind turbine technology, especially Adama-II wind farm, while taking into account the characteristic differences of the wind turbine. The main scope of this thesis deals with the mathematical modelling of DFIG, designing of controllers and to improve low voltage ride through capability and study and analysis of Grid converter control scheme. Further, to study and analysis the effect of voltage variation at grid side. Finally the voltage profile at the grid will be improved. The analyses is done by taking the DFIG based turbine of Adama-II wind farm as a case study to investigate the low voltage ride through capability and it will simulated by using MATLAB/Simulink software under various operating conditions.

1.6. Contribution of This Thesis

The major contribution of this thesis is to analyze low voltage ride through capability of wind turbine with the development of crowbar resistance protection scheme for DFIG to get better response from WT and to protect rotor side converter from an excess current, respectively. Crowbar resistance protection scheme is implemented, which is an effective solution for low

voltage ride through in DFIG based wind energy system controllers, protection scheme and mathematical modeling are performed in MATLAB/Simulink environment. Adama wind-II turbine is upgraded from the control capacitor bank and SVC to the developed crowbar protection. Crowbar protection scheme is developed inside MATLAB environment by combining normal diode set condition, resistance and ideal switches with its controlling mechanisms. The developed wind turbine system is simulated with MATLAB code for the back to back converter of the DFIG based wind turbine to improve low voltage ride through of the system. Finally integrate between MATLAB program and Simulink model is performed to show the analysis of low voltage ride through capability of complete system model under various fault Condition.

1.7. Outline of the Thesis

This thesis includes five chapters, the first chapter introduction part discussed about the background, statement of problem, objective of the study, motivation of the thesis, scope the study and outline of the thesis.

Chapter two is a literature review part in which different literatures are reviewed related to the study. The basic theoretical background theory related to low voltage ride through capability based wind turbine are briefly discussed in this chapter. Moreover the different types of faults during voltage dip and protection mechanism on wind turbine under DFIG with its general working principles are also presented in this chapter.

Chapter three deals with the methodology, in the third chapter methodology part was discussed about the wind turbine mathematical modeling, modeling of control mechanism, design of crowbar protection and numerical analysis of wind turbine at Adama-II wind turbine.

Chapter four deals with the result analysis and discussion about the modeled system which is developed in MATLAB simulation tool and the simulated results under different conditions.

Finally, in chapter six the conclusion, recommendation and future works of the thesis was discussed.

CHAPTER TWO

2. THEORETICAL BACKGROUND AND LITERATURE REVIEW

2.1. Literature Review

To obtain the necessary information's about the improved low voltage ride through capability of DFIG based wind turbine during grid integrated and detailed study of different resources are required. There are many researches that has been studied on the interconnection of DFIG to national grid and the different problems related to power quality are coming to the picture like voltage unbalance, disconnection of wind turbine from grid.

In 2014, Mali et al. [8] discussed the problem of improving low voltage ride through capabilities for grid connected wind turbine generator under the presence of grid voltage dips, a mismatch is produced between the generated active power and delivered reactive power to the grid. Low voltage ride through requirement demands management of this mismatch, which is a challenge for the wind energy conversion system (WECS). It was solved by inserting a chopper resistor into the DC link so as to dissipate the excessive energy in the form of heat during grid voltage dips. However, the temperature increase in the resistor may be a problem when voltage dip lasts relatively longer. The only problem was when fault occur at grid the side wind turbine will disconnect until the fault cleared.

In 2017, Behzad, et al. [9], described the low voltage ride through enhancement of DFIG based wind turbine using DC link switchable resistive type fault current limiter and proposes a novel DC link switchable resistive type fault current limiter (SRFCL) to improve the LVRT capability of the DFIG. The proposed approach was compared with the crowbar based protection method. Simulation studies were carried out in PSCAD/ EMTDC software. But it was not protected the power electronics converters.

In 2014, Shukla, et al. [10], discussed the low voltage ride through (LVRT) ability of DFIG based wind energy conversion system. By controlling the rotor and grid side converters, the DFIG characteristics was adjusted, so as to achieve maximum of effective power conversion or capturing capability for a wind turbine and to control its power generation with less fluctuation. Also it was discussed the major grid problems and grid codes for operation and grid connection of wind farms. But they were not discussed on the crowbar protection system, because without

crowbar converters will damaged even if wind turbine will disconnect from the grid. According to the grid code during the fault time it is not recommended to isolate wind turbine or others from national grid, it is better to find another alternative methods that is crowbar protection.

In 2017, Justo, et al. [11], studied the Enhanced crowbar less fault ride through (FRT) strategy for DFIG based wind turbines under three-phase voltage dip. It was proposed strategy avoids the engagement of a crowbar circuit by utilizing the PI controllers with modified feed forward compensators and series R- L circuit. The series R-L circuit is inserted between the rotor winding terminals and the AC side of rotor side power converter (RSPC), when the rotor overcurrent exceeds its threshold value during faults. Comparative studies with five grid code requirements are performed for a wind farm with 15WT to demonstrate the LVRT performances of the proposed scheme and conventional schemes using MATLAB/Simulink software. Finally the proposed scheme was designed to avoid the engagement of the crowbar circuit by employing the PI controllers with the modified feed forward compensators.

In 2016, Huang, et al.[12], described the current tracking control for doubly fed induction generator to ride through serious grid faults. The Proposes of scaled current tracking control for rotor side converter (RSC) to enhance its LVRT capacity without flux was observed. In that method, rotor current is controlled to track stator current in a certain scale. Under proper tracking coefficient, both the required rotor current and rotor voltage can be constrained within the permissible ranges of RSC, thus it can maintain DFIG under control to suppress overcurrent and overvoltage.

In 2011, Costa, et al. [13], introduced the robust controller for DFIGs of grid connected wind turbines. It was proposed a new stationary frame robust controller for DFIGs in grid connected WTs. The DFIG dynamic model has been obtained from linear voltage and flux equations in the $\alpha\beta$ coordinates.

In 2016, Preethi et al. [14], discussed the Improved Low Voltage Ride through Capability of a Fixed Speed Wind Generator using Dynamic Voltage Restorer. They were used single fixed speed wind turbines utilizing squirrel cage induction generators were used because they are robust, economical and simple in design. Three phase voltage sags and faults cause reduction in voltage at the point of interconnection to the grid when fixed speed wind turbines connected to squirrel cage induction generators are employed resulting in disconnection of wind turbine from

the grid. But the limitations of using fixed capacitors are reactive power compensation include damage to gearbox, less efficiency and inability to provide fast control of reactive power.

In 2014, Benbouzid et al. [15], discussed about the Second order sliding mode control for DFIG based wind turbines fault ride through capability enhancement using high order sliding mode control. Its advantage is no extra mechanical stress on the wind turbine drive train, but during the grid disturbance wind turbine will disconnect from the grid and the variation of frequency is lag.

In 2017, Rini et al. [16], introduced the, improved fault ride through capability of DFIG based wind turbines using synchronous reference frame control using dynamic voltage restorer (DVR). Its main goal is to mitigate the variation of voltage under the grid faults and to maintain the normal operating condition for DFIG WT. But DVR is old method and it not fully supply power to the grid during faults.

In 2018, Sitharthan et al. [17], discussed the improved fault ride through capability of DFIG wind turbines using customized dynamic voltage restorer. DVR used to compensate the grid voltage during the grid disturbance WT stay connected but is less efficient compared to the crowbar protections.

In, 2016, Ananth, et al, [18], discussed the Improved LVRT for grid connected DFIG using enhanced field oriented control technique with super capacitor as external energy storage system by using dynamic voltage restorer. The converter topology used a super capacitor energy storage system in parallel to a normal capacitor for additional reactive power support to further to improve performance of DFIG during the faults. The super capacitor energy storage system helps in maintaining nearly constant voltage profile across the dc link capacitor.

In 2018, Mahyar, et al. [19], discussed the appropriate crowbar protection for improvement of brushless DFIG LVRT during asymmetrical voltage dips using the crowbar resistance. Used to compensate the grid voltage under grid faults. And the dis advantage is that when the crowbar circuit is activated, the control loop of the machine is deactivated and the power electronic converter is bypassed.

In 2016, Shuying et al. [20], discussed the A SCR crowbar commutated with power converter for DFIG-based wind Turbines using silicon controlled rectifiers (SCRs). Used to dissipate the circulated over current on the rotor side converters. But due to the IGBT the cost and reliability

to the IGBT crowbar, the harmonics produced by its diode bridge are harmful to the LVRT performance.

In 2016, Sajjad et al. [21], discussed the A comprehensive review of low voltage ride through of doubly fed induction wind generators using DVR. The objective is to compensate the grid power during the grid disturbance by using the reactive power, but it is less efficient and is not fully controlled the RSC.

In 2012, You et al. [22], introduced Application of PLL in the Generator-side Converters for Doubly-Fed Wind Power Generation Systems using PLL. Its goal is the phase of positive sequence component can be obtained quickly and accurately, even if the grid voltage appears to be unbalanced and distorted. But is not complete design and WT is stay connected during the grid faults.

In 2018, Gomez et al. [23], discussed on the DFIG Analysis under Grid Voltage Sags Based on Symmetrical Components by using field -oriented control on PSIM software. The symmetrical and asymmetrical faults are analyzed under different conditions.

In 2016, Saroja, et al. [24], discussed the Low Voltage Ride Through of a Grid Connected Doubly Fed Induction Generator with Speed Sensor less Vector Control by using Model reference adaptive system. The protection strategy is to ensure a safe and stable operation of the system.

in 2016, Tadesse [25], discussed the study of doubly fed induction generator control under grid fault conditions by using proportional integral controller. The main objective of this paper is to study the DFIG under the grid disturbance and evaluate the performance of DFIG during voltage sag or dip by using PID controller. But during the grid disturbance high current will produce at the rotor side controller and it will be damaged the machine. So the wind turbine will be disconnected from the grid.

In 2010, Eshetu, [47], investigation and analysis of Ashegoda wind farm integration impact on Ethiopian grid by using Siemens power system simulator PSS/E. Aim of this work is making impact study, particularly operational impact, due to variability nature of wind power output, predictability and stability impacts. But no solutions for the low voltage ride through capability. So using crowbar protection the disconnection of wind turbine ca be protected during the grid disturbance to satisfy the low voltage ride through capability.

Table 2.1 Comparison of literature review

Author	Title	Method	Advantage	Limitation
Tadesse et al.[45]	study of doubly fed induction generator control under grid fault conditions	PID	To evaluate active and reactive power To model controller	WT will disconnected from the grid during faults
Sithartha n et al. [17]	improved fault ride through capability of DFIG wind turbines using customized dynamic voltage restorer	DVR	To inject voltage during grid fault	Less efficiency Old mechanism
A. Rini et al. [16]	improved fault ride through capability of DFIG based wind turbines using synchronous reference frame control	DVR	To mitigate voltage variation	Less efficiency Not fully controlled
Preethi et al. [14]	improved Low Voltage Ride through Capability of a Fixed Speed Wind Generator	DVR	To compensate voltage during dip condition	WT disconnect during fault unidirectional
Shuying et al. [20]	SCR crowbar commutated with power converter for DFIG-based wind Turbines	silicon controlle d rectifiers	To dissipate the high current circulated at the RSC	Produce harmonics

2.2. Theoretical Background

2.3 Wind Energy Conversion Systems

Wind energy is originated from the uneven heating of the atmosphere from the sun, the abnormalities from the earth's surface, and revolution of the earth. And it produces electricity by extracting mechanical energy of the air to drive the rotor of WT. Then it converts into electrical energy by using electrical generators. Rotor of the WT turns a shaft which is connected to

gearbox, and shaft transfer energy to gearbox. Gearbox normally have different size to increase rotational speed which is suitable to the generator, thus electricity is generated by converting rotational energy to electrical energy through magnetic field. The output power from the generator fed to a transformer, which is used to converts electricity for the utility [26].

The major components of a typical wind energy conversion system include a wind turbine, generator, and interconnection device and control systems. Wind turbines can be classified into the vertical axis type and the horizontal axis type. Most modem wind turbines use a horizontal axis configuration with two or three blades, operating either down wind or up wind. A wind turbine can be designed for a constant speed or variable speed operation. Variable speed wind turbines can produce 8% to 15% more energy output as compared to their constant speed counterparts, however, they necessitate power electronic converters to provide a fixed frequency and fixed voltage power to their loads [26].

2.3.1. Definition of Wind Turbine

A wind turbine is a device that converts kinetic energy from the wind into mechanical energy. The converted mechanical energy is also converted into electrical energy with the help of generators. Wind energy penetration is rapidly increasing over the past decades due to many merits of wind power generation, such as clean, short construction cycle, and low running cost. Nowadays, a doubly fed induction generator (DFIG) is the most employed generator for wind turbines [27].

Wind is caused due to the pressure differences across the surface of the earth do to the uneven heating via solar radiation. Wind turbines are designed to exploit the wind energy that exists at a location. Aerodynamic modeling is used to determine the optimum tower height, control systems, number of blades and blade shape [27]. Figure 2.1 shows the Adama-II wind turbine.

Figure 2-1 Adama-II wind plant [7]

From studies of fluid mechanics, this flow of air can be analyzed as mass flow with kinetic energy given by:

$$KE = \frac{1}{2}mV^2 \tag{2.1}$$

The power in wind is the Kinetic energy per unit time and as is expressed as:

$$P_w = \frac{1}{2}MV^2 \tag{2.2}$$

$$\frac{dm}{dt} = \rho AV \tag{2.3}$$

$$P_w = \frac{1}{2}\rho AV^3 \tag{2.4}$$

Where A is the area of the incident air stream

m Mass

M mass flow rate

V Speed of the wind, m/sec

ρ The density of the flow

P_w Wind power

As a result of these studies, the energy market has several types of wind turbines and these turbines can be divided into two classifications according to their orientation of the spin axis, structure or speed of the rotor. The distinctive classification in the market is according to the orientation of the spin axis and wind turbines can be divided into two: vertical axis and horizontal axis wind turbines [27]. Adama –II wind farm is installed horizontal axis wind turbines. The most common type of lift force wind turbines is the horizontal axis wind turbine HAWT. The rotor axis lies horizontally, parallel to the air flow. The blades sweep a circular

plane normal to the air flow, situated upwind (in front of the tower) or downwind (behind the tower). The main advantage of HAWTs is the good aerodynamic efficiency if blades are appropriately designed and versatility of applications.

2.4 Wind Turbine

The power an air mass of wind flowing at speed v_w through the swept area A can be calculated by [28, 29] as shown in equation (2.4).

The wind power captured by the blade and converted into mechanical power can be calculated using the following.

$$P_m = \frac{1}{2}\rho A V_w{}^3 C_p = \frac{1}{2}\rho \prod R^2 V_w{}^3 C_p \tag{2.5}$$

Where sweep area is $A=\Pi R^{2,}$ R= length of the blade (radius of the turbine rotor)

Availability of power in the air will reduced by a factor of power coefficient (C_p) which gives actual power at the rotor of WT is;

$$C_p = \frac{P_t}{P_{air}} \tag{2.6}$$

2.5 Gearbox

As the speed obtained from WT rotor is not to the level required by the generator, the gear box is needed to speed up.

$$G = \frac{n_m}{n_M} \tag{2.7}$$

$$N_s = \frac{120 f_s}{P} \tag{2.8}$$

Where G = Gear box ratio

P = number of poles

It is know that;

$$n_r = (1-S)N_s = \frac{(1-S)60 f_s}{P} \tag{2.9}$$

Where p is number of pole pairs

The substitute (2.5) into(2.4) gear box equaion will be as flows.

$$G = \frac{(1-S)60 f_s}{P * n_r} \tag{2.10}$$

Where n_r and n_M are the generator and turbine rated speeds in rpm, s is the rated slip, f_s is the rated stator frequency in Hz. In the case of Adama wind farm-II wind farm, the DFIG is 1800

rpm of generator speed, 19 rpm of turbine rated speed as shown in appendix A. Accordingly, G=1800/19=94.7 which is actually given in the appendix.

2.6 Generators Used In the Wind Industry

Traditionally wind turbine industry are used different type of generators for power generation, but presently doubly fed induction generators are popularly known and it will be discussed below.

2.6.1 Doubly Fed Induction Generator (DFIG)

Nowadays, Doubly Fed Induction Generator (DFIG) becomes one of the most popular generators in a variable wind turbine systems and it comprised of two back to back converters. One converter connects the DFIG stator to the grid, and the second converter is connected to the rotor of the machine through a DC link capacitor to achieve the variable speed necessary for maximum energy capture in a variable winds.

The doubly fed induction generator (DFIG) wind energy system is widely accepted in today's wind energy industry. The DFIG is essentially a wound rotor induction generator in which the rotor circuit can be controlled by external devices to achieve variable speed operation. A typical block diagram of the DFIG wind energy system is shown in Figure 2-2. The stator of the generator is directly connected to the grid through a transformer, whereas the rotor connection to the grid is done through power converters, harmonic filters, and the transformer [28].

In this scheme, stator is directly connected to the grid while the rotor circuit is connected to grid through an AC-DC-AC back to back frequency converter as shown in Figure 2-2. The rating of this converter is typically 25-30% of the total power rating of the generator. This is the main advantage of DFIG over other variable speed topologies as it provides same features at lesser cost and provides better efficiency [30].

The stator of the generator delivers power from the wind turbine to the grid and, therefore, the power flow is unidirectional. However, the power flow in the rotor circuit is bidirectional, depending on the operating conditions [31].

The power can be delivered from the rotor to the grid and vice versa through rotor side converter (RSCs) and grid side converters (GSC). Since the maximum rotor power is approximately 30% of the rated stator power, the power rating of the converters is substantially reduced in

comparison to the Wind energy conversion system (WECS) with full capacity converters. The converter's main aim is to compensate for the difference between the speed of the rotor and the synchronous speed with the help of slip control.

With variable speed operation, a DFIG wind energy system can produce more energy from the wind than a fixed speed WECS of the same capacity when the wind speed is below its rated value. The cost of the power converters and harmonic filters is substantially lower than that in the WECS with full capacity converters. The power losses in the converters are also lower, leading to improved overall efficiency. In addition, the system can provide leading or lagging reactive power to the grid without additional devices [27].

The DC capacitor linking stator and rotor side converters allows the storage of power from induction generator for further generation or to maintain the variation. To accomplish the full control of grid current, the DC link voltage must be increased to a level higher than the amplitude of grid line to line voltage.

The main characteristics of power electronics converter may be summarized as follows.

- Limited operating speed range (-30% to +20%).
- Small scale power electronic converter (reduced power losses and price).
- Complete control of active power and reactive power exchanged with the grid.
- Need for gearbox.
- Active and reactive power control of the machine while the grid side converter (GSC) keeps the voltage of the DC link constant.

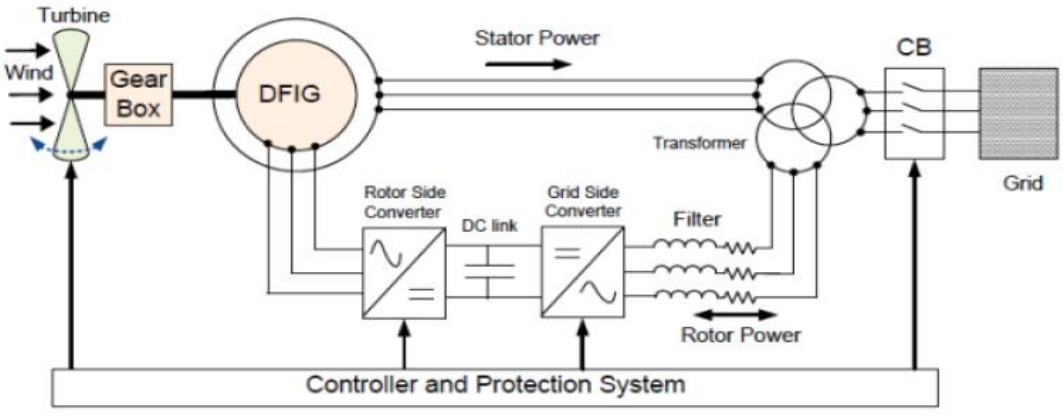

Figure 2-2 Simplified block diagram for DFIG wind energy conversion system [28].

2.6.2 Operation of Doubly Fed Induction Generator (DFIG)

Wind with certain speed is blown towards the vanes, thus driving the vanes to rotate. The vanes then drive the rotor hub to rotate, thus converting wind energy into mechanical energy. The converted mechanical energy will then drives the principal axis to rotate, and consequently electrical energy is produced by the doubly fed induction generator after accelerated by the speed up gearbox which increases relatively low rotating speed of the principal axis. The output of Adama-II wind farm DFIG is 690V is then converted into forms compliant with requirements of the power grid by external transformers 33kV before grid connection as shown in figure 2.2

If the generator operate in super synchronous mode (slip<0), power will be delivered from the rotor through the convertors to the grid, but if the generator operates in sub synchronous mode (slip>0) then the rotor will absorb power from the grid through the converters.

2.6.3 Advantage of Doubly Fed Induction Generator (DFIG)

One of the main advantages of the DFIG is that it provides variable speed using a small and economic power converter. These machines are controlled by a converter connected at the rotor, where the power is only a small fraction, approximately equal to the slip, of the stator power. This characteristic makes the DFIG especially suitable for applications where the slip is narrowly limited.

Advantages of the DFIG based on wind turbine generator system [31]

a) Improved system efficiency.
b) Reduced inverter cost, because inverter rating is typically 30% of total system power.
c) Power factor control can be implemented at lower cost.
d) It has a complete control of active and reactive power.
e) The DFIG is usually a wound rotor induction generator, which is simple in construction.

In a fixed speed wind turbine, the stator of the generator is directly connected to the grid. However, in a variable speed wind turbine, the machine is controlled and connected to the power grid through a power electronic converter.

Disadvantages of the DFIG based wind turbine generator system [31]

a) Needs slip rings and gearbox, which will require frequent maintenance.
b) Has limited fault ride through capability and needs protection schemes.

c) Has complex control schemes.

d) Sensitivity to electric grid disturbances.

2.7. Low Voltage Ride through (LVRT) Capability

In electrical power engineering, fault ride through (FRT), sometimes under voltage ride through (UVRT) or low Voltage Ride through (LVRT) has become a crucial feature of the wind turbine control system. The LVRT term is the capability of electrical generators to stay connected in short periods of time at lower electric network voltage. When the voltage of the grid is dropping it is essential that a wind turbine stay connected in order to prevent major blackouts. It is not only essential that the park stays connected. It is equally essential that the park is working actively to compensate for the faulty grid condition. Whether the LVRT capability of a wind farm is satisfying for meeting the requirements is defined in grid codes issued by the grid operator. The capability of meeting these demands is critical for whether the wind turbine is allowed to be connected to the grid or not [32].

Due to the random nature, faults imposed on the grid can occur anywhere within the connected system. Also, due to the transmission line impedance the voltages dip could be seen at the stator windings. The voltage dip can cause excessive currents on the rotor windings by the magnetic coupling. As a guaranteed mechanism, the DFIG automatically disconnects from the grid to protect the internal Power electronic converter from over currents as well as over voltage on the converter dc link, but using crowbar protection it is possible to save the power electronics converters [21].

Currently, the grid codes in most countries require that the large scale wind power plants must stay connected to the grid for a short period during the voltage dip by flowing the excess current to the crowbar resistor. This is so called LVRT capability of WTs. If the WTs are tripped off immediately after voltage sag, the grid voltage will drop further. Also, the system frequency will drop due to power imbalance. Then, the power system may be blackout due to a cascade of failures of generators. To prevent the system blackouts, the WTs must be equipped with the LVRT capability (crowbar protection must be needed).

The typical requirements for the LVRT capability of WTs in the grid codes are shown in figure 2.6. As shown in Figure. 2.3 (a), the WTs must keep connected to the grid, if the system voltage and fault duration remain in the shadow area. Because the voltage drop of the WT terminal

causes both over current in the windings and over voltage in the DC link, the additional protection devices should be installed [33].

Moreover, WTs must deliver the reactive current during the voltage dips to maintain the grid voltage. This voltage control must be activated within 20 ms after the voltage sag is detected. The required amount of the reactive current depend on the voltage dip, as indicated in Figure. 2.3 (b). The reactive current output of a WT should be within the shadow area. After the fault is cleared, WTs must continue to deliver the active power immediately with the gradient of at least 20% of the rated power per second [33].

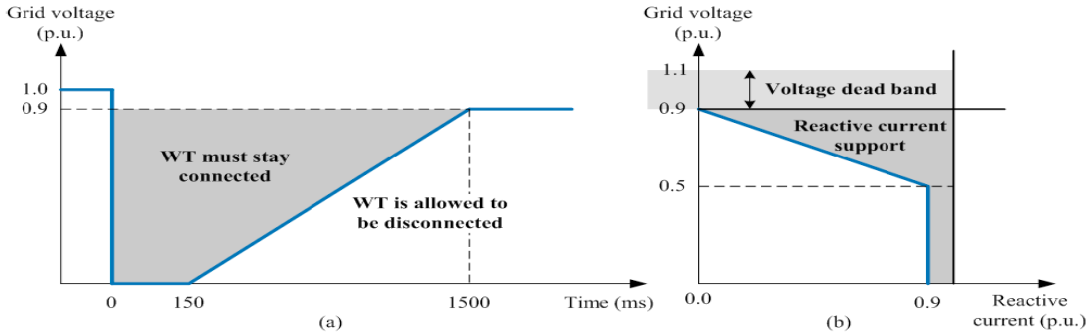

Figure 2-3. The grid code requirements that consist of (a) ride-through curve and (b) support curve of reactive current [33].

Under the fault conditions, there are two major problems for existing DFIG based on wind energy system**.**

a) High current for rotor side converter and high voltage on dc link.
b) Reconnection to recovered grid may cause stability issue.

Without proper control scheme, DFIG produce huge currents on the rotor side as the excitation current is low during faults. The generator flux is not maintained, when the stator voltage drops or negative rotating flux may appear if the system is strictly unbalanced.

2.8 Crowbar Protection Scheme

Crowbar is a device widely used to protect power electronic circuits against an overvoltage and under voltage condition in their power supply. It operates by putting a short circuit or low resistance path between the terminals. The circuit is therefore protected, meanwhile the short circuit current can cause, in over all, below out of an upstream fuse [28].

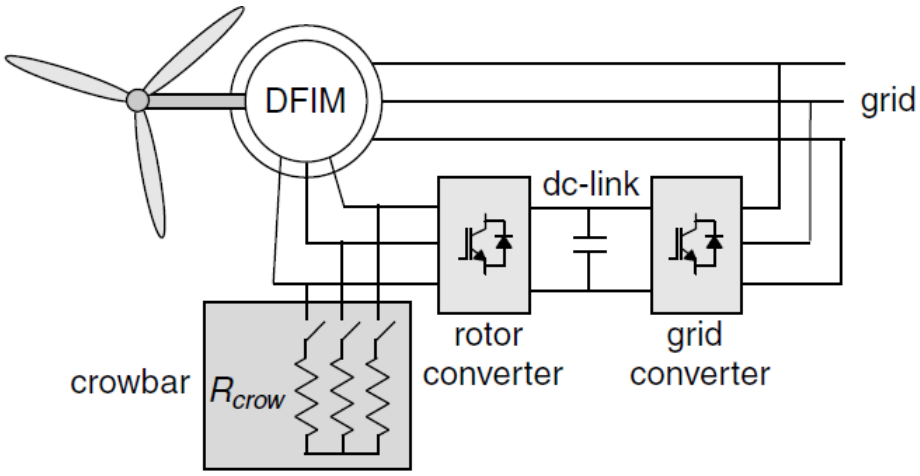

Figure 2-4. System equipped with a crowbar [28].

In wind turbines the crowbar is connected at the rotor side terminals as shown in Figure 2.4 and it prevents the overvoltage induced in case of voltages dips from damaging the rotor converter. It is activated, when an abnormal situation is detected like overcurrent in the rotor, overvoltage in the DC link, or low stator voltage. The rotor current is then diverted to the crowbar protection to prevent converters from damaging and the rotor converter is switched off, but power is delivered to the grid through the stator side [28].

Figure 2.5 shows the equivalent circuit of the system of figure 2.4 using the rotor model, when the crowbar is activated the circuit becomes an impedance divider. The converter voltage is then a fraction of the EMF induced in the rotor windings. Another way to understand how it works is the following, When the crowbar is connected, a large current circulates across the rotor, causing a huge voltage drop in the rotor internal impedance, $R`_r$ and $L`_r$ this reduces the remaining voltage at the rotor terminals.

In figure 2.4 the crowbar was made up of three resistors and three phase switch. Since the rotor current is AC, the switches must be bidirectional. In order to reduce the complexity and cost of the circuit, many manufacturers use the alternative circuit shown in Figure 2.6. This alternative diagram rectifies the rotor currents, in general, by means of a diode bridge, and hence it requires only one unidirectional switch. Neglecting the harmonics, both schemas are equivalent, if their resistances are fulfill the following relationship [28].

$$RcrowDC = \frac{\pi^2}{6} R_{crow} \tag{2.11}$$

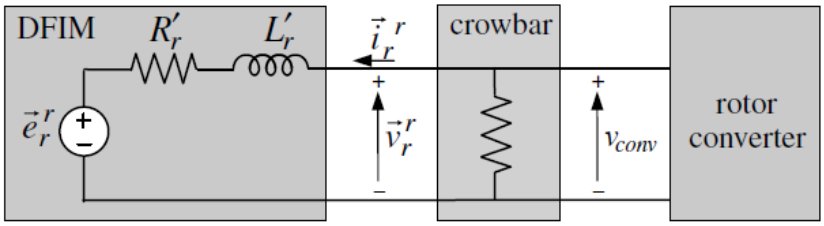

Figure 2-5 Equivalent circuit of the system when the crowbar is activated [28].

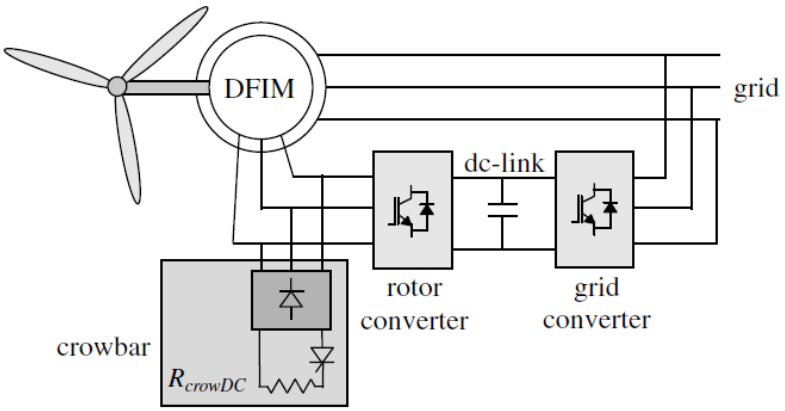

Figure 2-6 Alternative implementation of a crowbar [28].

Once the crowbar is activated, and it remains connected until the circuit breaker of the generator stops the short circuit current. In order to provide the LVRT capability, the crowbar short circuit has to be eliminated without disconnecting the turbine from the grid. Today most manufacturer's use the "active crowbar" in which the activation and also the deactivation can be actively controlled [34]. The activation and deactivation of crowbar protection scheme is shown at chapter four under the title of controlling of crowbar protection, also it is shows in the inside the Simulink model.

Modern versions of active crowbars are usually based on the scheme of Figure 2.6 and include at least one switch with cut off capability, such as a GTO or IGBTs. This design allows direct disconnection of the crowbar and instant rotor converter reactivation, enabling the continuation of normal operation in the turbine.

The active crowbar has an additional advantage, since the resistor can be connected and disconnected, it is possible to perform a pulse width modulation (PWM) in order to simulate a variable resistor [35]. It can be interesting, for example, to simulate a low resistance at the beginning of the dip, when the rotor current is very large, and to increase the resistance as the current decreases.

Another possibility of active crowbar is to obtain a variable resistance is to use different resistors that can be switched independently, as shown in Figure 2.7 depicts. At the beginning of the dip, the resistors can be connected simultaneously in order to provide a low resistance path to the rotor currents and to avoid exceeding the maximum voltage of the rotor converter.

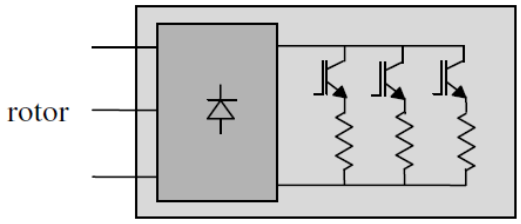

Figure 2-7 Active crowbar with a set of various resistors [28].

2.9 Dc Chopper Protection Scheme

The DC chopper is composed of power resistor which is connected in parallel to DC capacitor through a power switch. Switch will be off, if DC bus voltage is within the limits. When the fault occurs at the grid voltage will be drops. DC link capacitor will be over voltage during grid voltage dip. Inserting a chopper resistor into the DC link so as to dissipate the excessive energy in the form of heat during grid voltage dips. However, the temperature increase in the resistor may be a problem when voltage dip lasts relatively longer [36].

The DC link provides a decoupling of the generator side from the grid side, resulting in improved fault handling and active/reactive power control.

The chopper facilitates a voltage raising action from the converter terminals during the LVRT and thereby enabling a faster recover of the control of the DC link voltage the dc link voltage kept within its safe limits even though some oscillations remain to be a challenge for a smooth transition between the steady state and the fault state if required. The available oscillations may be in a long run deteriorate the performance and life duration of the power electronics components [27].The DC link voltage regulates the source current in the grid system, so the DC link voltage is maintained constant across the capacitor as shown in Figure 2.8 [29].

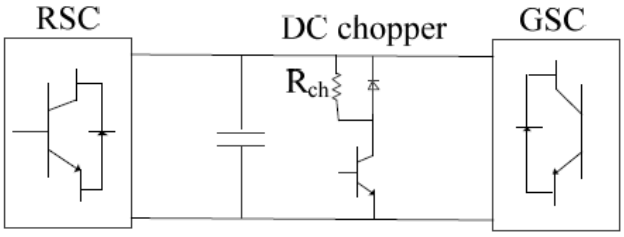

Figure 2-8 Schematic diagram of DC chopper protection circuit [37].

Normally DC link capacitor is located between the two power electronics converters and it serves as energy storage mechanism in order to maintain a constant voltage in its terminals. To derive the model of the DC link, the DC bus is dependent on the current through the capacitor its calculation will be as flows [28, 38].

$$q = CV$$

$$where \quad i = \frac{dq}{dt}$$

$$then \quad i = C\frac{dv}{dt}$$

$$V_{bus} = \frac{1}{C_{bus}}\int_{t_o}^{t} i_c dt \tag{2.12}$$

The current through the capacitor can be found as flows;

$$i_c = i_{r\_dc} - i_{g\_dc} - i_{res} \tag{2.13}$$

Where i_{res} current through the resistor (A)

i_{g_dc} dc current flowing from the dc link to the grid (A)

i_{r_dc} dc current flowing from left part to the dc link (A)

The DC currents can be calculated as follows from the output AC currents of the converters

$$i_{g\_dc} = S_{a\_g} i_{ag} + S_{b\_g} i_{bg} + S_{c\_g} i_{cg} \tag{2.14}$$

$$i_{r\_dc} = -S_{a\_r} i_{ar} - S_{br} i_{br} - S_{c\_r} i_{cr} \tag{2.15}$$

The current through the resistance is shown below;

$$i_{res} = \frac{V_{bus}}{R_{bus}} \tag{2.16}$$

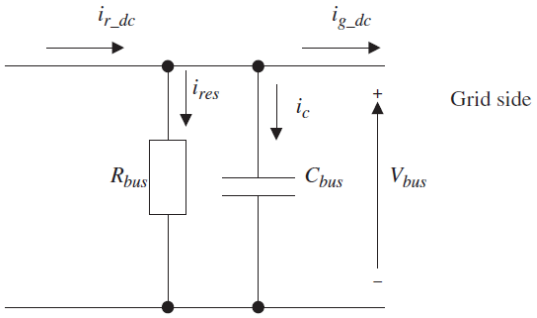

Figure 2-9 dc link system [28]

2.10. Analysis of the DFIG during Fault Time

2.10.1 Introduction

The stator of DFIG on wind turbine is directly connected to the grid and during the grid fault high current will produced. And the rotor winding are connected to the grid through back to back converters which is more sensitive to the grid faults. One of the main advantages of the DFIG is that it provides variable speed using a small and economic power converter. These machines are controlled by a converter connected at the rotor, where the power is only a small fraction, approximately equal to the slip of the stator power. This characteristic makes the DFIG especially suitable for applications where the slip is narrowly limited, such as wind turbines. However, as wind energy penetration increased and the number of wind turbines using the DFIG expanded, the main disadvantage of DFIG is it became more sensitivity to electric grid disturbances. A drop of one or more phase voltages can be mainly damaging for the electronic converter. A voltage dip causes high currents and over voltages in the rotor windings, which would damage the converter connected to their terminals, if no counter measures were taken [28]. In the following sub title different fault are analyzed.

2.10.2 Electromagnetic Force Induced In the Rotor

The electromagnetic force induced in the rotor windings varies considerably under the grid disturbances. This is the cause of the problematic behavior of DFIG under perturbations [28].

The voltage of the rotor expression will be as follows.

$$\overrightarrow{v_r^{\,r}} = R_r i_r + \frac{d\vec{\Psi}_{rr}}{dt} \tag{2.17}$$

The rotor flux is very similar to the stator flux imposed by the grid when the stator is directly connected to the grid. And the relationship between both the stator and rotor fluxes can be calculated as flows:

$$\vec{\psi}_r^{\,r} = \frac{L_m}{L_s}\overrightarrow{\psi_s}^{r} + \delta L_r \vec{i}_r^{\,r} \tag{2.18}$$

Where $\sigma=1-L^2_m/L_sL_r$ is the leakage coefficient. Combining Equations (2.12) and (2.13), the following expression is obtained.

$$\vec{V}_r^{\,r} = \frac{L_m}{L_s}\frac{d}{dt}\vec{\Psi}_r^{\,r} + (R_r + \sigma L_r \frac{d}{dt})\vec{i}_r^{\,r} \tag{2.19}$$

The rotor voltage might be divided into two terms. The first term corresponds to the EMF induced by the stator flux in the rotor. It is the voltage in the rotor open circuit terminals (where i_r =0). Thus, its expression is:

$$e_r^{\,r} = \frac{L_m}{L_s}\frac{d}{dt}\Psi_r^{\,s} \tag{2.20}$$

Or, if the variables are exposed in a stator reference frame.

$$\vec{e}_s^{\,r} = \frac{L_m}{L_s}(\frac{L_m}{L_s}\vec{\Psi}_s^{\,s} - j\omega_m\vec{\Psi}_r^{\,s}) \tag{2.21}$$

2.10.3 During The Normal Operation of DFIG

During normal operation, the three phase voltage are balanced and have constant amplitude and frequency shifted by 120^0 each other.

$$V_a = V_g \cos(\omega_s + \phi)$$

$$V_b = V_g \cos(\omega_s + \phi - \frac{2\pi}{3})$$

$$V_c = V_g cos(\omega_s + \phi - \frac{4\pi}{3})$$

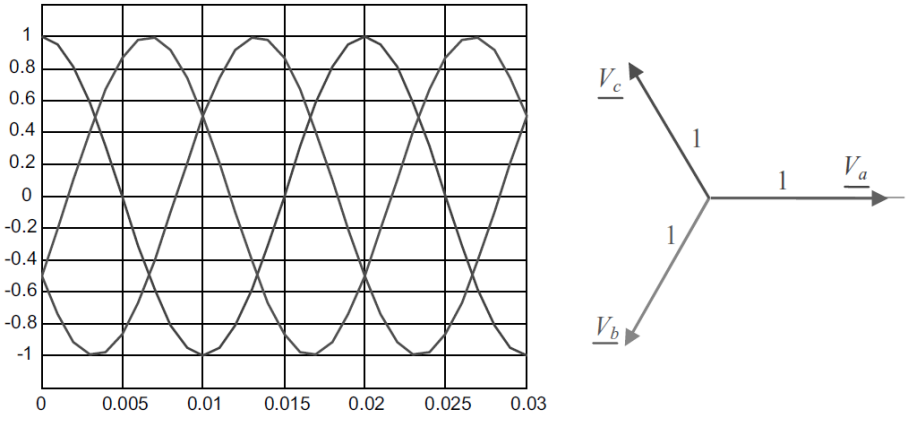

Figure 2-10 Balanced system [28].

The space vector of the stator voltage is a rotating vector of constant amplitude V_g that rotates at synchronous speed of ω_s.

$$\vec{V}_s^{\,s} = V_g e^{i\phi} e^{j\omega_s t} = \sqrt{2}Vg e^{i\omega_s t} \tag{2.22}$$

Where Vg is grid phasor voltage (rms)

Voltage drop in stator resistance R_s is significantly smaller than stator voltage drop (~1%) this can be neglected and the stator phasor flux will found as flows.

$$\psi_s = \frac{V_g}{j\omega_s} \tag{2.23}$$

At steady state stator flux is rotating vector at constant amplitude directly to the grid voltage and synchronous speed.

$$\vec{\Psi}_s^{\ s} = \sqrt{2}\Psi_s e^{i\omega_s t} = \frac{V_g e^{j\phi}}{j\omega_s} e^{j\omega_s t} \tag{2.24}$$

From the rotor windings the rotational speed of the stator flux is the result of the synchronous speed and the electrical rotor speed that is the slip frequency. If the machine operates at synchronous frequency rotor winding have constant flux and no EMF.

The rotor reference frame will be expressed as flow.

$$\vec{\Psi}_r^{\ s} = \vec{\Psi}_s^{\ s} e^{-j\omega_m t} = \sqrt{2}\Psi_s e^{j(\omega s - \omega m)t} = \sqrt{2}\Psi_s e^{j\omega_r t} \tag{2.25}$$

The variable flux will thus produce an EMF proportional to the slip frequency.

$$\vec{e}_r^{\ r} = \frac{L_m}{L_s}\frac{d}{dt}\vec{\Psi}_s^{\ r} = j\omega_r \frac{L_m}{Ls}\vec{\Psi}_s^{\ r} \tag{2.26}$$

Amplitude of EMF can be stated as function of stator voltage.

$$|E| = \omega_r \frac{L_m V_g}{L_s \omega_s} = Vg\frac{L_m}{L_s}s \tag{2.27}$$

The machine operates by the slip of 25%, voltage is relatively low it should note that this voltage is refers to stator side and there is faults. Using the phasor notation, the phasors are three complex numbers with 120^0 phase shift will shows below.

$$\begin{bmatrix} V_a \\ V_b \\ V_c \end{bmatrix} = \begin{bmatrix} V_g e^{j\varphi} \\ V_g e^{j\varphi - \frac{2\pi}{3}} \\ V_g e^{j\varphi - \frac{4\pi}{3}} \end{bmatrix} = Ve^{j\varphi}\begin{bmatrix} 1 \\ a \\ a^2 \end{bmatrix}$$

The three sequence can be expressed from the phasor of the three phase of the original system;

Where 'a' is unitary vector at the angle of 120^0 and $a^2 = a^* = 1 < 240^0$ $a^3=1$ and $1+a+a^2=0$.

Positive sequence is denoted by subscript 1 ($a \to b \to c$) and negative sequence is by 2 ($a \to c \to b$). From the phasor of three phase can be calculated three sequcence as flows;

$$\begin{bmatrix} V_{1,a} \\ V_{2,a} \\ V_{0,a} \end{bmatrix} = \frac{1}{3}\begin{bmatrix} 1 & a & a^2 \\ 1 & a^2 & a \\ 1 & 1 & 1 \end{bmatrix} . \begin{bmatrix} V_a \\ V_b \\ V_c \end{bmatrix} \quad (2.28)$$

Where V_a V_b V_c are phasors of phases a b and c

$V_{1,a}$, $V_{2,a}$ and $V_{a,0}$ the phasore of phase a of positive, negative and zero sequences respectively.

2.10.4 Three Phase Voltage Dips

Fault involves all the three phase is known as symmetrical or balanced faults. Usually symmetrical fault is three phase to ground fault. Voltage dip is one the faults and it is an unexpected drop of one or more voltage phases and it said to be three phase, symmetrical, or balanced dip if the drop is the same in the three phases. This fault could be caused, for example, by inrushing currents at motor start up or by a near short circuit between the three phases and the ground. The cause of symmetrical faults are lightning, heavy winds, trees falling across the line and vehicles colliding with the tower. And their effects are flow of excess current, abnormal voltage and induce over voltage.

In electrical machine with symmetrical windings have positive, negative and zero sequence. Zero sequence create leakage flux, if the machine have neutral ground but in most neutral is isolated and zero sequence voltage have no effect it can be isolated. By ignoring the zero sequence grid voltage can reduced into the sum of positive and negative sequence. Using the space vector natation can be found the following.

$$\overrightarrow{V_s^s} = \sqrt{2}V_1 e^{j\omega_s t} + \sqrt{2}V_2 e^{-j\omega_s t} \quad (2.29)$$

The machine can be considered as a linear system, if it is not saturated steady state will be the addition of two terms that's called the positive components of the stator voltage ψ_1 and negative voltage ψ_2.

By neglecting the stator resistance:

$$\overrightarrow{\psi_{s1}^s} = \frac{\sqrt{2}V_1}{j\omega_s} e^{j\omega_s t}$$

$$\overrightarrow{\psi_{s2}^s} = \frac{\sqrt{2}V_2}{-j\omega_s} e^{-j\omega_s t} \quad (2.30)$$

Due to the natural flux surge the three phase dip, the total flux will be continuous and it is the sum of three fluxes.

$$\overrightarrow{\psi_s^s} = \overrightarrow{\psi_{s1}^s} + \overrightarrow{\psi_{s2}^s} + \overrightarrow{\psi_{sn}^s} \quad (2.31)$$

These are the total stator flux on the positive, negative and the neutral. The positive ($\overrightarrow{\psi_{s1}^{s}}$) and negative ($\overrightarrow{\psi_{s2}^{s}}$) fluxes are the steady state fluxes, a function of the grid voltage. The natural flux, in contrast, is a transitory flux, independent on the grid voltage. Its initial value ψ_{n0} guarantees no discontinuity in the total flux. In three-phase voltage dips, this initial natural flux is a function of depth whereas in asymmetrical dips, it depends as well on the type of fault (single phase, and phase to phase) and on the time of appearance.

Each flux can induce EMF in the rotor based on its amplitude and its relative speed with respect to rotor winding. Voltage produced in the open circuit is the sum of the three terms.

$$\overrightarrow{e_r} = \overrightarrow{e_{r1}} + \overrightarrow{e_{r2}} + \overrightarrow{e_{rn}} \tag{2.32}$$

The first term can found by substituting into equation 2.22 the flux obtain in equation 2.31 then the rotor reference frame will be as flows.

$$\overrightarrow{e_{r1}^{r}} = \sqrt{2}V_1 \frac{L_m}{L_s} S e^{jS\omega_s t}$$

$$\overrightarrow{e_{r2}^{r}} = \sqrt{2}V_2 \frac{L_m}{L_s} (2 - S) e^{-(2-S)\omega_s t} \tag{2.33}$$

From equation (2.34) author understand the first voltage is low and it is relative to the slip. Its frequency is equivalent to the slip frequency that is a few hertz. The next voltage, is increased by a factor close to 2, and consequently its amplitude could be vital if the asymmetrical ratio of the dip is large. Since the slip is usually small, its frequency is approximately twice the grid frequency.

$$\overrightarrow{e_{rn}^{r}} = -\frac{L_m}{L_s} j\omega_m \overrightarrow{\psi_{sn}^{r}} \tag{2.34}$$

Three phase dips and emf induced by natural flux are similar and the only difference are at the initial value of the flux it depend on the other factors besides the dip. Then the natural flux is fixed with the stator, the frequency of this emf is similar to the rotor speed, that is, nearly the grid frequency.

2.10.5 Single Phase Dip (Unsymmetrical Faults)

A fault that involves only one or two phase is known as unsymmetrical faults that is single line to ground, line to line and double line to ground faults are example of unsymmetrical faults. The most common grid fault in power system is a short circuit between one lines to ground. The dip voltage creates due to the short circuit in phase ‘a’ , positive and negative sequence have equal

impedance and voltage at phase 'b' and 'c' are remain the same. The phasors of the phase voltages can be express as flows.

$$\begin{aligned}\sqrt{2}V_a &= v_{pre}(1-p)\\ \sqrt{2}V_b &= v_{pre}a^2\\ \sqrt{2}V_c &= v_{pre}a\end{aligned} \tag{2.35}$$

$\sqrt{2}$ Indicates the phasor are expressed in rms value and p is the pair of poles of the Machine.

$$\begin{bmatrix}\sqrt{2}V_1\\ \sqrt{2}V_2\\ \sqrt{2}V_0\end{bmatrix} = \frac{1}{3}\begin{bmatrix}1 & a & a^2\\ 1 & a^2 & a\\ 1 & 1 & 1\end{bmatrix}.\begin{bmatrix}V_{pre}(1-p)\\ V_{pre}a^2\\ V_{pre}a\end{bmatrix} = V_{pre}\begin{bmatrix}1-\frac{p}{3}\\ \frac{-p}{3}\\ \frac{-p}{3}\end{bmatrix} \tag{2.36}$$

The natural flux can be found from the initial setting by considering the total flux is also must be contentious.

$$\begin{aligned}\vec{\psi}_s(t_0^-) &= \vec{\psi}_s(t_0^+)\\ \vec{\psi}_s(t_0^-) &= \vec{\psi}_{s1}(t_0^+) + \vec{\psi}_{s2}(t_0^+) + \vec{\psi}_{sn}(t_0^+)\end{aligned} \tag{2.37}$$

By using the above expression initial natural flux can be derived.

$$\vec{\psi}_{no} = \overrightarrow{\psi_s^s}(t_0^-) - \overrightarrow{\psi_{s1}^s}(t_0^+) - \overrightarrow{\psi_{s2}^s}(t_0^+) \tag{2.38}$$

The amplitude of the natural flux depends on the positive and negative flux at time t. the timing of the fault. If the dip voltage starts at t_0=0 natural frequency will be zero because at this time positive and negative fluxes are aligned and their sum will equals to the flux before the fault as shown in figure (2.11).

$$\begin{aligned}\overrightarrow{\psi_s^s}(0^-) &= \frac{V_{pre}}{j\omega_s}\\ \overrightarrow{\psi_s^s}(0^+) &= \frac{V_{pre}(1-p/3)}{j\omega_s} + \frac{-V_{pre}\frac{p}{3}}{-j\omega_s} = \frac{V_{pre}}{j\omega_s}\end{aligned} \tag{2.39}$$

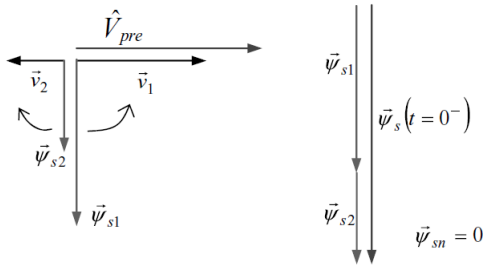

Figure 2-11 Space vectors of the stator flux for an 80% single phase dip starting at t_0=0 [28]

In figure 2.12 the curve drown by flux during dip is create an elliptical and this is common characteristics in an unsymmetrical voltage dip due to the presence of two flux rotating in opposite directions. The two flux vectors add constructively and destructively twice per period, which gives rise to the major and minor axes of the ellipse, respectively as shown in figure 2.12.

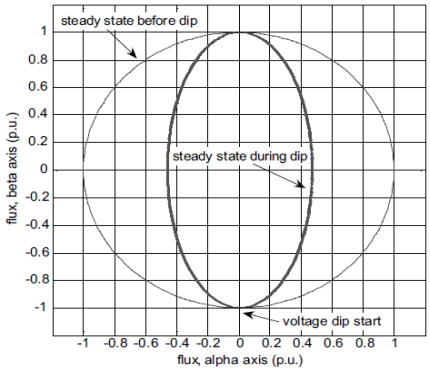

Figure 2-12 Stator flux trajectory for an 80% single phase dip starting at t_0=0 [28].

If dip starts at t_0 =T/4 the worst condition happed. In this case the initial natural flux value is large because the positive and negative fluxes are at the beginning dip opposed as shown in figure 2.13.

Total flux must be the same before and after the beginning of the faults and the initial value will be calculated as flows.

$$\overrightarrow{\psi_s^s}\left(\frac{T^-}{4}\right) = \frac{jV_{pre}}{j\omega_s}$$

$$\overrightarrow{\psi_s^s}\left(\frac{T^+}{4}\right) = \frac{jV_{pre}(1-p/3)}{j\omega_s} + \frac{jV_{pre}p/3}{j\omega_s} + \overrightarrow{\psi_{n0}}$$

$$\overrightarrow{\psi_{n0}} = \frac{{V_{pre}}^2/_3 p}{\omega_s} \qquad (2.40)$$

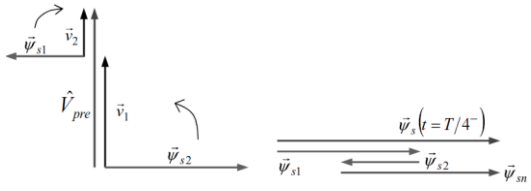

Figure 2-13 Space vectors of the stator flux for an 80% single-phase dip starting at t_0 =T/4 [28].

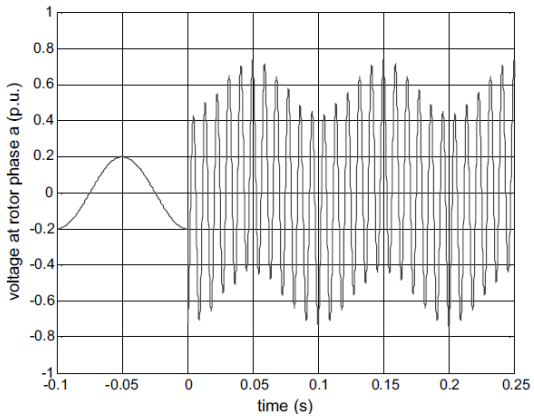

Figure 2-14 Voltage across rotor phase for an 80% single phase dip starting at t_0=0 [28].

2.10.6 Equivalent Model during the different faults

During the normal operation time there is only positive flux in the stator and EMF induced is proportional to the slip. Also the resistance seen from rotor is almost equals to the rotor resistance as shown in figure 2.15.

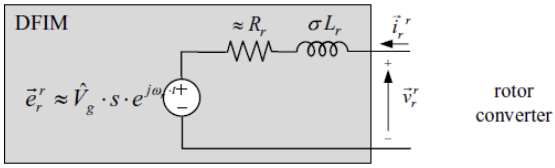

Figure 2-15 Equivalent circuit for normal operation [28].

During three phase voltage dips the stator flux is composed of positive and neutral flux. And the EMF produced by the positive flux can be neglected because it is relatively small compared to the EMF produced by the natural flux as shown in figure 2.16.

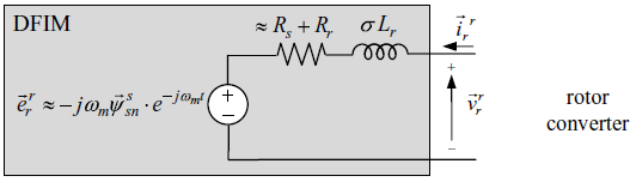

Figure 2-16 Equivalent circuit for three phase voltage dips [28].

Finally asymmetrical voltage dip produce neutral and negative flux, even though the positive flux will remain in the stator. This flux can be ignored and the behavior of the machine is determined by the negative flux as shown in figure 2.17. The stator resistance affects the rotor converter it appears in the circuit multiplied by 2.

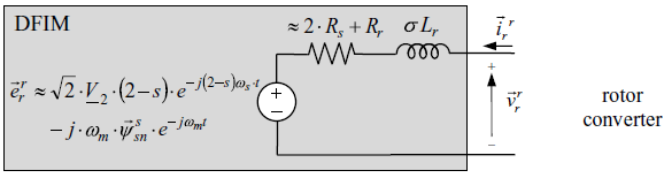

Figure 2-17 Equivalent circuit for asymmetrical voltage dips [28].

Generally DFIG under healthy conditions when the EMF induced in the rotor is small and proportional to the sleep. The EMF induced on voltage dip is remarkable larger, it depend on the rotational speed and transient of the voltage. During three phase voltage dip, the stator voltage drops to zero, and the flux which is not generated by any stator voltage is called natural flux. During general voltage dip, stator flux can be separated in to positive, negative and natural frequency.

Positive flux rotate at synchronous speed and is always existent, including during regular operation of the machine and it induce EMF proportional to the sleep. And the negative flux is only appears in case of asymmetrical faults since it is generated by negative sequence of the grid voltage. Also it rotates at synchronous speed but in opposite direction. Natural flux is a transient flux that produced due to voltage differences and it decays exponentially in asymmetrical faults and it depends on fault time (0.8 to 1.5 s). As the negative and natural fluxes rotates at a relatively high speed with respect to the rotor they produce voltages in the rotor that are higher than those appear under regular operation. If the value of voltage exceeds that rotor converter, current will not controlled consequently over current will be appear and power electronics converter will be damaged [28].

2.11 Power Curve of Adama-II Wind Turbine Generation

According to Betz rules, the value of the power coefficient features a theoretical limit connected with 59.7 %. And a typical power curve of Adama-II wind farm power curve is shown in figure 2.18 [29].

a) Cut in wind speed, is the starting speed to generate power, which is vary between 3- 4 m/s wind speed of Adama-II wind turbine has 3.5 m/s cut in wind speed.
b) Rated wind speed, which is the rated power output (1.5MW), it will generate continuously with the speed on 10-15 m/s as shown in figure 2.18. Adama-II wind turbine has 12 m/s rated wind speed.

c) Cut out wind speed, when this wind speed exceeds 20–25 m/s the particular wind generators are commonly brought to be standstill avoiding high mechanically skillful loads within the turbine components. This wind speed is called the shortened out breeze speed.

As described in Figure 2.18 the cut in wind speed, as the name indicates that the wind speed at which the turbine starts to operate and deliver power. The blade should be able to capture enough power to compensate for the turbine power losses.

The rated wind speed is the speed at which the system produces nominal power, which is also the rated output power of the generator. The cut out wind speed is the highest wind speed at which the turbine is allowed to operate before it shut down. If the wind speed is above the cut out speed, the turbine must be stopped, to prevent materials from excessive wind is presented [28].

Power curve of the WTGS indicates the power generating power of the WTGs under different wind speed. The WTGs power curve is shown as fig. 2.18. The WTGs starts generating and outputs power when the speed reaches the cut in speed, as the wind speed increased, the output power increases as well, output power of the WTGs reaches the rated value 1.5 MW when the rated wind speed is achieved, when the wind speed exceeds the rated value, it will be controlled at limit value through variable control, e.g. rated power 1.5 MW for Adam-II wind farm.

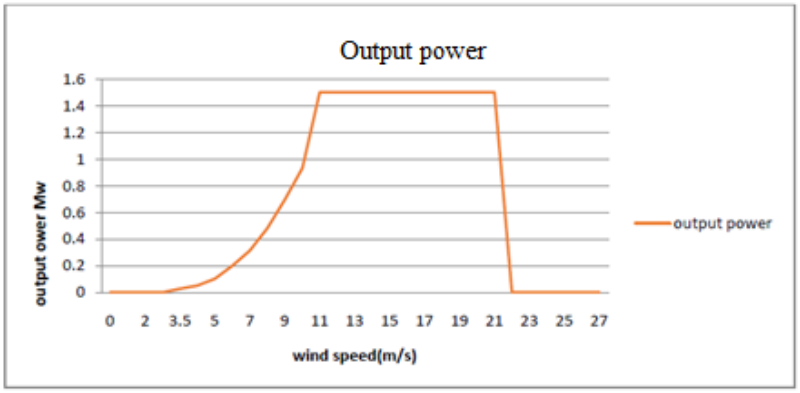

Figure 2-18 Turbine mechanical power versus wind speed curve.

The wind turbine is described by the power it generates through WT and it is a function of the wind velocity, air density, radius of the turbine and power coefficient for the tur bine. Blades of the turbine play significant role in energy capture. If the radius of WT rotor is large, then it will capture large amount of energy from the wind [28, 29, 39].

Wind turbine can only extract part of the power from the wind, which is limited by the Betz limit (maximum 59.7 %). This fraction is described by the power coefficient of the turbine, C_p, which is a function of the blade pitch angle and the tip speed ratio.

Power coefficient (C_p), the ratio of the wind kinetic energy that the wind rotor receives and of all wind kinetic energy over the sweeping area of the blades, indicates the wind energy utilization efficiency. Initial value of C_p for WTG under study is approximates 0.34. When the wind speed reaches the cut in speed, C_p keeps stable above 0.48. When the wind speed exceeds the rated value, to ensure stable output power and to reduce impact of the wind on the WTGS, C_p value drops. For the DFIG under study, C_{pmax} of 0.4865 is used [28, 29, 39].

CHAPTER THREE

3. METHODOLOGY AND MODELING OF DFIG BASED ON WIND TURBINE

3.1. Methodology

The first step towards processing this thesis is started with reviewing different literatures, where all the theoretical information regarding the improved low voltage ride through capability of DFIG based on wind turbine is gathered and comparison of previous similar research is studied. The work of different authors has been reviewed under literature review. The total task of data collection was accomplished through;

- From recorded data and equipment specifications
- By interviewing people working on the site and
- Through prepared questionnaires

This work will discussed the low voltage ride through capability (LVRT) of DFIG based wind turbine of Adama-II wind farm to stay connected with grid under different fault conditions. Previously wind turbine is disconnected during the fault conditions. But using the method of crowbar resistance protection, it is possible to make wind turbines stay connected to the grid under the grid disturbance.

3.2. Modeling of DFIG Based Wind Turbine

3.2.1 Structure of the Machine and Electric Configuration

Doubly fed induction machine (DFIG) is a term commonly used to define an electrical machine, which has been used over many decades in various applications, often in the range of megawatts of power and also less usually in the range of few kilowatts. This idea of the machine is as an alternative to more common asynchronous and synchronous machine. It can be beneficial in applications that have inadequate speed range allowing a reduction in the size of the supplying power electronic converter as for instance in variable speed generation water pumping and so on. The typical scheme of the DFIG is shown in figure 3.1. The stator is supplied by three phase voltage directly from the grid at constant amplitude and frequency, creating the stator magnetic field. The rotor is also supplied by three phase voltage that take different amplitude and frequency at steady state in order to reach different operating conditions of the machine like speed and torque.

This is attained by using back to back voltage source converter (VSC), three converter, as denoted in the simple schematic diagram. Those converters used to control the whole DFIG operating point and to achieve the power exchange through the rotor to the grid. Vector control techniques active and reactive power of DFIG will be controlled according in [28, 40].

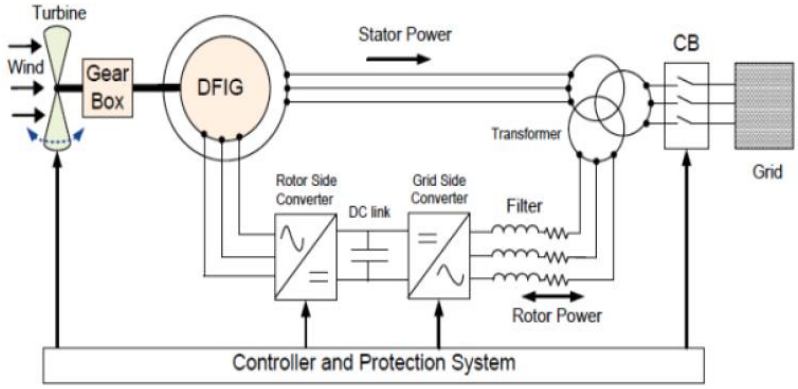

Figure 3-1 General supply of configuration of DFIG [40].

3.2.2 Aerodynamic Model

In wind turbine simulation with FRT capability is desirable to involve the aerodynamic model during grid disturbance. Turbine rotor blades extract some kinetic energy from the flow of air in the wind and transform this energy into rotational mechanical energy. In order to obtain the amount of mechanical energy transformed by the turbine blade firstly the kinetic energy of moving object in the air should be found using equation (2.3). The magnitude of this equation depends on air density and wind velocity [28, 40].

Therefore the mechanical power of the wind turbine extracted from the wind is as flows in equation (2.3). And the power of the moving air passing across an area could be found as it shows in equation (2.4).

After it calculating the power of the wind the power that extracted wind turbine can be also calculated. Since the air flow must be continues behind the blades to extract power only a fraction of the kinetic energy can be absorbed by the blades of the wind turbine. The tip speed ratio can be defined as the ratio of the blade tip speed and wind speed as;

$$\lambda_t = \frac{\omega_t R}{V_w} \text{ [rad]} \tag{3.1}$$

Where R is the length of the blades (radius of the turbine rotor), besides as the rotor structure can be changed by changing the pitch angle of the blades also C_p will be changed. The power of output turbine can be extracted by using equation (3.2).

$$P_w = \frac{1}{2}\rho A V_w^3 C_p(\lambda\beta) \tag{3.2}$$

Where $C_p(\lambda,\beta)=0.5176(\frac{116}{\lambda_i}-0.4\beta-5)e^{\frac{21}{\lambda_{i+0.0068\lambda}}}$ (3.3)

By rearranging the above equation λ_i can be express as flows:

$$\lambda_i = \frac{1}{\frac{1}{(\lambda+0.08\beta)}-\frac{0.035}{1+\beta^3}} \tag{3.4}$$

Where ω the turbine rotor speed and

R is the radius of the wind turbine blade.

Thus any change in the rotor speed or the wind speed induces change in the tip speed ratio leading to power coefficient variation. in this way the generated power is affected according to [28, 40].

The mechanical power captured by the turbine can also be expressed in terms of torque.

$$P_M = T_t * \omega_t \quad \text{and} \quad T_t = P_M/\omega_t \tag{3.5}$$

Substituting equation ($P_M = \frac{1}{2}\rho A V^3_w C_P = \frac{1}{2}\rho\pi R^2 V^3_w C_P$) and ($\lambda t = \frac{\omega_t R}{V_w}$ into (3.6).

$$T_t = \frac{1}{2}\rho\pi R^3 C_t V^2 \tag{3.6}$$

Where, C_t is the coefficient of torque. The coefficients of power and torque are related by this equation.

$$C_p(\lambda) = C_t * \lambda$$

The most straight forward way to represent the torque and power coefficient C_p is by means of analytical expression as a functions of tip step ratio (λ) and the pitch angle (β). One expression usually used and easy to adapt different turbines are as flows.

$$C_p = k_1(\frac{k_2}{\lambda_i} - k_3\beta - k_4\beta^{k5} - k_6)(e^{k7/\lambda_i}) \tag{3.7}$$

K_1=0.46, K_2=151, K_3=0.58, K_4=0.002, K_5=2.14, K_6=13.2, K_7=-18.4

$$\lambda_i = \frac{1}{\lambda + 0.02\beta} - \frac{0.003}{\beta^3 + 1} \tag{3.8}$$

With the tip step ratio,

$$\lambda = \frac{\omega_t R}{v_w}$$

The following relations can be used during modeling.

$$T_G' = T_G * G \tag{3.9}$$

$$J_G' = T_G * G^2 \tag{3.10}$$

$$\omega_t = \frac{T_t - T_g'}{J_t - J_g'} \tag{3.11}$$

Where J_t & J_g are turbine and generator inertias respectively [28, 40].

3.3 Dynamic Modeling of DFIG

3.3.1 α-β Model

To develop the dynamic α-β model of the DFIG, space vector theory is applied to the basic electric equations of the machine and gain, as in the steady state model that was considered the machine is assumed both ideal and linear. Figure 3.2 shows the three different rotating reference frames typically utilized to develop space vector based on models of the DFIG. The stator reference frame (α-β) is stationary reference frame, the rotor reference frame (DQ) rotates at ω_m and the synchronous reference frame (dq) rotates at ω_s. Subscripts "s", "r" and "a" are used to denote that one space vector is reference to the stator, rotor and synchronous reference frames respectively [40].

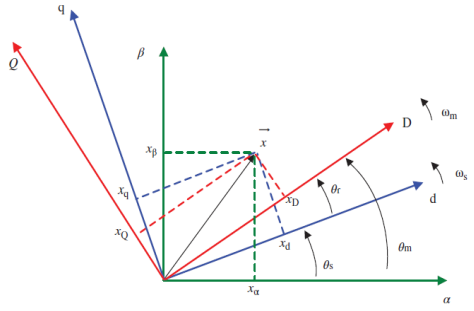

Figure 3-2 Different reference frames to represent space vectors of the DFIG [40].

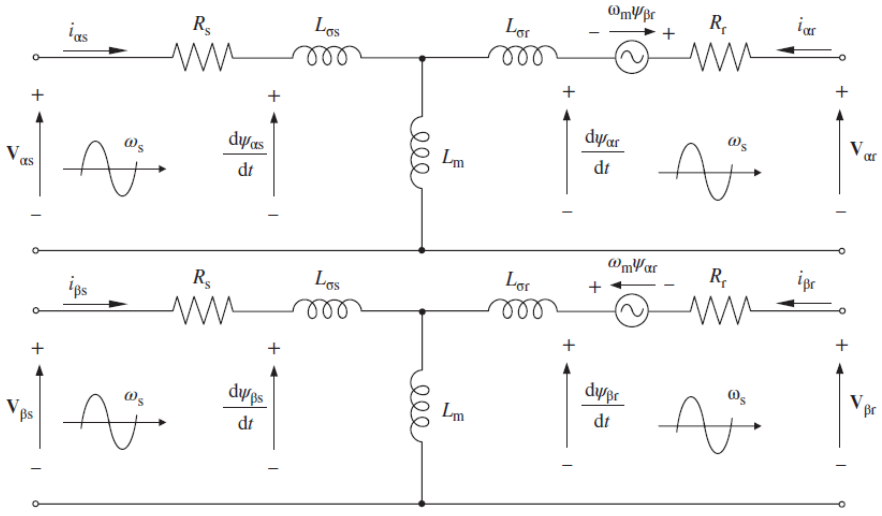

Figure 3-3 Equivalent Model of the DFIG in the α-β reference frame [40].

The three coils of the stator and rotor independently by using space vector theory, can be characterized by two stationary α-β coils for the rotor and two revolving coils DQ for the rotor, providing the following voltage equations based on figure 3.3.

$$\vec{V}_s^{\,s} = R_s\vec{i}_s^{\,s} + \frac{d\vec{\psi}_s^{\,s}}{dt} \tag{3.12}$$

$$\vec{V}_r^{\,r} = R_r\vec{i}_r^{\,r} + \frac{d\vec{\psi}_r^{\,r}}{dt} \tag{3.13}$$

If the voltage equations are represented in stationary reference frame α-β, the rotor equation must be multiplied by $e^{j\theta_m}$, which yields the following set of equations.

$$\vec{V}_s^{\,s} = R_s\vec{i}_s^{\,s} + \frac{d\vec{\Psi}_s^{\,s}}{dt} \rightarrow \begin{pmatrix} V_{\alpha s} = R_s i_{as} + \dfrac{d\Psi_{\alpha s}}{dt} \\ V_{\beta s} = R_s i_{\beta s} + \dfrac{d\Psi_{\beta s}}{dt} \end{pmatrix} \tag{3.14}$$

$$\vec{V}_r^{\,s} = R_r\vec{i}_r^{\,s} + \frac{d\vec{\Psi}_r^{\,s}}{dt} - j\omega_m\vec{\psi}_r^{\,s} \rightarrow \begin{pmatrix} V_{\alpha r} = R_r i_{\alpha r} + \dfrac{d\Psi_{\alpha r}}{dt} + \omega_m\Psi_{\beta r} \\ V_{\beta r} = R_r i_{\beta r} + \dfrac{d\Psi_{\beta r}}{dt} - \omega_m\Psi_{\alpha r} \end{pmatrix} \tag{3.15}$$

In a similar way, it is possible to derive the stator and rotor flux expressions in space vector in a stationary reference fame.

$$\vec{\psi_s^s} = L_s\vec{\imath_s^s} + L_m\vec{\imath_r^s} \rightarrow \quad \begin{cases} \psi_{\alpha s} = L_s\, i_{\alpha s} + L_m\, i_{\alpha s} \\ \psi_{\beta s} = L_s\, i_{\beta s} + L_m\, i_{\beta s} \end{cases} \tag{3.16}$$

$$\vec{\psi_r^s} = L_m\vec{\imath_s^s} + L_r\vec{\imath_r^s} \rightarrow \quad \begin{cases} \psi_{\alpha r} = L_s\, i_{\alpha r} + L_r\, i_{\alpha r} \\ \psi_{\beta r} = L_m\, i_{\beta s} + L_r\, i_{\beta r} \end{cases} \tag{3.17}$$

Where;

$V_{\alpha s}$, $i_{\alpha s}$	α-axis stator voltage and current
$V_{\beta s}$, $i_{\beta s}$	β-axis stator voltage and current
$V_{\alpha r}$, $i_{\alpha r}$	α-axis rotor voltage and current
$V_{\beta r}$, $i_{\beta r}$	β-axis rotor voltage and current
$\psi_{\alpha s}$	α-axis stator flux linkage
$\psi_{\alpha r}$	α- axis rotor flux linkage
$\psi_{\beta s}$	β -axis stator flux linkage
$\psi_{\beta r}$	β -axis rotor flux linkage
L_m	Mutual inductance (H)
L_{mr}	rotor leakage inductance (H)
L_{ms}	Stator leakage inductance (H)
R_r	Rotor resistance (Ω)
T_g	Electrical torque.
R_s	Stator resistance((Ω))

Hence from the set of equations derived, the α-β equivalent circuit is developed as represented in Figure 3.4. There is one equivalent circuit for each α-β coordinate, in which all the voltage, current and flux magnitude are with a frequency of ω_s. On the other hand, the active and reactive power of the stator and rotor side can be calculated according to the following equations.

$$P_s = \frac{3}{2}(V_{\alpha s}\, i_{\alpha s} + V_{\beta s} i_{\beta s}) \quad (3.18)$$

$$P_r = \frac{3}{2}(V_{\alpha r}\, i_{\alpha r} + V_{\beta r} i_{\beta r}) \quad (3.19)$$

$$Q_s = \frac{3}{2}(V_{\beta s}\, i_{\alpha s} - V_{\alpha s} i_{\beta s}) \quad (3.20)$$

$$Q_r = \frac{3}{2}(V_{\beta r}\, i_{\alpha r} - V_{\alpha r} i_{\beta r}) \quad (3.21)$$

Where P_s, P_r, Q_s and Q_r are active and reactive power of the stator and rotor respectively calculated from α-β axes voltage and currents. While the electromagnetic torque, created by the

DFIG, can be calculated by the following equivalent expressions, where p is the number of poles and T_g is the electrical torque[41].

$$T_{em} = \frac{3}{2} P I_m = \frac{3}{2} P(\psi_{\beta r} i_{\alpha r} - \psi_{\alpha r} i_{\beta r}) \tag{3.22}$$

$$Tem = \frac{3}{2} P \frac{L_m}{L_s} I_m\{\overrightarrow{\psi_s}\ \overrightarrow{\imath_r} *\} = \frac{2}{3} P I_m\{\overrightarrow{\psi_s^*}\overrightarrow{\imath_s}\ \}$$

$$Tem = \frac{3}{2}\frac{L_m}{L_r} p I_m\{\overrightarrow{\psi_r^*}\ \overrightarrow{\imath_s}\} = \frac{3}{2}\frac{L_m}{\sigma L_r L_S} \mathrm{PI_m}\{\overrightarrow{\psi_r^*}\ \overrightarrow{\psi_s}\} = \frac{3}{2} L_m P I_M\{\overrightarrow{\imath_s}\ \overrightarrow{\imath_r^*}\} \tag{3.23}$$

Where again $\sigma = 1 - L\,m\ 2/Ls.Lr$.

The following expression shows one of them in which the state space vector is composed of the stator and rotor fluxes.

$$\frac{d}{dt}\begin{bmatrix}\overrightarrow{\psi_S^s} \\ \overrightarrow{\psi_r^s}\end{bmatrix} = \begin{bmatrix}\frac{-R_s}{\sigma L_s} & \frac{-R_s L_m}{\sigma L_s L_r} \\ \frac{R_s}{\sigma L_s L_r} & \frac{-\mathrm{R}_r}{\sigma L_r} + j\omega_m\end{bmatrix}\begin{bmatrix}\overrightarrow{\psi_S^s} \\ \overrightarrow{\psi_r^s}\end{bmatrix} + \begin{bmatrix}\overrightarrow{V_S^s} \\ \overrightarrow{V_r^s}\end{bmatrix} \tag{3.24}$$

Therefore, by adding the mechanical motion equation that describes the rotor speed behavior.

$$T_{em} = T_{load} = J\frac{d\Omega}{dT} \tag{3.25}$$

With J, the inertia of the rotor and T_{load}, the load torque applied to the shaft.

3.3.2 dq- Model

In this section, the model differential equations of the DFIM are developed using the space vector representation in the synchronous reference frame and considering core loss. Again, the voltage equations are equivalent to the voltage equations derived from the classic model of the DFIM. The space vector model of the DFIG can be also represented in a synchronously rotating frame as shown in the figure 3.4.

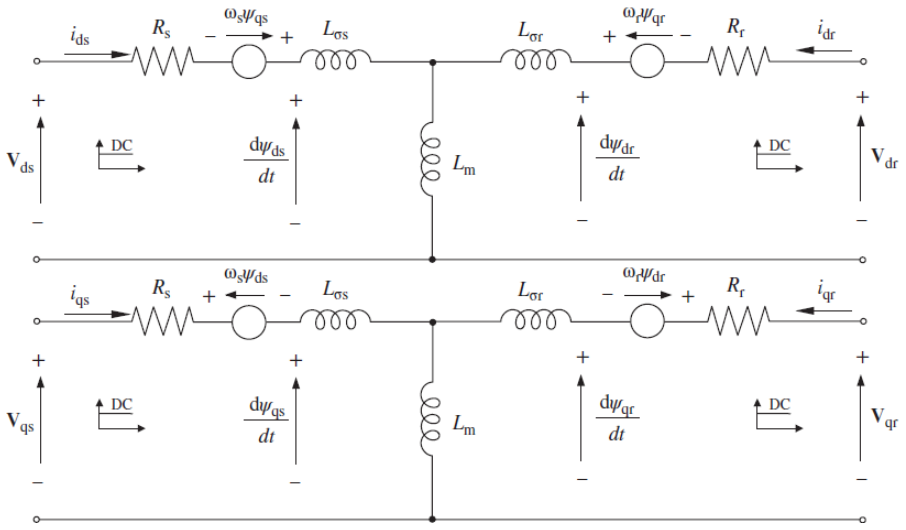

Figure 3-4 Equivalent Model of the DFIG in d-q reference frame [40]

By multiplying the voltage expressions eq. 3.1 by $e^{j\theta_s}$ and $e^{-j\theta_r}$ e-j respectively, the d-q voltage equations will be.

$$\overrightarrow{V_s^a} = R_s\,\overrightarrow{i_s^a} + j\omega_s\,\overrightarrow{\psi_s^a} \rightarrow \begin{cases} V_{ds} = R_s\,i_{ds} + \frac{d\psi_{ds}}{dt} - \omega_s\psi_{qs} \\ V_{qs} = R_s\,i_{qs} + \frac{d\psi_{qs}}{dt} + \omega_s\psi_{ds} \end{cases} \tag{3.26}$$

$$\overrightarrow{V_r^a} = R_r\,\overrightarrow{i_r^a} + j\omega_r\,\overrightarrow{\psi_r^a} \rightarrow \begin{cases} V_{dr} = R_r\,i_{dr} + \frac{d\psi_{dr}}{dt} - \omega_r\psi_{qr} \\ V_{qr} = R_r\,i_{qr} + \frac{d\psi_{qr}}{dt} + \omega_r\psi_{dr} \end{cases} \tag{3.27}$$

Similarly, the fluxes yield will be;

$$\overrightarrow{\psi_s^a} = L_s\overrightarrow{i_s^a} + L_m\overrightarrow{i_r^a} \rightarrow \begin{cases} \psi_{ds} = L_s\,i_{ds} + L_m i_{dr} \\ \psi_{qs} = L_s\,i_{qs} + L_m i_{qr} \end{cases} \tag{3.28}$$

$$\overrightarrow{\psi_r^a} = L_m\overrightarrow{i_s^a} + L_r\overrightarrow{i_r^a} \rightarrow \begin{cases} \psi_{dr} = L_s\,i_{ds} + L_r i_{dr} \\ \psi_{qr} = L_s\,i_{qs} + L_r i_{qr} \end{cases} \tag{3.29}$$

3.4. Fault Detection and Control of DFIG Based Wind Turbine System

Wind turbine have certain control systems. Horizontal axis turbine have to be oriented to face of the wind. In high winds, it is desirable to reduce the drive train loads and protect the converters, transformers and the power electronic equipment from damaging by high speed coming to turbine.

3.4.1. Maximum Power Point Tracking (MPPT) Control Methods

The MPPT with indirect speed control of a variable speed wind turbine below the rated wind speed is achieved by controlling the generator. And it consists of taking as the electromagnetic

torque reference interrelated to the maximum power curve each turbine rotational speed value and using the dynamically stable nature of the variable speed control of wind turbine. This is called the indirect speed controller.

The main objective of MPPT is to maximize wind power captured at different wind speeds by adjusting the speed of turbine and the optimal tip speed ration is λ_{opt} is maintained. The relation between the mechanical power, speed and torque of a wind turbine can be used to determine the optimal speed or torque reference to control the generator and achieve the MPPT operation in [28, 29, 42].

When the turbine is working on at maximum power point,

$$\lambda_{opt} = \frac{R\omega_t}{V_v}, \quad C_p = C_{p\text{-}max,} \text{ and } C_t = C_{t\text{-}opt} \tag{3.30}$$

Where aerodynamic torque extracted by the turbine is given by;

$$T_t = \frac{1}{2}\rho\pi R^5 \frac{C_{p,max}\omega_t^2}{\lambda_{opt}^3} \tag{3.31}$$

That is

$$T_t = \frac{1}{2}\rho\pi R^5 \frac{C_{p,max}\omega_t^2}{\lambda_{opt}^3} = K_{opt\text{-}t}\,\omega_t^2 \tag{3.32}$$

$$K_{opt-t} = \frac{1}{2}\rho\pi R^5 \frac{C_{p,max}}{\lambda_{opt}^3} \tag{3.33}$$

Where - T_t Aerodynamic torque

V_v wind speed

$C_{p\_max.}$ Maximum power coefficient

λ_{opt} Specific speed

3.4.2 Pitch Angle Control

Pitch angle control is used to determine the expected blade pitch angle based on desired angular speed and real power. The pitch angle is kept constant at zero degree, when the measured electronic output power is under its normal value. When the wind speed is below its rated speed, the pitch angle will be kept as zero value to maximize the power coefficient of the wind turbine. When the power output becomes too high, it sends a corrective signal to the blade pitch mechanism which immediately pitches the rotor blades slightly of the wind. Generally wind turbine are capable of operating with either fixed speed or variable speed. Now a days variable speed wind turbines have pitch correction mechanism. The reason for the increase in choice of variable speed wind turbines during the recent years are reduction of both the mechanical structure stresses, acoustic stress and the possibility to control active and reactive power.

Very small changes in the pitch angle can lead to a huge change on the output power. Pitch angle control is expressed as, optimization of power output, below rated speed the pitch setting should be at its optimum value to give maximum power. Prevention of input mechanical power from exceeding design limits, above rated wind speed, pitch angle control provides a very effective means of regulating aerodynamic power and loads produced by the rotor.

Maximizing fatigue loads of the turbine mechanical components one pitch controlled wind turbine, the turbine electronic controller checks the power output of the turbine several time per second. When the power output becomes too high, it sends an order to the blade pitch mechanism, which immediately pitches the rotor blades slightly out of the wind. Conversely the blades are turned back into the wind whenever the wind drops again. That's is the reason why crowbar protection is recommended to stay connected WT to the grid.

As author explained before the equation of pitch angle will be;

$$P_m = \frac{1}{2}\rho A V_w^3 C_p(\lambda\beta) \tag{3.34}$$

$$C_p(\lambda,\beta) = C_1\left(\frac{C_2}{\lambda} - C_3\beta - C_4\right)e^{\frac{C_5}{\lambda_i}} + C_6\lambda \tag{3.35}$$

$$\frac{1}{\lambda_I} = \frac{1}{\lambda+0.08\beta} - \frac{0.035}{\beta^3+1} \tag{3.36}$$

As shown in figure 3.5 performance coefficient will reach its maximum value when the pitch angle is zero and then tip ratio result from this is the nominal value.

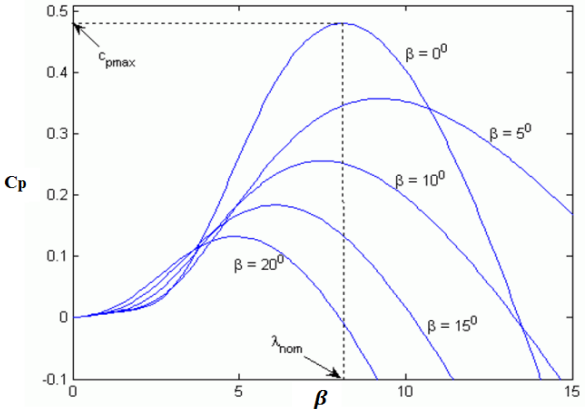

Figure 3-5 C_p as a function of pitch angle and tip speed ratio. [29]

3.4.3 Protection of DFIG Using Crowbar Resistor

The crowbar protection mechanism can provide low voltage ride through condition for the DFIG. It does not allow current to pass through, when the wind generator is operating under normal condition. The crowbar operates while the DC Link voltage is increasing, when short circuit fault

occurs at the grid, so that no current is supplied to the converter of the rotor side and that of the grid. Thus, the transient flux causing the overcurrent on the rotor decreases.

When short circuit fault occurs at the grid side, the crowbar circuit provides a current discharge path to the DFIG rotor windings and RSC. This helps in preventing damage to the devices due to overcurrent. Therefore, it is very important to select the right value for crowbar resistance. When the crowbar resistance is small, the DFIG short circuit characteristics are similar to an asynchronous induction generator with a small resistance in its rotor windings. The rotor current is too large which is unfavorable to RSC. Therefore, crowbar resistance value is basically at a high level, not less than 30 times the DFIG rotor resistance. When short circuit fault occurs, the crowbar protection is activated. It obstructs the trigger pulses of the RSC, which has not been disconnected from the system. If the crowbar resistance is too large, then the voltage on the crowbar resistance may be higher than the DC bus voltage.

In case of sever grid fault short circuit current rise at the stator parts and it will transfer to the rotor side, consequently converters will be damaged. Now a days DFIG have a number of protection system, one of them is crowbar protection and it helps to dissipate high current without disconnecting turbine from the national grid that is called LVRT capability. In crowbar protection two parameter are wisely chosen to protect from damaging the rotor converters, when large number of currents are produced. Those are resistance R_{crow} and its activation time.

When choosing concerning the crowbar resistance.

a) If low value of resistance was chosen high short circuit current will be faced. Then crowbar switch will be oversized and the value of electromagnetic torque will high.
b) By using higher resistance rotor current could be minimized. But if the value of resistance is high, crowbar will not have enough power to push rotor voltage. During this time the produced rotor current rotate across the converters through fly wheeling diodes.

To protect the rotor converters voltage must be satisfied the following conditions.

$$V_r < \frac{V_{bus}}{\sqrt{3}} u \tag{3.37}$$

Where V_r rotor peak voltage

V_{bus} voltage of DC link and

U Turn ratio.

The crowbar circuit diagram consist of diode for rectifier the rotor current and thyristor connected in series with crowbar resistance R_{crow} shown in figure 3.6 . Crowbar does not work as a chopper and the thyristor is turned on, when the value of DC voltage V_{dc} maximum in value.

$$V_{dc} \geq V_{dc\,max.} \tag{3.38}$$

At the same time circuit of the rotor will separated from the side of the rotor converter and it connected to the crowbar. And it remains connected to the crowbar still circuit breaker isolate from the system.

During the crowbar protection the constant time of damping DC component at the stator and rotor can express as [43].

$$\tau_s = \frac{L_s L_r - L_m^2}{R_s L_r} \tag{3.39}$$

$$\tau_r = \frac{L_s L'_r - L_m^2}{R'_{rc} L_s} \tag{3.40}$$

Where τ_s DC components in stator

τ_r DC components in rotor

L_s Stator inductance

L_r rotor inductance

L_m magnetizing inductance

R_s stator resistance per phase

If the crowbar is turn off the damping time constant of DC component of stator will be higher than because of the open circuit of rotor. The time constant of τ_{so} can be express as flows.

$$\tau_{so} = \frac{L_s}{R_r} \tag{3.41}$$

The simulation of crowbar indicates that in smaller R_{crow} rotor voltage was low but high electromagnetic torque and over current induces. For high value of R_{crow} lower electromagnetic torque, low current and higher rotor over voltage will produce.

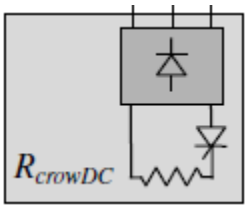

Figure 3-6 block diagram of crowbar protection [40]

The value of resistor can be calculating using the following equations [44, 45];

$$R_{crow} = \frac{U_{dco}}{\sqrt{6} I_{rmax}} = \frac{U_{dco}}{\sqrt{6} h I_{rn}} \tag{3.42}$$

Where h is acceptable multiple rotor normal current.

During voltage dip stator flux couldn't directly be there at the stator voltage variations, and large fault current will be generated the stator and short circuit will be present at DFIG. Let the voltage dip is zero at t=0, the following relationship is happens [45, 46].

$$\psi_s(t) = \frac{U_s(t_0)}{j\omega_s} e^{-t/T_s} + \frac{U_s(t_0)}{j\omega_s} e^{-j\omega_s t} \tag{3.43}$$

$$\psi_r(t) = \psi_{rdco} e^{-j\omega_r t} * e^{-\frac{t}{T_r}} + \psi_{rf0} * e^{i\omega_s t} \tag{3.44}$$

Where ω_r rotor angular frequency

ω_s Base angular frequency

ψ_{rf0} forced rotor flux component

ψ_{rdc0} DC component of the rotor flux at the occurring instant of the dip.

The equivalent circuit diagram of DFIG with the crowbar protection including rotor resistance R_r and crowbar resistance R_{crow} are shown below [44].

According to IEEE the maximum value of crowbar resistance is limited at 70 times of the rotor resistance to protect the rotor side converters from high rotor current and it avoids the flow of high current through rotor side converters and dc link capacitor. Four different value of crowbar resistance are affected to the DFIG during fault conditions (10 to 40 times rotor resistance) [39].

The different value of crowbar resistor are calculated as follows.

$$R_{crw} = 10 * R_r = 10 * 0.011074 = 0.11074\ \Omega$$
$$R_{crw} = 20 * R_r = 20 * 0.011074 = 0.22148\ \Omega$$
$$R_{crw} = 30 * R_r = 30 * 0.011074 = 0.33222\ \Omega$$
$$R_{crw} = 40 * R_r = 40 * 0.011074 = 0.44296\ \Omega$$
$$R_{crw} = 70 * R_r = 70 * 0.011074 = 0.77518\ \Omega$$

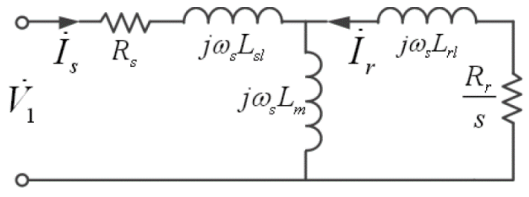

Figure 3-7 Positive sequence equivalent circuit of DFIG with crowbar [43].

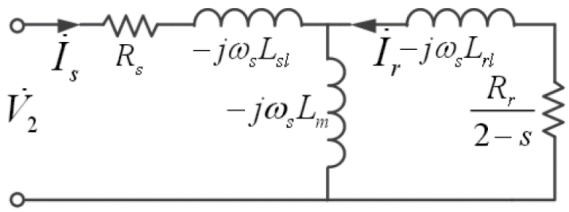

Figure 3-8 Negative sequence equivalent circuit of DFIG with crowbar [44].

By taking equation (3.47 and (3.48) value of stator and rotor fault current will be shown below [44, 46].

$$I_S = \frac{-\omega_s L_r + j\frac{R_r}{S}}{-\omega_s L_s \frac{R_r}{S} + j\omega_s^2 (L_m^2 - L_s L_r)} V_1 e^{-j\omega_s t} + \frac{\omega_s L_r + j\frac{R_r}{2-S}}{\omega_s L_s \frac{R_r}{2-S} + j\omega_s^2 (L_m^2 - L_s L_r)} V_1 e^{-\omega_s t} +$$

$$\frac{-\omega_s L_r + j\frac{R_r L_S (L_m - L_r)}{(S-1)(L_m^2 - L_S L_r)}}{-\omega_s L_s \frac{R_r}{S-1} + j\omega_s^2 (L_m^2 - L_s L_r)} \left[V_s - (V_1 - V_2) e^{\frac{-t}{\tau_s}} + L_m A e^{\frac{t}{\tau_s}} e^{i\omega_s t} \right] \quad (3.45)$$

$$I_r = \frac{\omega_s L_m}{-\omega_s L_s \frac{R_r}{s} + j\omega_s^2 (L_m^2 - L_s L_r)} V_1 e^{i\omega_s t} + \frac{-\omega_s L_m}{\omega_s L_s \frac{R_r}{2-s} + j\omega_s^2 (L_m^2 - L_s L_r)} V_2 e^{-i\omega_s t} + \frac{\omega_s L_{m+j\frac{R_r L_S (L_m - L_S)}{(S-1)(L_m^2 - L_S L_r)}}}{-\omega_s L_s \frac{R_r}{S-1} + j\omega_s^2 (L_m^2 - L_s L_r)} [V_s -$$

$$(V_1 - V_2) e^{\frac{t}{\tau_s}} - L_s A e^{\frac{t}{\tau_s}} e^{i\omega_r t}] \quad (3.46)$$

The rectified crowbar current (I_{crow}) from the figure of DFIG rotor current can be calculated as flows.

$$I_{crow} = \frac{(|I_{ra}| - I_{ra} + |I_{rb}| - I_{rb} + |I_{rc}| - I_{rc})}{2} \quad (3.47)$$

And the dc voltage over the crowbar will be calculated as flows.

$$V_{crow} = R_{crow} I_{crow} - V_{CB\_semic} \quad (3.48)$$

Where V_{CB_semic} is voltage drop across the thyristor

In the above scheme of the crowbar used thyristors used as a switches. Once the crowbar is activated thyristor remain until the circuit breaker of the generator stops the short circuit current. To deliver the LVRT capability crowbar short circuit as to be removed without separating the turbine from the grid.

3.4.3.1 Control Strategy of Crowbar Protection Based DFIG

To protect the rotor side converter from tripping due to over currents in the rotor circuit or overvoltage in the DC link during grid voltage dips a crowbar is installed in DFIG wind turbines which is connected to the rotor windings of the DFIG. When the crowbar is activated the rotor side converters pulses are disabled and the machine behaves like a squirrel cage induction machine directly coupled to the grid. The magnetization of the machine that was provided by the

RSC in nominal condition is lost and the machine absorbs a large amount of reactive power from the stator and thus from the network, which can further reduce the voltage level and is not allowed. Triggering of the crowbar circuit also means high stress to the mechanical components of the system as the shaft and the gear.

Thus, from network and from machine mechanical point of view a crowbar triggering should be avoided. Anyway, to compare the presented technique here with a conventional DFIG wind turbine system protected by a crowbar circuit, simulation results including crowbar protection are examined. Therefore the crowbar resistance is designed. The value of the crowbar resistance should be chosen carefully. There are two requirements that give an upper and a lower limit to the crowbar resistance. It should be high enough to limit the short circuit rotor current and it should be low enough to avoid too high voltage in the rotor circuit. If the voltage across the crowbar terminals rises above the DC-link voltage of the RSC high currents will flow through the antiparallel diodes of the converter. There are approaches limiting the operation time of the crowbar to return to normal DFIG operation with active and reactive power control as soon as possible. When the absolute value of the rotor current reaches a maximum threshold value the crowbar is fired and the RSC is blocked. When the rotor transients have died out and the absolute value of the rotor current is below a minimal threshold value the crowbar is switched off and the RSCs control is restarted. A reset of the integral values of the RSCs current and power control before restart is necessary to avoid over currents.

The crowbar protection that uses IGBT switches to short the rotor. This enhances considerably the operation of the device, with a faster elimination of the rotor transients usually within 100 ms and therefore faster regain of control. After deactivation of the crowbar, full controllability over the wind turbine behavior is resumed as it shows in figure 4.2. The conventional crowbar control realizes the LVRT protection by blocking the rotor side converter circuit and introducing additional rotor winding resistances that actually dissipate the produced energy. In contrast, the proposed control strategy can transform the additional output power into the WT kinetic energy by temporarily increasing the generator rotor speed during the grid faults, thus effectively limiting the oscillations in the currents.

During rotor crowbar activation, the generator rotor windings are short circuited through the crowbar circuit, and the rotor currents are limited accordingly to the crowbar resistor dimensioning.

3.4.4. Vector Control of DFIG Using AC/DC/AC Converter

Vector control is one of the best methods used in doubly fed induction generator based on wind turbine. In this method active and reactive power of the stator will be controlled through the rotor current of vector control.

3.4.4.1 Vector Control of Rotor Side Converter (RSC)

The main objective of rotor side converter is to control active and reactive power separately. Active and reactive power are not directly controlled but by controlling of rotor current is possible to control. And it operates in stator flux d-q reference frame. Rotor side converter structure have inner and outer loop, which is the inner loop regulates direct rotor current is proportional to the stator reactive power, and he quadrature rotor current related to torque or stator power.

From the model of DFIG by substitute equation (3.14) and equation (3.15) into (3.13) can be found equation (3.53) of rotor voltage as a function of stator flux and rotor current (ψ_{qs}= 0) as shown in figure 3.9.

$$V_{dr} = R_r i_{dr} + \sigma L_r \frac{d}{dt} i_{dr} - \omega_r \sigma L_r i_{qr} + \frac{L_m}{L_s} \frac{d}{dt} |\overrightarrow{\psi_s}|$$

$$V_{qr} = R_r i_{qr} + \sigma L_r \frac{d}{dt} i_{qr} - \omega_r \sigma L_r i_{dr} + \omega_r \frac{L_m}{L_s} |\overrightarrow{\psi_s}| \quad (3.49)$$

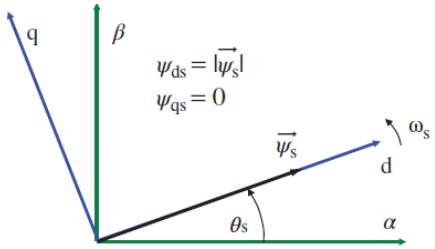

Figure 3-9 Synchronous rotating dq reference frame aligned with the stator flux space vector [28]

From equation 3.3 let the voltage drop in stator resistance is low stator flux is constant, because it is directly connected to the grid therefore, $d|\psi_s|/dt = 0$. For the reference frame transformation the angle θ_r must be estimated. The controller must be achieved in dq coordinates, but rotor voltage and current must be transformed into DQ coordinates. First obtain the angle of stator voltage space vector and subtract 90^0 from estimated angle θ_s will get.

Based on the figure 3.10 the control scheme current loop works with the rotor current refers to stator side, even though the conversion to rotor referred quantity is performed at the

measurement stage for the current and before the creation of the pulse for the converts for the voltage.

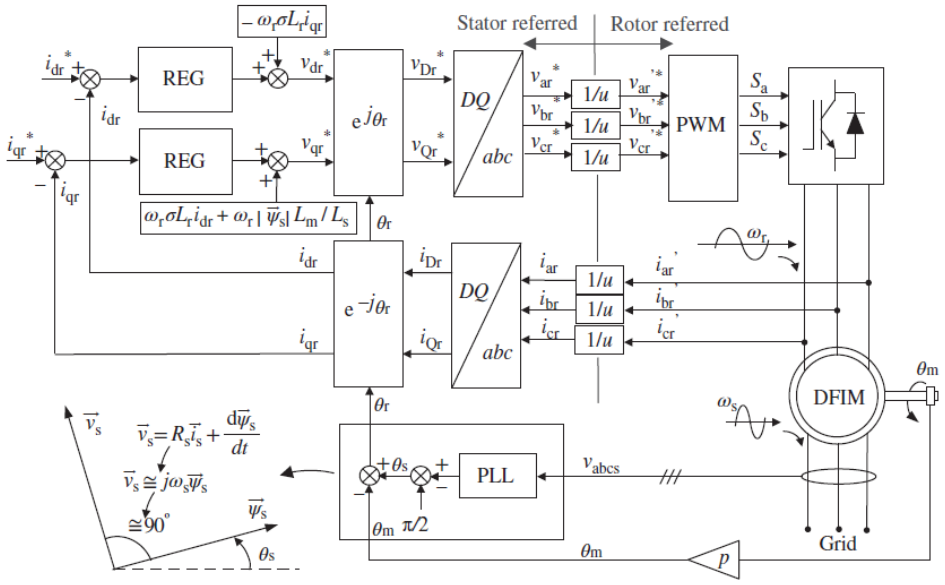

Figure 3-10 current control loops of DFIG [28].

The simplified stator flux torque and space vector expression in dq frame as follows.

$$T_{em} = \frac{3}{2} p \frac{L_m}{L_s} \left(\psi_{qs} i_{dr} - \psi_{ds} i_{qr}\right) \rightarrow T_{em} = -\frac{3}{2} p \frac{L_m}{L_s} \left|\overrightarrow{\psi_s}\right| i_{qr} \rightarrow T_{em} = K_T i_{qr} \qquad (3.50)$$

From this the q rotor current component is proportional to the torque that is with i_{qr} it is possible to control the torque and consequently speed of the machine. By developing the stator reactive power expression in dq frame, the compact expression, which reveals that i_{dr} is responsible of Q_s.

$$Q_s = \frac{3}{2}\left(V_{qs} i_{ds} - V_{ds} i_{qs}\right) \rightarrow Q_s = -\frac{3}{2} \omega_s \frac{L_m}{L_s} \left|\vec{\psi}_s\right| \left(i_{dr} - \frac{\left|\overrightarrow{\psi_s}\right|}{L_m}\right) \rightarrow Q_s = K_Q \left(i_{dr} - \frac{\left|\overrightarrow{\psi_s}\right|}{L_m}\right) \qquad (3.51)$$

The complete vector control of DFIG will show in figure 3.14, and the stator is directly connected to the grid at constant stator flux amplitude provides by the grid voltage $\left|\overrightarrow{\psi_s}\right| \cong \left|\overrightarrow{V_s}\right| / \omega_s$ stator flux will be.

$$\left|\overrightarrow{\psi_s}\right| = \psi_{ds} = L_s i_{ds} + L_m i_{dr} \qquad \psi_{qs} = 0 = L_s i_{qs} + L_m i_{qr} \qquad (3.52)$$

3.4.4.2 Vector Control of Grid Side Converter (GSC)

Grid side converter consist of GSC, grid filter, grid voltage and its main objective is to maintain the capacitor voltage of DC link based on the direction and magnitude of rotor power with unity power factor reactive power is zero. GSC permits bidirectional power flow to exchange active power to the grid as well as from the grid and reactive power is transformed from DFIG to the grid through stator. GSC is modeled with directional ideal switches and the property of rectifier

(AC to DC) and as inverters (DC to AC). By controlling the semiconductor ideal switch will be created with ideal diode in antiparallel to permit the flow of current both directions.

During sudden voltage dip occur the stator flux of DFIG cannot involve to its final steady state as stator voltage and its expression will be.

$$\frac{d\overrightarrow{\psi_s^s}}{dt} = \overrightarrow{V_s^s} - \frac{R_s}{L_s}\overrightarrow{\psi_s^s} + R_s\frac{L_m}{L_s}\overrightarrow{\imath_r^s} \tag{3.53}$$

The stator flux of each phase is the sum of a sinusoidal and exponential with constant time of L_s/R_s. Based on the figure 22 (a) the equivalent of the DFIG voltage dip analysis will be.

$$\overrightarrow{V_r^r} = \frac{L_m}{L_s}\left(\overrightarrow{V_s^r} - j\omega_s\overrightarrow{\psi_s^r}\right) + \left[R_r + \left(\frac{L_m}{L_s}\right)^2 R_s\right]\overrightarrow{\imath_r^r} + \sigma L_r\frac{d}{dt}\overrightarrow{\imath_r^r} \tag{3.54}$$

Rotor current is recognized as a function of stator and rotor functions. The space vector diagram is shows in figure 3.11(b). $\overrightarrow{V_s^r}$ is the sum of dominant $\overrightarrow{V_r^r}$ and $j\omega_s\overrightarrow{\psi_s^r}$. The unexpected change in stator voltage should be conveyed by unexpected rotor voltage to protect high increase in the rotor current. The stator flux slowly decreases as shows in figure 3.12 the required voltage is higher than the steady state caused by dip voltage.

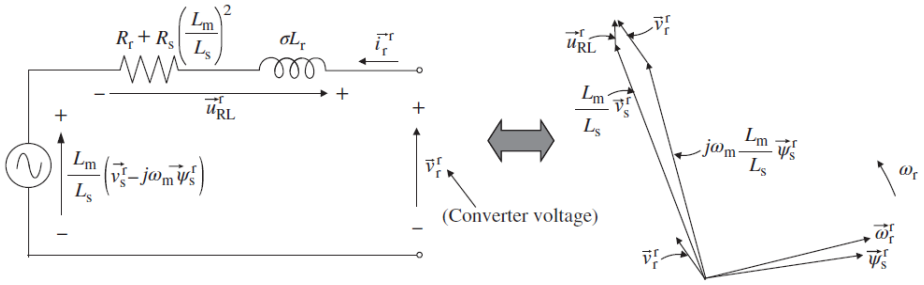

Figure 3-11 (a) Equivalent of DFIG for analysis of dip voltage and (b) space vector diagram at sub synchronism in a generator mode [28].

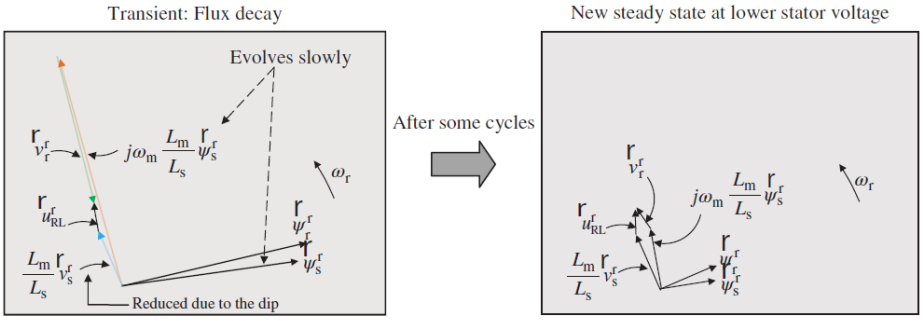

Figure 3-12 Evolution of the space vector magnitudes from the first instant when the stator voltage is reduced until the steady state reached at the dip [28].

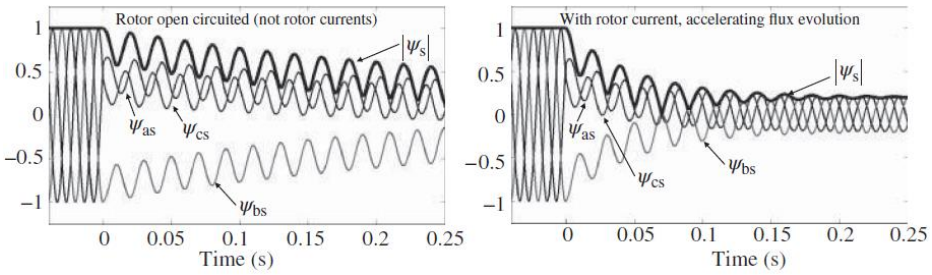

Figure 3-13 Stator flux growth in p.u during 80% voltage dip [28].

When the stator voltage dip is 100% it is the worst situations at this time rotor voltage is replaced by stator voltage that has been disappeared. Due to the voltage drawback wind turbine based on DFIG proposed additional crowbar protections is used to solve dip voltage. As mentioned earlier to protect from over current produced by loss of control crowbar protection will be activated.

The block diagram of DFIG with its crowbar protection is depicted is shows below.

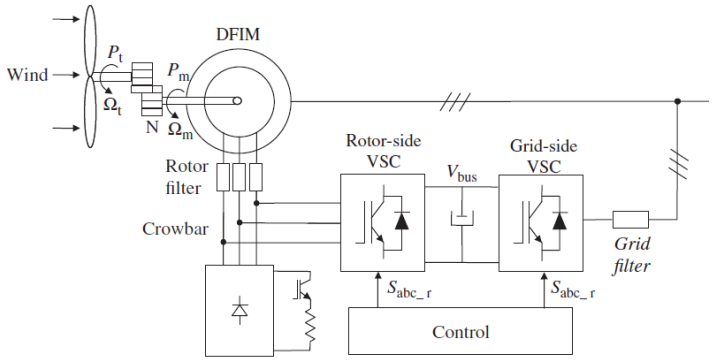

Figure 3-14 (a) System equipped with three phase DC crowbar protection [28].

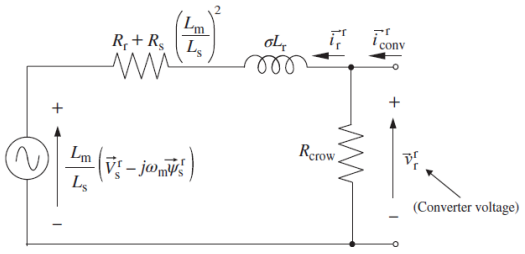

Figure 3-15 (b) one phase equivalent circuit of the system when the crowbar is activated [28].

3.5. Phase Locked LOOP (PLL)

Phase locked loop (PLL) is used to estimate the angle of the grid voltage θ_g, in a closed loop way. PLL strive for synchronization to a sinusoidally varying three phase variable on the grid voltage. By using the dq coordinates of the voltage with which it is required to be synchronized 'd' component of the grid voltage (V_{dg}) must be aligned with the 'd' rotating reference frame.

The estimated θ_g must be modified till voltage (V_{qg}) is zero. At that time the rotating reference frame dq and the grid voltage space vector are synchronized and aligned to the axis. In figure 3.16 shows the closed loop PLL structure takes ABC voltage inputs and transform into dq by using its own angle.

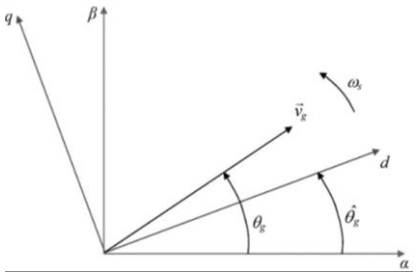

Figure 3-16 Grid voltage angle estimation with PLL [28].

PLL must be running continuously with the control strategy, since the angle doesn't have constant magnitude but modified according to the angular speed of the grid voltage.

Frequency and Amplitude Control using PLL

Frequency of the stator voltage results from the sum of the frequency related to the mechanical speed and rotor current frequency. Amplitude of the stator voltage for a given speed and load is proportional to the rotor current amplitude and frequency. However, for the rotor current frequency equal to the slip frequency, the only way to obtain a reference amplitude of the generated voltage is to maintain adequate rotor current amplitude. Control of the grid side converter is similar to the case of a grid connected system, as a superior control loop for this converter is used for stabilization of the DC-link voltage. A phase-locked loop (PLL) which synchronizes on the positive sequence component of the 3-phase primary voltage V_1. The output of the PLL (angle $\Theta=\omega_t$) is used to compute the direct axis and quadrature -axis components of the AC 3-phase voltage and currents (labeled as v_d, v_q or i_d, i_q). Measurement systems are measuring the d and q components of AC positive-sequence voltage and currents to be controlled as well as the DC voltage Vdc.

3.6. Analysis of DFIG Based Of Adama-II Wind Farm Turbine and Power Converter

It is possible to calculate all the electrical components of wind turbine and associated converters. The parameters related to ω_s (frequency of stator voltage and currents), ω_r (frequency of rotor voltage and current) and ω_m (rotor electrical speed) is shows in [28].

$$\omega_s = \omega_r + \omega_m \tag{3.55}$$

And the relationship between mechanical speed of the shaft $\omega_{mech.}$ and electrical speed ω_{elec} depend on the pole pair of the machine.

$$\omega_{mech} = p\omega_{elec} \text{ [Rad/sec]} \tag{3.56}$$

The slip of the machine is defined as follows and it can reduce simplified form using equation 3.57.

$$S = \frac{\omega_s - \omega_m}{\omega_s} = \frac{\omega_r}{\omega_s} \tag{3.57}$$

Stator winding is directly connected to the grid and the synchronous frequency (ω_s) is Constant (1500 rpm). But frequency of rotor voltage and current (ω_r) depends on the shaft electrical speed (ω_m), which leads to three operating mode of the machine depends on the speed is shown below [15].

$\omega_m < \omega_s \rightarrow \omega_r > 0 \rightarrow S > 0 \rightarrow$ Sub synchronous operation

$\omega_m > \omega_s \rightarrow \omega_r < 0 \rightarrow S < 0 \rightarrow$ Super synchronous operation

$\omega_m = \omega_s \rightarrow \omega_r = 0 \rightarrow S = 0 \rightarrow$ Synchronous operation

If the machine operates in sub synchronous mode then the rotor will absorb power from the network through the converters, but if the machine works in super synchronous power will be delivered from the wind turbine to the grid through the converters.

3.6.1 Reasons for Choosing Crowbar Protection

Capacitors are usually connected to fixed speed wind turbines to enhance the system voltage because they are a sink of reactive power. Mechanically switched fixed shunt capacitors can enhance the systems voltage stability limit. Also, voltage regulated by the wind generators equipped with only fixed capacitors can become higher than the voltage limit. Hence, a fixed capacitor cannot serve as the only source of reactive power compensation. The maximum compensating current of the SVC decreases linearly with the ac system voltage and the maximum var output decreases with the square of the voltage. When the continuity of the control SVC is discontinuous and slow response time. So these are not fulfil the low voltage ride through capability of the wind turbine, if disturbance occurs at the grid side wind turbine will definitely disconnect from the national grid this one of the disadvantage. But crowbar protection is used to maintaining continuous active and reactive power control during the grid fault also used for enhancement of LVRT capability of DFIG. To protect the rotor side converter from tripping due

to over currents in the rotor circuit or overvoltage in the DC link during grid voltage dips a crowbar is installed in conventional DFIG wind turbines connected to the rotor windings of the DFIG.

3.6.2 Super and Sub Synchronous Operation of DFIG

From the above expression sub synchronous mode generator operates below the synchronous ω_s speed and the slip is positive. In super synchronous mode generator operates above the synchronous speed ω_s and its slip is negative in value (as induction generator) [47].

In figure 3.17 is an example of slip versus mechanical power of DFIG wind turbine. DFIG is in generating mode, when the mechanical power is negative in value. To harvest maximum power from the wind turbine maximum power point is used it illustrated in figure 3.16. Rotor speed of the generator is within the range of $0.5\omega_s$ to$1.2\ \omega_s$ as shows in the figure 3.17 with corresponding to arround 58% full speed range. Wind energy have sufficient speed range since the power generated at 42% of the rated speed one 0.072% p.u (0.42) only 7.4% of rated power. DFIG operates until 0.0 p.u or 30% above the synchronous speed.

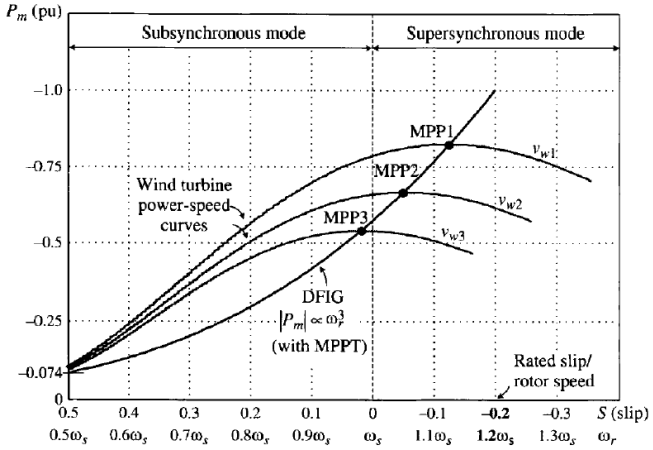

Figure 3-17 Power speed characteristics in a DFIG wind energy system with MPPT control [26].

Depend on the sign of the slip rotor circuit can receive or deliver power from or to the grid. In case of negative slip mechanical power (P_m) will be delivered to the grid through stator and rotor circuits. The rotor power (P_r) is transmitted to the main grid through power electronics converters, whereas stator power (P_s) is directly connected to the grid. Ignoring losses in generator and converters power delivered to the grid (P_g) is mechanical power (P_m) shows at figure 3.17 (a).

In case of positive slip shows in figure 3.18(b) rotor receives power from the grid. Both P_m and P_r are delivered to the grid through the stator. During sub synchronous mechanical power is lower than supper synchronous and stator power is the sum of P_m and P_r.

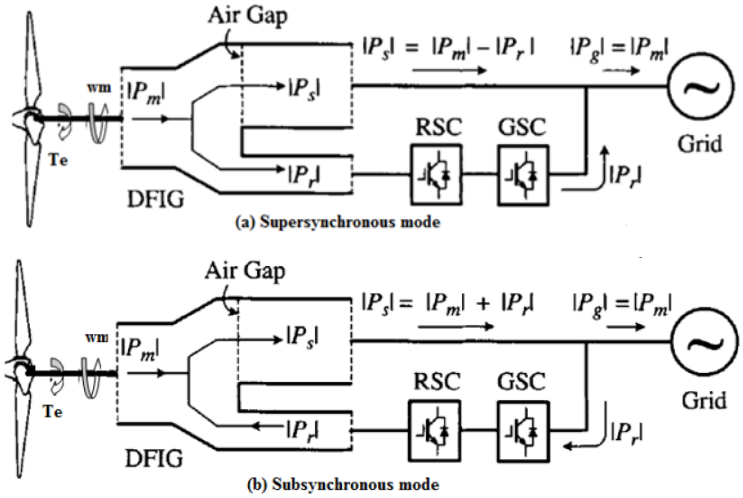

Figure 3-18 Power flow in DFIG wind energy conversion system [47]

3.6.3. Analysis of Steady State Equivalent Circuit of DFIG with RSC

Under the operation of unity power factor of rotor side converter the derivation of steady state analysis of equivalent impedance of rotor side converter based on the DFIG will be performed depicted in figure 3.19.

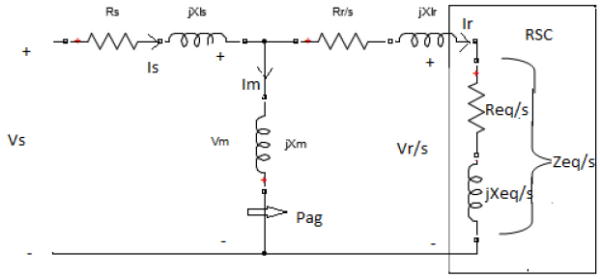

Figure 3-19 equivalent circuit of steady state DFIG with RSC [47].

RSC impedance equivalent is defined by

$$\overline{Z_{eq/S}} = \mathrm{R}_{eq/S} + jX_{eq}/s = R_{eq} + j\omega_{sl}L_{eq} \qquad (3.58)$$

ω_{sl} is the angular slip frequency

L_{eq} equivalent inductance of the RSC

In actual rotor winding frequency of rotor current flowing into the converter is ω_{sl} not ω_s and to find the impedance equivalent impedance refers to stator side as in equation 3.62 will be devide by slip.

$$\frac{\overline{Z_{eq}}}{S} = \frac{R_{eq}+jX_{eq}}{S} = \frac{R_{eq}+j\omega_{sl}L_{eq}}{S} = \frac{R_{eq}}{S} + j\omega_s L_{eq} \tag{3.59}$$

Where $\omega_{sl} = S.\omega_s$ and the air gap power of generator can be calculated by;

$$P_{ag} = 3(V_s - I_s R_s)I_s \tag{3.60}$$

Also from the induction machine air gap can also calculated by;

$$P_{ag} = \frac{\omega_s T_m}{p} \tag{3.61}$$

Where T_m the mechanical torque

P the number of pole pair of generator, substitute equation (3.65) into (3.64) it will

$$Pag = 3(V_s - I_S R_s)I_s = \frac{T_m \omega_s}{p} \tag{3.62}$$

By rearaging equation (3.2) equation (3.63)will get.

$$R_s I_s^2 - V_s I_s + \frac{T_m \omega_s}{3p} \tag{3.63}$$

Express equation (3.63)in the form of I_s

$$I_s = \frac{V_{s\pm}\sqrt{V_s^2 - \frac{4R_s T_m \omega_s}{3p}}}{2R_s} \tag{3.64}$$

To find rotor current and voltage author used figure (27), voltage across the branch will be.

$$\overline{V_m} = \overline{V_s} - \overline{I_s}(R_s + j\omega_s L_{ls}) \tag{3.65}$$

Stator voltage and current are;

$$\overline{V_s} = V_s < 0^0 \text{ and}$$

$$I_s = i_s < 180^0 \tag{3.66}$$

DFIG in the generating mode of unity power factor the stator and current are 180^0 out of phase. Magnetizing current, rotor current and rotor voltage can be calculated as flows;

$$\overline{I_m} = \frac{\overline{V_m}}{j\omega_s L_m} \tag{3.67}$$

$$\overline{I_r} = \overline{I_s} - \overline{I_m} \tag{3.68}$$

$$\frac{\overline{V_r}}{S} = \overline{V_m} - \overline{I_r}(\frac{R_r}{S} + j\omega L_{lr}) \tag{3.69}$$

By Rearange equation (3.72) can found as;

$$\overline{V}_r = S\overline{V_m} - \overline{I_r}(R_r + jS\omega L_{lr}) \tag{3.70}$$

Rotor current and voltage related to the equivalent to resistance and reactance (X_{eq},) by;

$$\frac{\overline{V_s}/_S}{I_r} = \frac{R_{eq.}}{S} + {jX_{eq}}/_S \tag{3.71}$$

From equation (3.71)

$$R_{eq} + jX_{eq} = \frac{\overline{V}_r}{I_r} \tag{3.72}$$

3.7. Analysis of Adama-II Wind Farm Turbine

Wind farm is the collection of individual wind turbines those are separated from each other. So its modeling is necessary. Adama-II wind farm has DFIGs with the capacity of 153 MW, 690 V, 50Hz; 1800 rpm with 102 turbines with nominal output power of 1.5 MW of each turbines. The parameters of generator are listed at Appendix A-1.

Adama-II wind power farm turbine generator specifications

- Type — three blade up wind
- Blade length — 37 meter
- Rated power — 1.5 MW
- Startup wind speed — 3.5 m/s
- Rated wind speed — 12 m/s
- Cut off wind speed — 25m/s
- Generator — DFIG
- Rated output voltage — 690 V
- Turbine rotor speed range — 9.5-21 m/s
- Rotor diameter — 77 m

Adama-II wind farm also has control model parameter in revolution per minute (rpm) with cut in speed is 1000 rpm, limit speed is 1800 rpm and shutdown speed is 2000 rpm. Adama wind farm-II is divided into 8 clusters, one cluster has 11 turbines and the rest seven clusters have 13 turbines. Adama-II wind farm equivalent impedance of RSC will be explained below.

Adama-II wind farm equivalent power is;

$$P_{eq} = 1.5 * 102 = 153\ MW$$

From equation (3.68) stator current will be calculated by;

$$I_s = V_s \pm \frac{\sqrt{v_s^2 - \frac{4R_s T_m \omega_s}{3p}}}{2R_s}$$

The express in the form of torque(T_m)

$$T_m = \frac{3P(V_s^2 - (2R_s I_s - V_s)^2)}{4R_s \omega_s} \quad (3.73)$$

Depend on the manufactures manual rated stator current is 1110 A during negative sign it works as generating mode and pair pole is 2.

$$T_m = \frac{3P(V_s^2 - (2R_s I_s - V_s)^2)}{4R_s \omega_s} = \frac{6\left(\frac{690^2}{\sqrt{3^2}} - \left(2 * 0.006243 * 1110 - \frac{690}{\sqrt{3}}\right)^2\right)}{4 * 0.006243 * 2 * 50 * \pi} = 8.3KNm$$

From the manufacturer report the stator side current under constant frequency test is 1053 A. it is almost equals to with rated current 1110 A, and it has negative sign during generating mode. Which is 5% variation due to the losses and from equation (3.69) the magnetizing voltage branch is calculated by;

$$\overline{V_m} = \overline{V_s} - \overline{I_s}(R_s + j\omega_s L_{ls}) = \frac{690}{\sqrt{3}} r - 1110 < 180^0 [0.006243 + (j100\pi * 0.000198822)]$$

$$= 398.37 + 6.93 + j69.33 = 405.2997 + j69.33 = 411.18669 < 9.707^0$$

Magnetizing current will calculated using equation (3.71).

$$I_m = \frac{411.18669 < 9.707^0}{(100\pi * 0.003976) < 90^0} = 328.95 < -80.893^0 A = 52.06578 - j324.8\ A$$

Rotor current

$$I_r = I_s - I_m = -1110 - [52.06578 - j324.8] = -1162.0658 + j324.8 = 1206.6 < -15.6^0$$

Rotor voltage

$$\overline{V_r} = s\overline{V}_m - \overline{I}_r(R_r + j\omega_s L_{lr}) = -0.2[405.2997 + j69.33] - [(-1162.0658 + j324.8)] *$$

$$(0.011074 - j0.2 * 100\pi * 0.000198811)] = -80.06 - j13.86 - [-12.91 + j14.56 +$$

$$j3.594 + 4.054] = -72.248 - j31.991 = 79.014 < 23.88^0$$

Where S=$\frac{\omega_s - \omega_r}{\omega_s} \cong -0.2$

Or using $|V_r| \approx |SV_s| = \overline{V_s} - \overline{I_s}(R_s + j\omega_s L_{ls})V_r = \frac{0.2 * 690}{\sqrt{3}} = 79.67\ V$

RSC equivalent impedance rated speed is given by

$$\overline{Z}_{eq} = \frac{\overline{V}_r}{\overline{I}_r} = \frac{79.014 < 23.88^0}{1209.6 < -15.6^0} = 0.0653 < 39.48^0$$

And the equivalent resistance and reactance are;

$$R_{eq} + jX_{eq} = \frac{\overline{V}_r}{\overline{I}_r} = 0.0504 + j0.0415$$

$$R_{eq} = 0.0504\Omega$$

$$X_{eq} = 0.0415\Omega$$

To find the mechanical power at 1800 rpm using the rotor current of 1206.6 A is as flows.

$$P_m = 3{I_r}^2\left(R_r + R_{eq}\right)\frac{1-S}{S}$$

$$P_m = 3 * 1206.6^2(0.01107 + 0.0504) * \frac{1 + 0.2}{-0.2} \cong -1610.9\ KW$$

Rotor power will be calculated as flows.

$$P_r = 3{I_r}^2 R_{eq} = 3 * 1206.6^2 * 0.0504 = 220.13\ KW$$

Stator and rotor winding power loss will be.

$$P_{cu,s} = 3{I_s}^2 R_s = 3 * 1110^2 * 0.006243 = 23.1\ KW$$

$$P_{cu,r} = 3{I_r}^2 \mathrm{R}_r = 3 * 1206.6^2 * 0.011074 = 48.337\ KW$$

The value of stator active power will be;

$$P_s = 3V_s I_s\, cos(\varphi_s) = 3 * \frac{690}{\sqrt{3}} * 1110 * cos(180^0) = -1326.6\ KW$$

The negative sign indicates that the machine oprates in generating mode (slip is less than zero).

The value of total power delivered to the grid will be calculated as below.

$$\left|P_g\right| = |P_s| + |P_r| = 1326.6 + 220.13 = 1546.73\ KW$$

The total power loss at the stator and rotor winding is;

$$P_{loss} = P_{cu,s} + P_{cu,r} = 23.1 + 48.337 = 71.44\ KW$$

Value of efficiency under 1800 rpm is

$$\eta = \frac{P_g}{P_m} = \frac{1546.73}{1610.9} * 100 = 96.01\%$$

3.7.1. Converter Equivalent Impedance at 2000 RPM (Slip is Less than Zero)

When the generator operates at its maximum speed of 2000 rpm, 690V, 50Hz and 1.5 MW, the variables I_s, T_m, V_m, I_m, I_r, V_r, equivalent resistance and inductance will be calculated as flows;

$$I_s = \frac{V_s \pm \sqrt{V_s^2 - \frac{4R_s T_m \omega_s}{3p}}}{2R_s} = -1365.03A$$

$$T_m = -(2000/1800)^2 * 8.3 = -10.247KNm$$

Magnetizing voltage (V_m) is;

$$V_m = V_s - I_s(R_{s+} j\omega_s L_{ls}) = \frac{690}{\sqrt{3}} - (-1365.03)[0.006243 + j100\pi * 0.000198822]$$
$$= 398.23 < 12.33^0$$

The magnetizing current is calculated by (I_m) :

$$\overline{I}_m = \frac{\overline{V_m}}{j\omega_s L_m} = \frac{398.23 < 12.33^0}{(100\pi * 0.00397) < 90^0} = 320 < -77.67^0$$

The rotor current will be calculated as the following equations;

$$I_r = I_s - I_m = -1365.03 - [68.33 - j312.62] = -1433.36 + j325.62$$

And the value of rotor voltage is;

$$V_r = -0.333[398.23 < 12.33^0]$$
$$- [(-1433.36 + j325.62) * (0.011074 - j0.333 * 100\pi * 0.00019822)]$$
$$= 135.94 < 27.65^0$$

Where $S = \frac{\omega_s - \omega_r}{\omega_s} = -0.333$

The value of equivalent reactance and resistance for the rotor side converter is

$$\overline{Z_{eq}} = \frac{V_r}{I_r} = 0.070375 + j0.060233$$

$$R_{eq} + jX_{eq} = \frac{\overline{V}_r}{\overline{I}_r} = 0.070375 + j0.060233$$

3.7.2. Converter Equivalent Impedance at 1500 RPM (Synchronous Speed)

In synchronous speed, slip is zero and the shaft electrical speed (ω_m) is equals to with the synchronous frequency (ω_s) at 1.5 MW, 1500 rpm, 690 V and 50Hz. During the operation of 1500 rpm the following parameters will be calculated as follows.

$$I_s = \frac{V_s \pm \sqrt{V_s^2 - \frac{4R_s T_m \omega_s}{3p}}}{2R_s} = -774.84\ A$$

$$T_m = -(1500/1800)^2 * 8.3 = -5.764\ KNm$$

Voltage of magnetizing will be calculated as;

$$V_m = V_s - I_s(R_{s+} j\omega_s L_{ls}) = \frac{690}{\sqrt{3}} - (-774.84)[0.006243 + j100\pi * 0.000198822]$$

$$Vm = 406.1 < 6.845^0$$

Magnetizing current I_m

$$\overline{I}_m = \frac{\overline{V_m}}{j\omega_s L_m} = \frac{406.1 < 6.845^0}{(100\pi * 0.00397) < 90^0} = 325.61 < -83.155^0$$

Rotor current I_r

$$I_r = I_s - I_m = -774.84 - [38.81 - j323.29] = -813.65 + j323.29 = 875.524 < -21.7^0$$

Rotor voltage is

$$V_r = sV_m - I_r(R_r + js\omega_s L_{lr}) = -I_r R_r = 875.524 < -21.7^0 * 0.011074 = 9.7 < -21.7^0$$

The value of resistance and reactance for rotor side converter will be calculated as flows.

$$\overline{Z_{eq}} = \frac{V_r}{I_r} = \frac{9.7 < -21.7^0}{875.524 < -21.7^0} = 0.0111 < 0^0 = 0.0111 + j0$$

The slip is zero, consquenntlly the simplified equation will be can be written as.

$$I_r R_r = I_r R_{eq.}$$

And the equivalent resistance and reactance are;

$$R_{eq} = -R_r = 0.0111\ \Omega$$

$$X_{eq} = 0\ \Omega \qquad \text{because slip is zero}$$

When the generator of wind turbine operates at synchronous speed, slip frequancy and slip is zero. This indicates that DC current will flow by rotor circuit induction generator operates as wound rotor synchronous generator by creating rotor flux DC currnt through DC exciter. Mechanical power delivered to the national grid at zero slip and 875.524 A, will be calculated as flows.

$$P_m = T_m \omega_m = -5.764 * 2 * 1500 * \frac{\pi}{60} = -937.32\ KW$$

The value of rotor power is;

$$P_r = 3 * {I_r}^2 R_{eq} = -3 * 875.524^2 * 0.0111 = -25.23\ KW$$

The rotor and stator winding power loss is;

$$P_{cu,s} = 3{I_s}^2 R_s = 3 * 774.84^2 * 0.006243 = 11.244\ KW$$

$$P_{cu,r} = 3{I_r}^2 R_r = 3 * 875.524^2 * 0.011074 = 25.466\ KW$$

The value of active power at the stator side will be calculated as flows.

$$P_s = 3V_s I_s\, cos(\varphi_s) = 3 * \frac{690}{\sqrt{3}} * 774.84\, cos(180^0) \cong -926\ KW$$

The total grid power is;

$$P_g = P_s - P_r = 926 - 25.23 = 900.77\ KW$$

The total power loss at stator and rotor winding will be;

$$P_{loss} = P_{cu,s} + P_{cu,r} = 11.244 + 25.466 = 36.71\ KW$$

$$\eta = \frac{P_g}{P_m} = \frac{900.77}{937.32} = 96.1\%$$

3.7.3 Equivalent Impedance of Converters at 1000 RPM

In 1000 rpm the value of slip is positive and it indicates sub synchronous speed machine will works as a motor mode. The same procedure as an author calculated in the previous section, also

for 1000 rpm will be calculated for rotor current, rotor voltage, equivalent impedance and resistance as shown below.

When the generator operates at 1.5 MW/690V, 50Hz and 1000 rpm the value of stator current will be calculated as depicted below.

$$I_s = \frac{V_s \pm \sqrt{V_s^2 - \frac{4R_s T_m \omega_s}{3p}}}{2R_s} = -346.68\ A$$

$$\mathrm{T_m} = -\left(\frac{1000}{1800}\right)^2 * 8.3 = -2.562\ \mathrm{KNm}$$

Magnetizing voltage V_m and current I_m will be;

$$\mathrm{V_m} = \mathrm{V_s} - \mathrm{I_s}(\mathrm{R_{s+}} j\omega_s \mathrm{L_{ls}})$$

$$V_m = \frac{690}{\sqrt{3}} - (-346.68)[0.006243 + j100\pi * 0.000198822]$$

$$V_m = 400.534 + j21.65 = 401.12 < 3.094^0 = 400.53 + j21.65$$

$$\overline{I}_m = \frac{\overline{V_m}}{j\omega_s L_m} = \frac{401.12 < 3.094^0}{(100\pi * 0.00397) < 90^0} = 321.61 < -86.906^0 = 17.36 - j321.14$$

Rotor current I_r and rotor voltage will be calculated as ;

$$I_r = I_s - I_m = -346.68 - [17.36 - j321.14] = -364.04 + j321.14 = 485.44 < -41.42^0$$

$$V_r = sV_m - I_r(R_r + js\omega_s L_{lr})$$

$$V_r = 0.33[400.53 + j21.65] - [-(364.04 + j321.14) * (0.011074 + j0.33 * 100\pi * 0.000198822)]$$

$$V_r = 132.175 + j7.1445 - [-(485.44 < -41.42^0) * (0.011074 + j0.021)]$$

$$V_r = 132.175 + j7.1445 - \left(-(485.44 < -41.42^0) * (0.024 < 62.2^0)\right)$$

$$V_r = 132.175 + j7.1445 - (-(11.651 < 20.79^0))$$

$$V_r = 132.175 + j7.1445 - (-10.9 + j4.135) = 143.075 + j11.28 = 143.19 < 4.51^0$$

Where slip is S= $\frac{(1500-1000)}{1500}$ = 0.33333

Equivalent value of resistance and reactance are

$$\overline{Z_{eq}} = \frac{V_r}{I_r} = \frac{143.19 < -4.51^0}{485.44 < -41.42^0} = 0.3 < 36.91^0 = 0.24 + j0.2$$

$$R_{eq} = 0.24\Omega$$

$$X_{eq} = 0.2\Omega$$

The simplified steady state equivalent circuit of maximum torque on DFIG at maximum slip as shown in figure 3.20. Compared with figure 3.20, the magnetizing branch is moved to the left of stator circuit magnetizing inductance and is higher than stator resistance and it indicates less errors.

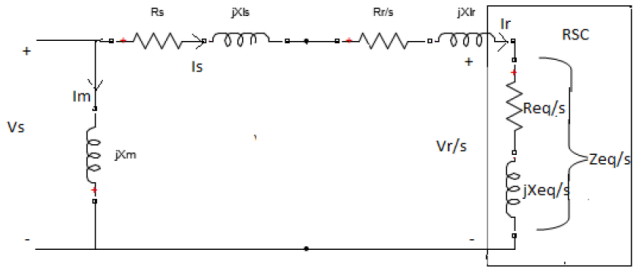

Figure 3-20 equivalent circuit of DFIG at maximum torque

Using figure 3.20 the maximum torque of the generator can be derived as flows.

$$T_m = \frac{P_{ag}}{\frac{\omega_s}{P}} = \frac{1}{\frac{\omega_s}{p}} * \frac{\left(3{I_r}^2\right)\left(R_r + R_{eq}\right)}{s}$$

$$T_m = \frac{P_{ag}}{\omega_s/p} * \frac{3{V_s}^2}{(R_s+\frac{R_r}{s}+R_{eq}/s)^2+(X_{ls}+X_{lr}+X_{eq}/s)^2} * \frac{R_r+R_{eq}}{s} \quad (3.74)$$

The maximum torque T_{max} and the slip at the maximum torque sT_{max} can be obtained by setting $dT_m/ds = 0$.

$$S_{Tmax} = \pm\sqrt{\frac{(R_r+R_{eq})^2+{X_{eq}}^2}{{R_s}^2+(X_{ls}+X_{lr})^2}} \quad (3.75)$$

The plus and minus signs in the above equation signify the sub- and super synchronous modes of operation.

It is valid for both sub and super synchronous mode of operations.

From the above calculations an author conclude the following points;

- During synchronous conditions the value of equivalent reactance rotor is zero indicates that DC current will flow into the circuit of the rotor and it produce DC current.
- During sub synchronous operation rotor voltage decrease until generator speed increases and it starts increase at super synchronous conditions. From this author says that power will be delivers to the grid at super synchronous mode of operations. During the generator running from sub synchronous to super synchronous rotor voltage will vary slowly and current of the rotor

will increased. During the operation of super synchronous mode of equivalent resistance is positive means that power will be flow from rotor to converter and in sub synchronous mode equivalent resistance is negative means that power will flow to the rotor.

3.7.4. Steady State of DFIG with Wind Energy Conversion System at Unity Pf

Under this sub title the area of power conversion of DFIG wind energy system is discussed. From chapter three equivalent circuit can be facilitated the steady state analysis of the DFIG wind energy system.

The electrical power can be calculated easily by the following equations.

$$P = 3I^2R$$

Where the rotor power is transferred from or to the rotor side converter. By neglecting the rotational losses of the turbine the power transferred or dissipated in the generator can be calculated by the following equations.

$$P_m = \frac{3I^2\left(R_r + R_{eq}\right)(1-S)}{s}$$

$$P_r = 3I^2R_{eq}$$

$$P_{cu,r} = 3I_r^2R_r$$

$$P_{cu,s} = 3I_r^2R_s$$

$$P_s = 3V_sI_scos\emptyset_s$$

$$P_s = \frac{P_m}{(1-S)}$$

$$P_r = -SP_s$$

Where $\emptyset s$ is the stator power factor angle and the power is delivered to the grid is the sum of stator and rotor power shows below.

$$\left|\mathrm{P_g}\right| = \begin{cases} |\mathrm{P_s}| - |\mathrm{P_r}| & \text{used for super synchronous mode} \\ |\mathrm{P_s}| + |\mathrm{P_r}| & \text{for sub synchronous mode} \end{cases}$$

During super synchronous operating mode the equivalent resistance of the rotor side converter has a positive and the rotor power is positive. This indicates that the resistance consumes power similar to the winding resistance. In sub synchronous operating mode the value of equivalent resistance is negative and the rotor power is negative. This implies that the rotor circuit receives power from the grid through the power electronics converters.

CHAPTER FOUR

4. SIMULATION RESULT AND DISCUSSION

4.1 Introduction

In this chapter, the simulation results of DFIG that was modelled and simulated using Simpowersystem toolbox under the MATLAB/Simulink/ programming is discussed. The model of DFIG includes different controllers in its design as it shows in figure 4.1.The overall block diagram of Adama-II wind farm by using MATLAB/ Simulink is shown below.

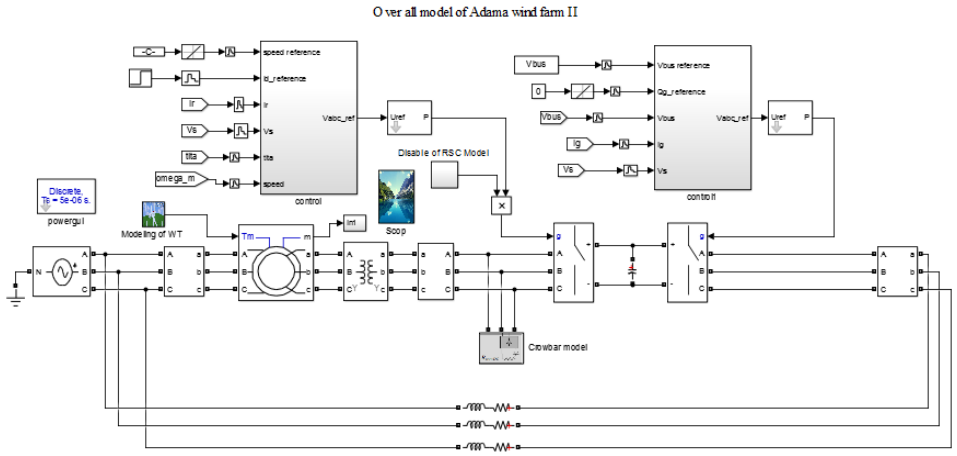

Figure 4-1 over all Simulink model of Adama-II wind farm with single turbine

The operating principle of the machine is either as a generator or motor mode. The operation will detect by the sign of the mechanical torque. If the mechanical torque is positive, it acts as a motor mode and if the mechanical torque is negative, the machine acts as generator. The ideal switch is used with appropriate switching logic. The symmetrical faults will be analyzed using crowbar resistor protection circuits and DFIG based wind energy conversion system under MATLAB/Simulink environment. The DFIG was implemented with the crowbar protection system to improve the operation of DFIG under different grid fault conditions. In addition, wind turbine will supply power to the grid all time even during fault conditions. The rotor side control (RSC) extracts maximum power from the wind turbine and improves reactive power requirement during grid fault.

The grid side converter (GSC) used to maintain almost constant voltage of the DC link voltage and voltages at the point of common coupling (PCC) to maintain equal value. GSC also used to correct the desired reactive power for the system and the crowbar protection is made up for

semiconductor switch device and resistance to protect the stator winding and power electronic converters.

4.2. Activation and Deactivation of Crowbar Protection

Crowbar is to be used to protect the system from loss of current control and increase in DC link Voltage. The crowbar shorts the rotor winding at severe voltage dip. It is connected at the first stage of the dip when the rotor emf is at its highest level. Once the transient flux has decayed and rotor emf is no longer hazardous, the crowbar can be disconnected, so that the machine can continue its normal operation. When the crowbar is connected, it causes the rotor current to increase but this doesn't affect the RSC, as it's disconnected and its current is zero. This means that DFIG is not controlled anymore and it acts as typical squirrel cage induction machine.

The SimPowerSystems DFIG model doesn't have block of crowbar protection. Therefore, it is developed by the combination of normal diode with set condition, resistance and ideal switches with its controlling mechanisms in MATLAB environment. Normally the switch is open but it will close during short circuit when rotor current or DC link capacitor voltage becomes too high. Voltage dip will perform at 3 seconds and the crowbar protection will activates within 100 milliseconds as it shows in figure 4.2.

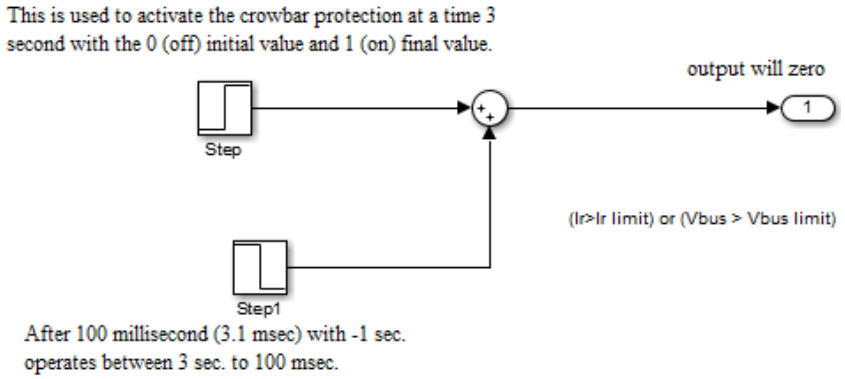

Figure 4-2 Activation and deactivation time of crowbar protection

The operation time of crowbar protection is between 3 second to 100 milliseconds (00:00:03 to 00:00:03:100). Once the voltage dip is detected, crowbar protection will be activated and the stator flux will dump quickly as shows in chapter three figure 3.11. The recovery time of the voltage dip is between 3.5 to 4.17 seconds and by using the crowbar resistance protection the stator flux will be dumped. As the crowbar protection activated, the GSC and RSC are protected from over voltage. All the energy and over current are flowing to the crowbar protection. During

the dip, all the current will be provided by the reference voltage. Once the dip voltage detected, crowbar protection will be activated.

4.2. Simulated Result of Existing System with the Help of Capacitor Bank

A. The simulated results of stator voltage on the rotor side converters shown below.

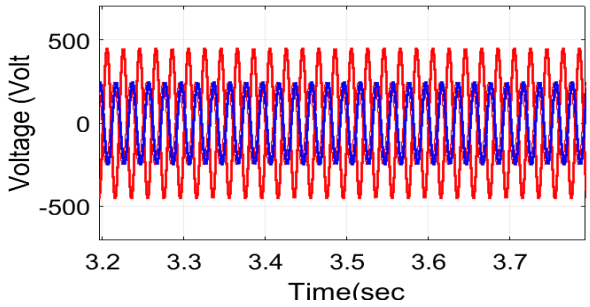

Figure 4-3 simulated result of stator voltage

From figure 4.3 it is clear that the stator voltage at the PCC is not balanced, they didn't have equal amplitude and frequency. So it leads to the mismatch of the voltage with national grid, consequently it will cut from the grid.

B. The simulation result of torque on the rotor side converters shown in the figure 4.4.

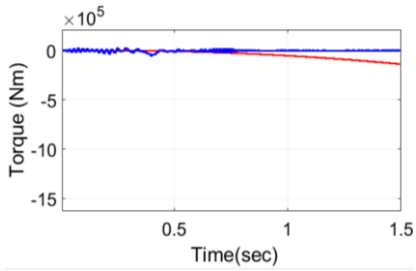

Figure 4-4 simulation result of torque

From figure 4.4 it is clear that the value of torque is initially the same with the reference torque, after some time it leads to the negative directions. But during normal condition the simulated result starts at negative sign.

C. Simulated results of current on q-axis is depicted as follows.

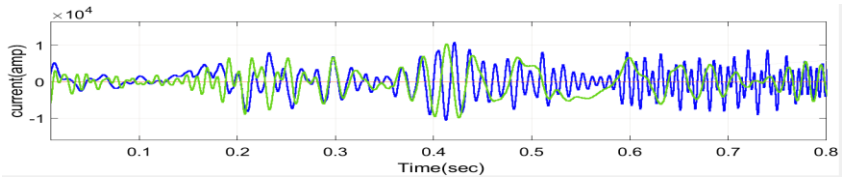

Figure 4-5 simulated result of I_q

As it shows from figure 4.5 the behavior of rotor side current the reference current for the quadrature with the voltage which controls the reactive power at the PCC. The simulated current across q- components is distorted and it can't control the reactive power, so crowbar protection is needed to control.

D. Simulated results of current on d-axis

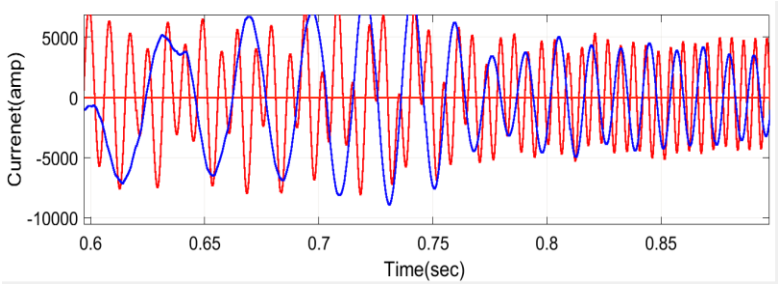

Figure 4-6 simulated result of current on d- axis

From figure 4.6 the simulated result of current across the d-component which controls the active power flows, but as it shows the output current is distorted it can't controlled itself, so the active power at the PCC is of Adama wind farm –II is not controlled.

E. Simulated results of stator current

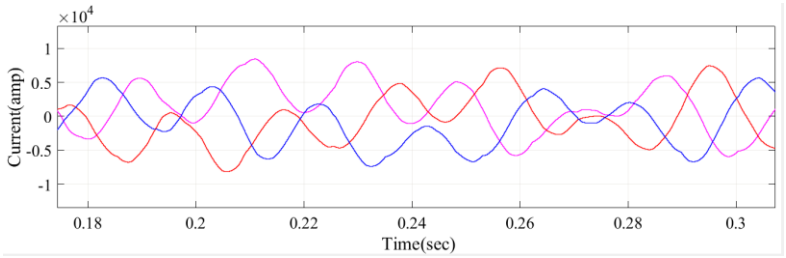

Figure 4-7 simulated result of stator current

From figure 4.7 it is clear that the stator current at the PCC is distorted and it is usually degradation of the signal. They have different amplitude and different frequency. It differs from its conventional sine wave shape.

F. Simulated results of V_{dr}

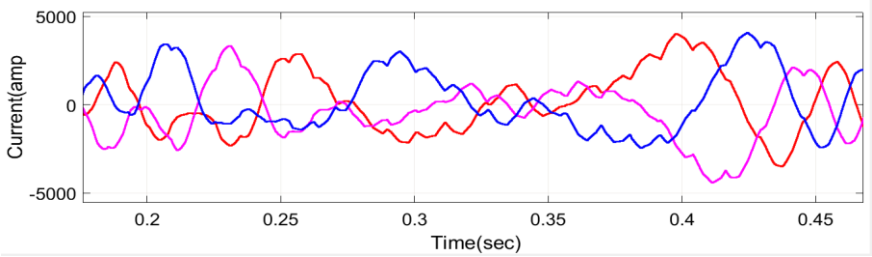

Figure 4-8 simulated result of simulated result of v_{dr}

The voltage across the d-component on the rotor is distorted and they haven't equal amplitude and frequency. So the reactive power of the grid is not controlled.

G. Simulated results of grid current

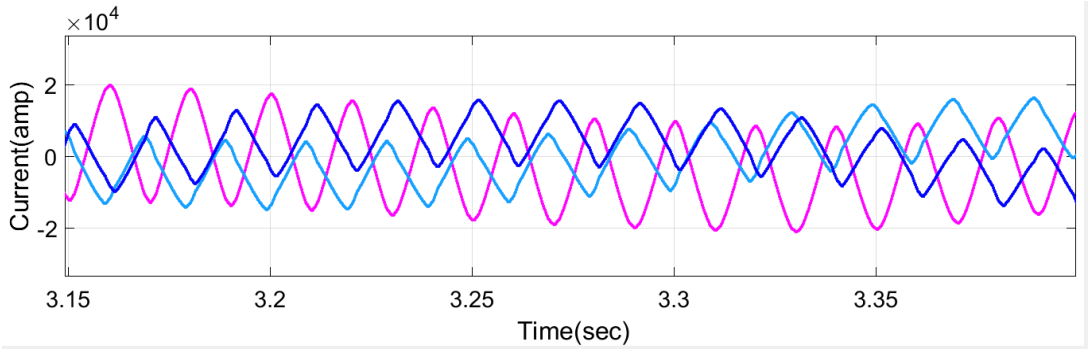

Figure 4-9 simulated result of grid current grid side

At the normal condition the stator current is pure sinusoidal to deliver sufficient power and voltage to the national grid but during the fault condition as it shows from figure 4.9 the signal of grid current is distorted, consequently the grid voltage is not controlled.

4.3 Asymmetrical Fault Analysis under Different Voltage Dip

Asymmetrical faults are faults those involve only one or two phase and these faults will not affect three phase at the same manner. From the overall Simulink model of asymmetrical voltage dip with a positive and negative sequence, voltage dip faced at 3 second and it will removed at 3.9 second.

4.4 Simulation Results of DFIG under Asymmetrical Fault on RSC

The simulation results of asymmetrical fault without crowbar protection on the rotor side converter are shown below. The rotor side converter is in healthy condition and rotor current is balanced by imposing the negative sequence zero for the rotor reference. The block diagram of

the RSC is shown below. The RSC controller is integrated with the generator rotor side of DFIG. The main objective of the RSC is to control both the active and reactive power of the DFIGs stator terminal. During normal operation, the RSC controller controls the stator active power with the help q-axis rotor current components (i_{qr}) and the reactive power is controlled by the d-axis rotor current component (i_{dr}). In this way the RSC controller main objective is achieved.

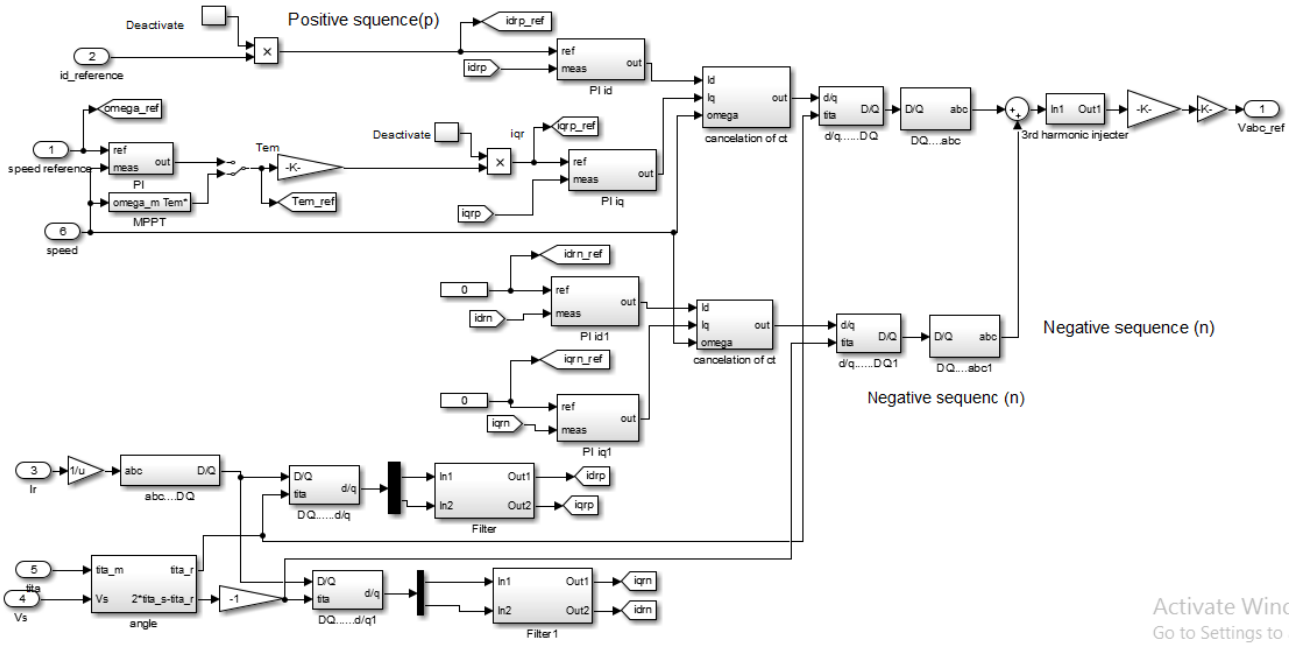

Figure 4-10 Modeling of RSC on asymmetrical fault

A. Simulation Result of Speed, iq ,Vdr and Torque on the RSC

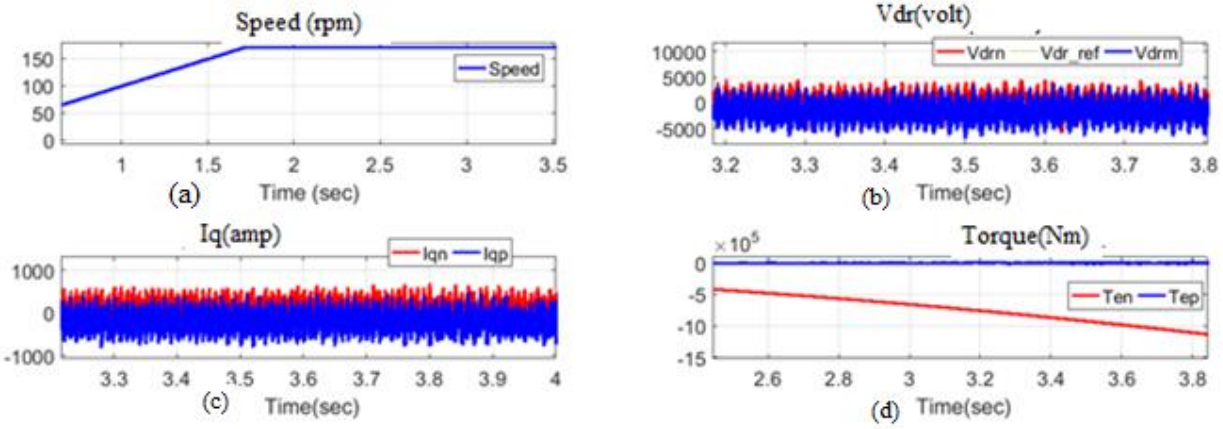

Figure 4-11 simulation result on the RSC

From figure 4.11 (a) it is clear that the speed of the wind turbine is increased and the rotor voltages at d-axis figure 4.11 (b) are not balanced due to the asymmetrical faults and they are not controlled. In figure 4.11 (c) also have negative and positive currents on q-axis are also not controlled and it oscillates with some cycle at different amplitude. The actual torque in normal condition is constant but during asymmetrical faults as shown in the figure 4.11 (d), it leads to negative directions, below the reference torque.

A. Simulation of Current and Voltage at q- Components

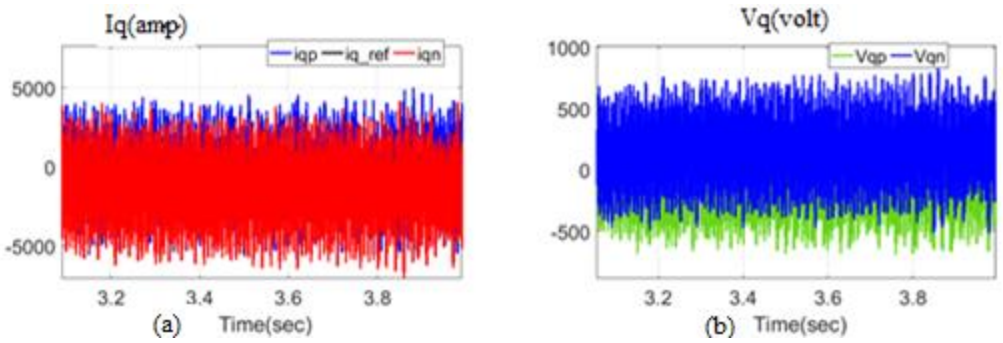

Figure 4-12 simulation result of current and voltage at q-component

As shown in the figure 4.12 (a), the negative and positive currents are depicted and the simulated results of current and voltage at q- component are unbalanced. They have different amplitude and frequency. During the voltage dip, unbalanced currents are not affected the three phase lines equally. The voltage dip is occurred at 3 seconds and unbalanced output current oscillates until the voltage recovered at 3.9 second.

B. Simulation of Stator Voltage

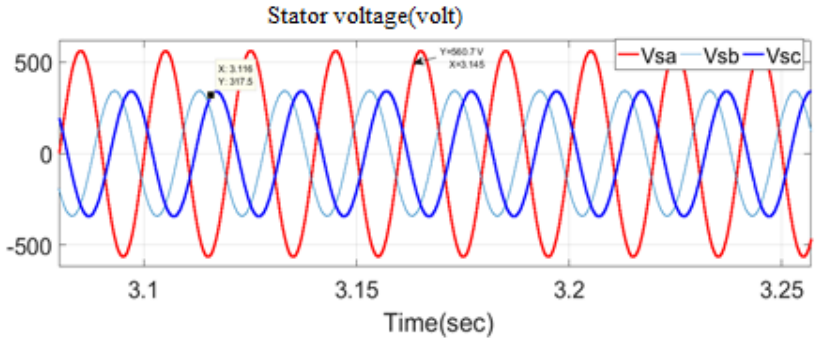

Figure 4-13 simulation result of stator voltage at asymmetrical faults

Based on the simulation results of figure 4.13, it is clear that the basic concept of power system fault that during asymmetrical faults, the system leads to disconnect wind turbines from the national grid. The power of wind turbine is delivered to the grid at different frequency and amplitude due to the grid faults. But using crowbar protection, power will be supply through stator or reactive power to compensate the grid voltage. The stator voltage will dip at 3 second until it will recovers and the output of stator voltage are oscillates at different amplitude and frequency. These are not affected equally for the three phases. During asymmetrical fault the stator voltage is not controlled.

4.5 Simulation Results of DFIG under Asymmetrical Fault on GSC

During the normal conditions, the system will be addressed to avoid negative sequence of the stator current for reducing the stator currents. But in the GSC, under asymmetrical faults, the system is not balanced as shown in the following figure 4.14.

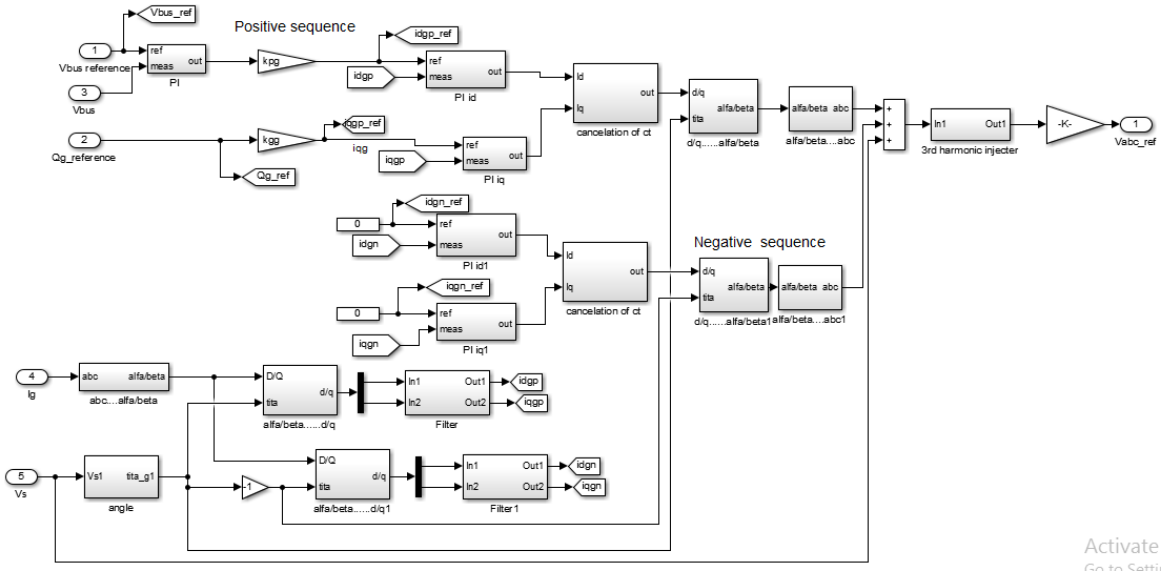

Figure 4-14 modeling of GSC under asymmetrical faults

A**. simulation result bus voltage and grid current on d-axis**

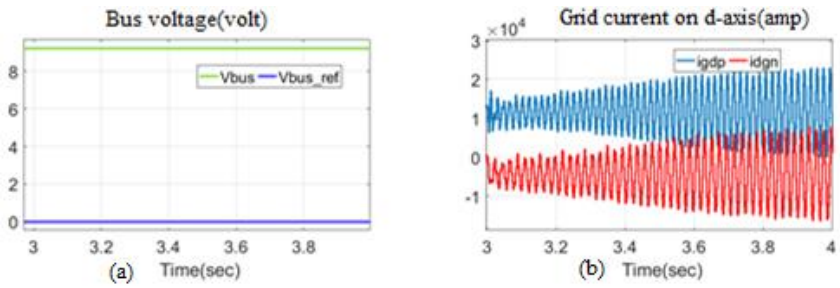

Figure 4-15 simulation result bus voltage and grid current on d-axis

From figure 4.15 (a), it is clear that the value of bus voltage is constant above the reference bus voltage and it is similar to the calculated value, but from figure 4.15 (b) the grid current at d-component contains negative as well as positive sequence and unbalanced current, which will be delivered to the grid.

B. Simulation of stator voltage and grid current

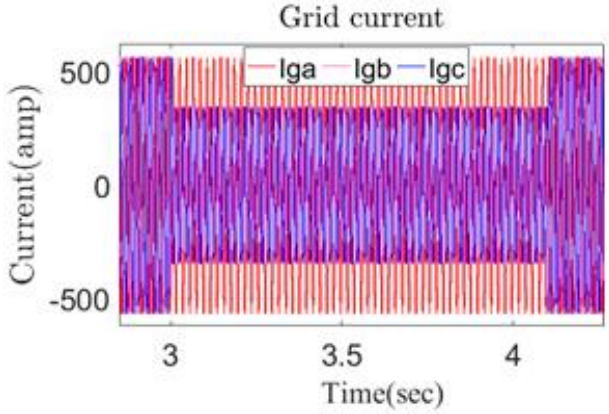

Figure 4-16 Simulation of stator voltage and grid current

From figure 4.16 it is clear that the simulated result of grid current during asymmetrical fault is not balanced during the occurrence of voltage dip at three (3 sec). But before the fault it is balanced the whole lines and also after the fault is cleared the simulated result is balanced. During the dip voltage the simulated results have different amplitude.

4.6 Simulation Results of DFIG LVRT Capability under Symmetrical Fault

The simulation results of DFIG under symmetrical fault condition shown the variation in crowbar current, stator voltage, stator flux, rotor current, stator current and the actual torque, as shown below. By increasing crowbar resistance value, rotor current will be made decrease.

A. The Stator Voltage During Fault Analysis Conditions

During the fault condition, the simulated disturbance of three phase fault produced symmetrical voltage dip at the wind turbine terminal for 100 ms period. The crowbar detected it after 100 ms from its occurrence. There is no current flow to the crowbar resistance before the fault, but after the protection system detected the grid fault, current will pass through crowbar resistance.

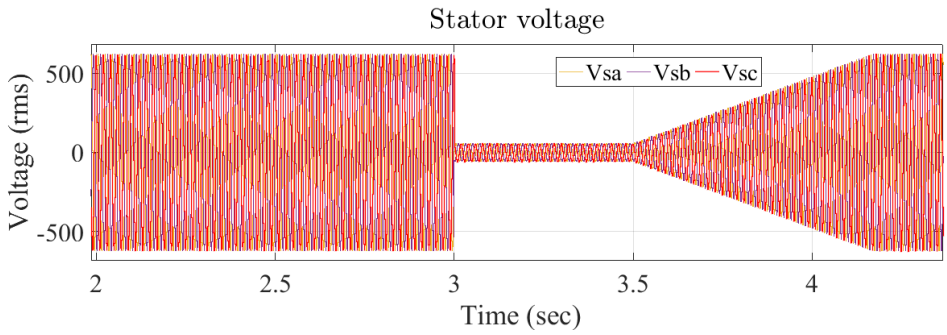

Figure 4-17 Stator voltage during fault analysis

Figure 4.17 presented the simulation results for the LVRT performance of DFIG system, with three phase symmetrical fault. When the grid fault occurs, crowbar protection suddenly activated and the value of voltage at the PCC is reduced to zero. When the voltage dip faced at 3 seconds, the value of current is high and it circulated at the rotor side converters, consequently the machinery of WT will lose or damage and the destruction of power system network will be faced. During the occurrence of voltage dip at 3 second, crowbar will activate and the stator voltage will recovered at 3.5 to 4.17 seconds. With the help of crowbar protection, WT will supply continuously at different voltage dips.

Stator voltage dip starts at 3 sseconds and during this time, high current will pass through the crowbar protection as shown in figure 4.18 (a) and it dissepates.

B. The Stator Flux and Crowbar Current during Fault Conditions

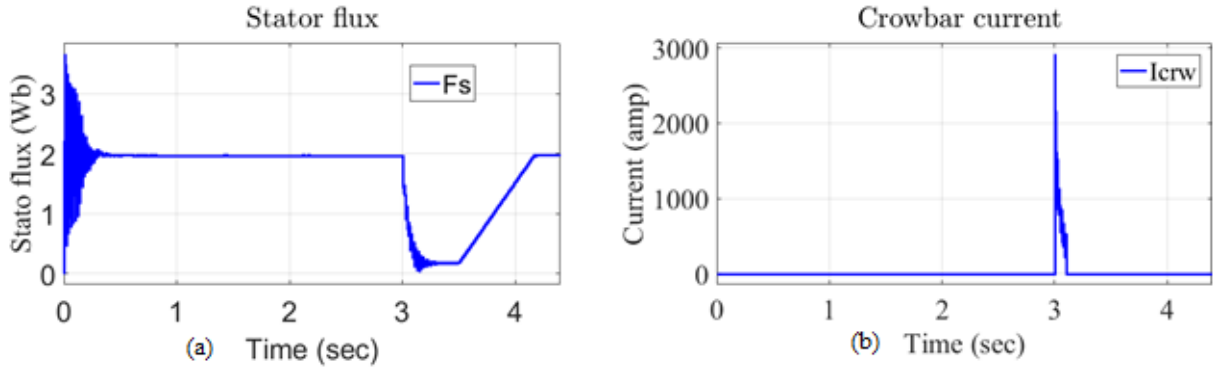

Figure 4-18 (a) crowbar current during fault analysis (b) stator flux during fault analysis

From figure 4.18 (a) it is clear that during the voltage dip, crowbar current is suddenly overshoot at time 3 seconds because of the grid faults. The value of crowbar current can be higher or small, depending on the value of crowbar resistance. Further, the over current produced at the rotor side converter will dissipate with the help of crowbar resistor protection. Figure 4.18 (b) presented that once the voltage dip is detected, crowbar protection will be activated and the stator flux will dump quickly at 3 second, until it will be recovered to its original value. As stator voltage decreased, stator flux also decreased and it became the normal condition after the voltage is recovered.

4.7 Simulation Results of DFIG LVRT Capability with Crowbar Protection on RSC

As shown in figure 4.19, RSC has a number of controller mechanisms. The main target of rotor side control is to control the active and reactive power independently. By controlling the rotor current, it can be controlled the active and reactive power indirectly. The simulation results for LVRT on DFIG with a crowbar activated are depicted below with the detail description of each rotor current and torque.

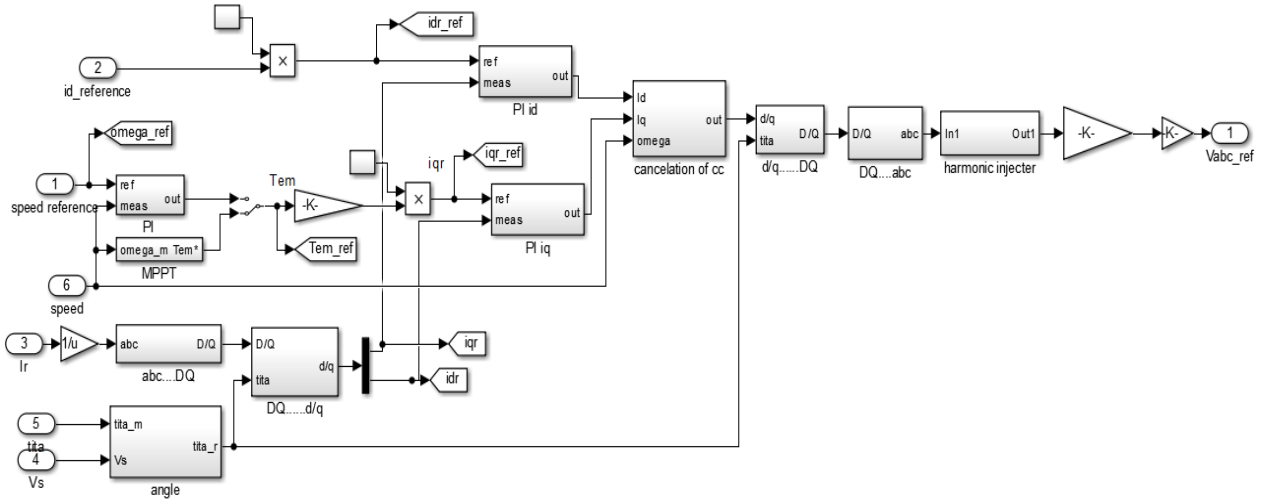

Figure 4-19 modeling of rotor side control under LVRT

When the crowbar is activated at voltage dip, the rotor side converter will disable by using simple steps in order to protect it.

A. Simulation Result of Speed and Quadrature of Rotor Side Control

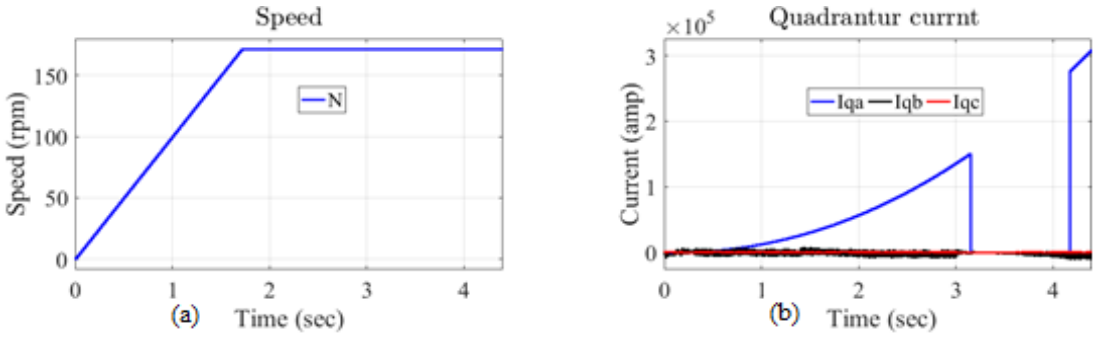

Figure 4-20 Speed and quadrature current Rotor Side Control

Based on the simulation results in figure 4.20 (a) the speed of wind turbine in RPM is gradually increased until it comes rated wind speed which is generate power continuously using the crowbar protections. And also from figure 4.13(b) the simulated result of quadrature current of one phase is gradually increased but during the crowbar activation time it will decay to zero and at a time 4.17 second increased.

B. Voltage Across d-Axis And Torque On Rotor Side Control (V_{dr})

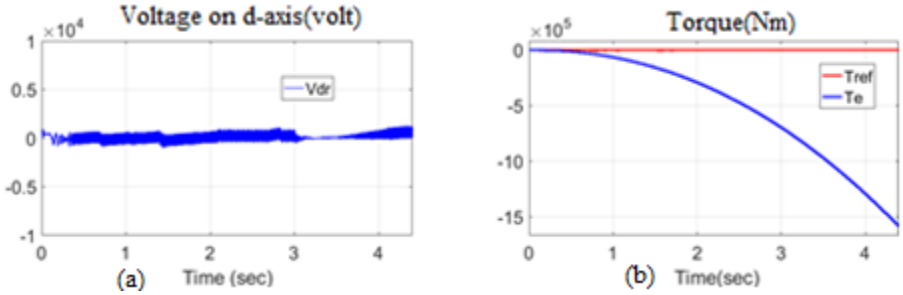

Figure 4-21 Voltage across d-axis and torque on rotor side control

Above figure presented V_{dr} and torque during normal operation. Reactive power is almost zero. For high wind speed, the speed of turbine is limited and therefore, output power is also limited. So figure 4.21 shown the value of torque, which leads to negative value because fault is occurred and to compensate the stator voltage, reactive power, must be delivered to the grid.

C. Stator Voltage on Rotor Side Control

The simulation of stator voltage on grid side converter, which is based LVRT of DFIG wind turbine is performed using the crowbar protection. The main cause of stator over voltage is due to the damage of rotor side control in a few milliseconds during grid disturbance. From the figure

4.22 it is clear that before the fault, DFIG is in steady state condition. But at time 3 second, stator voltage will be dropped to zero due to fault.

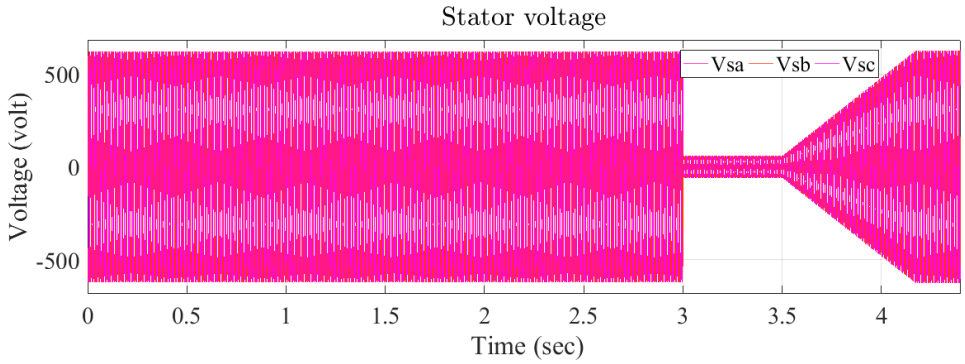

Figure 4-22 Stator voltage on rotor side control

4.8. Simulation Results of DFIG LVRT with Crowbar Protection on GSC

The grid side converter shown in figure 4.23 and it is used to adjust voltage of DC capacitor. For that purpose, d-axis of the rotating reference frame is used in d-q transformation and it is associated with the positive sequence of the grid voltage.

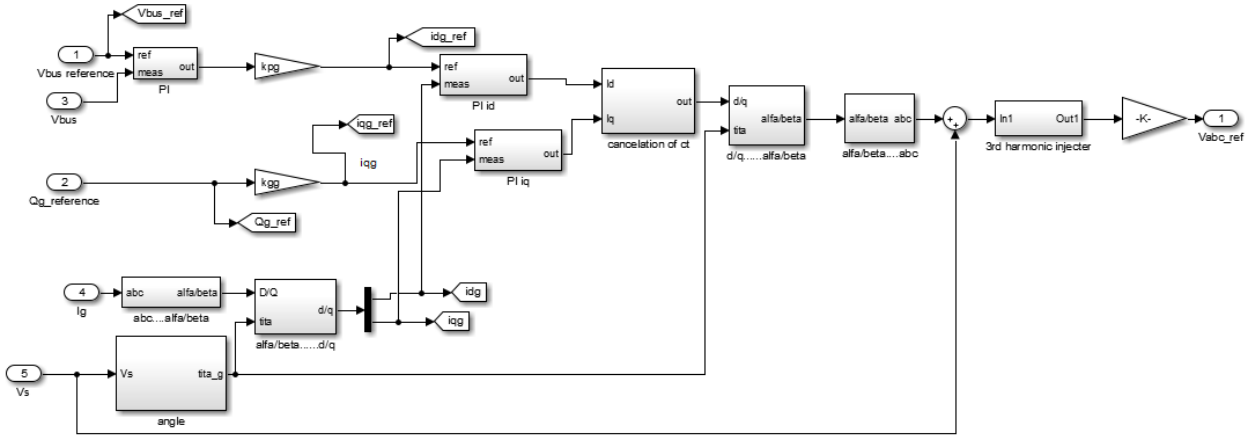

Figure 4-23 modeling of grid side control under LVRT

The simulation of grid side converter shows that almost constant voltage in the terms of DC link voltage at the PCC is obtained. The GSC is rapidly correct the desired reactive power for the wind turbine. So the crowbar protection can be protected the stator winding and the rotor side converters from damaging.

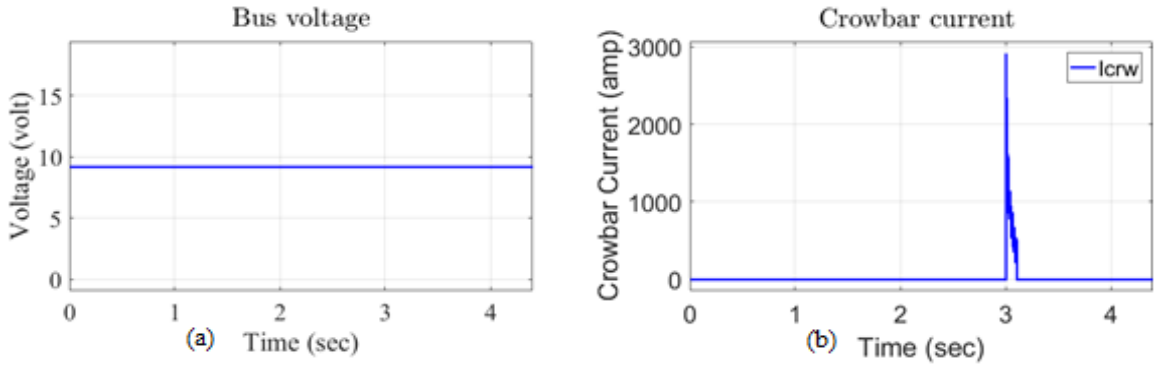

Figure 4-24 Bus voltage and reactive power at grid side control

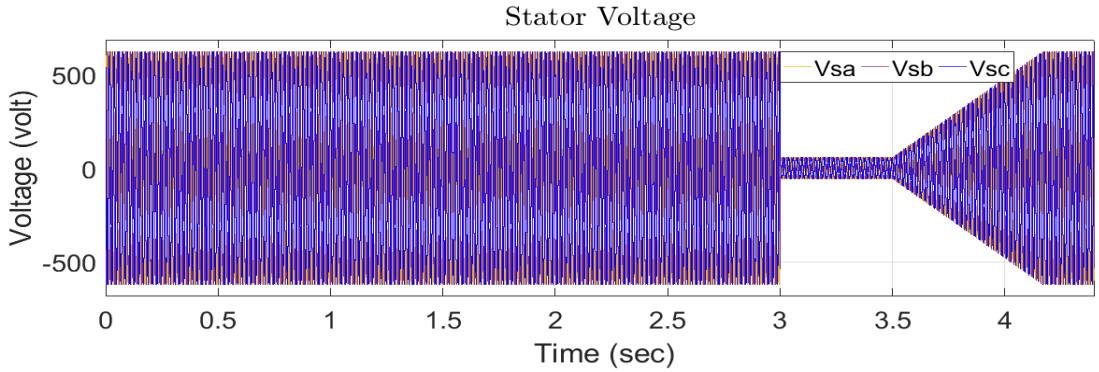

Figure 4-25 Stator voltage of grid side control

From figure 4.24 (a) it is clear that the value of bus voltage is constant around 9 volts and it is similar in value with the calculated value. It is important to maintain the DC-link bus voltage constant as system may get unstable if DC-link bus voltage increases beyond certain limits and it is also leads to power electronics converters failure. Also in figure 4.24(b) the value of crowbar current during the fault condition is over shooting. Before the fault and after the fault the value of crowbar current is the same, because the switch of crowbar resistor protection is open. When fault occurs the switch of crowbar protection will activate consequently high rotor current faced at the rotor side then the high rotor current will start flow to the crowbar protection and crowbar current will high in order to protect the rotor side converter. Generally, the crowbar protection resistance is instantly activated whenever the voltage dip occurs. When the crowbar is activated, it needs to disable the rotor side control converter (RSC) in order to protect.

4.9. Simulation Results of DFIG on RSC under Steady State Condition

Wind power integration has an influence on steady state and transient stability of the power system and it depends on their penetration level. The main concept of steady state torque control of an induction motor is stretched to transient states of operation in the high performance. The

main reasons, which raise steady state stability issues, are the large scale wind energy penetration to the grid. Figure 4.26 shown the modeling of DFIG at rotor side control (RSC), under steady state condition.

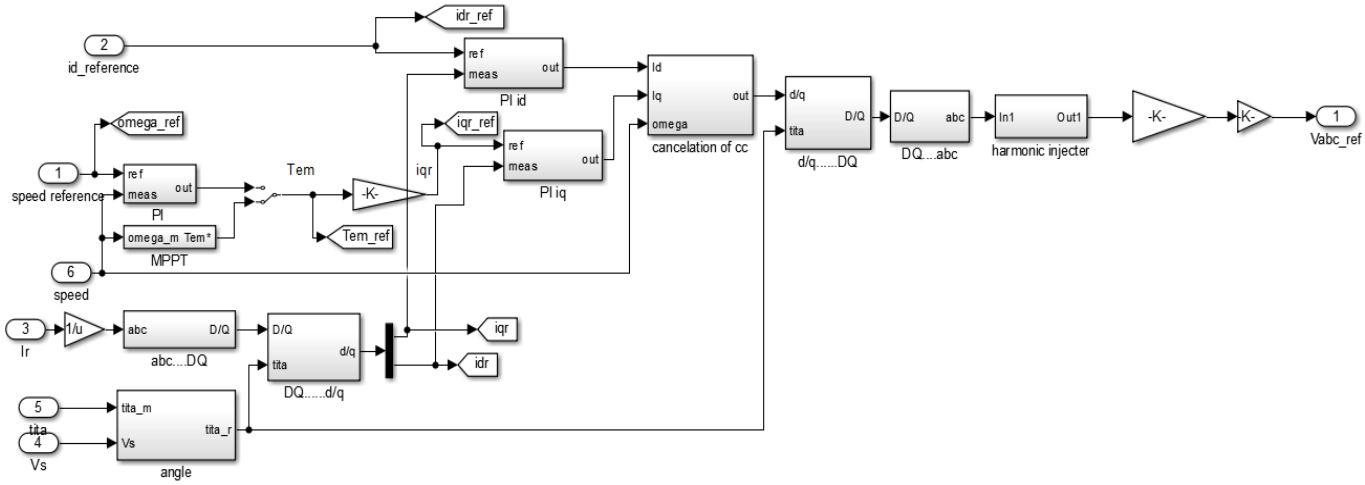

Figure 4-26 Modeling of RSC under steady state

A. Speed and Current Across q-axis Under Steady State Condition on RSC

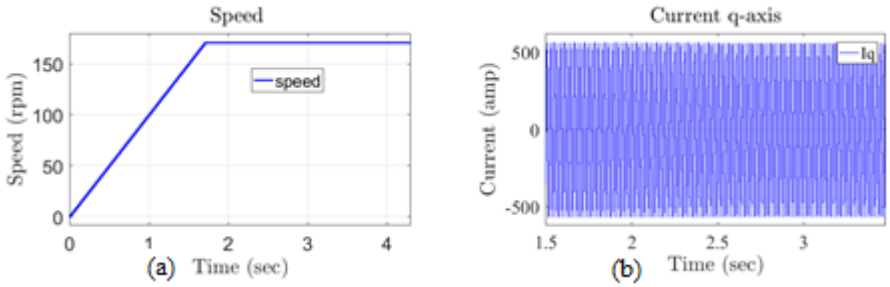

Figure 4-27 simulation result of speed and I_q on steady state condition

From the above figure 4.27 it is clear that under steady state, speed and current are in normal operating conditions. The current under q- components is balanced with the same amplitude.

B. Speed and Voltage at d-axis Under Steady State on RSC

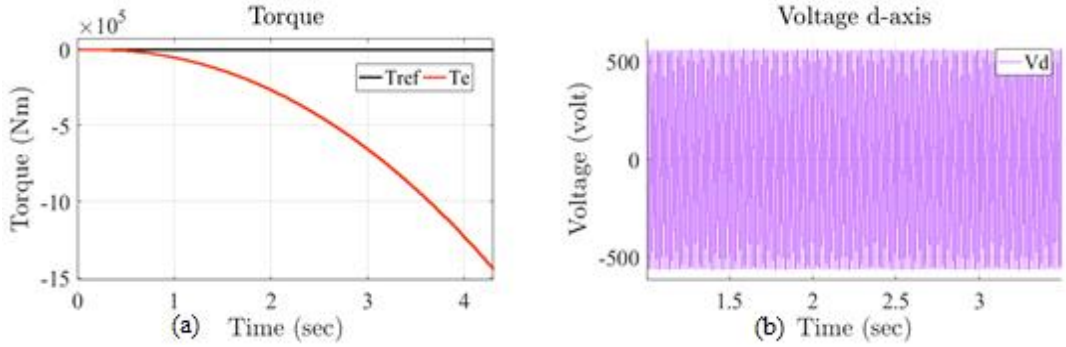

Figure 4-28 simulation result of torque and V_{dr} on steady state condition

From the figure 4.28, it clear that the voltage on d-component is balanced and it is of the same amplitude and frequency as available in the healthy condition of the system. The simulated result of torque indicated that the machine is in generating mode.

C. Voltage on q-axis and current on d-axis

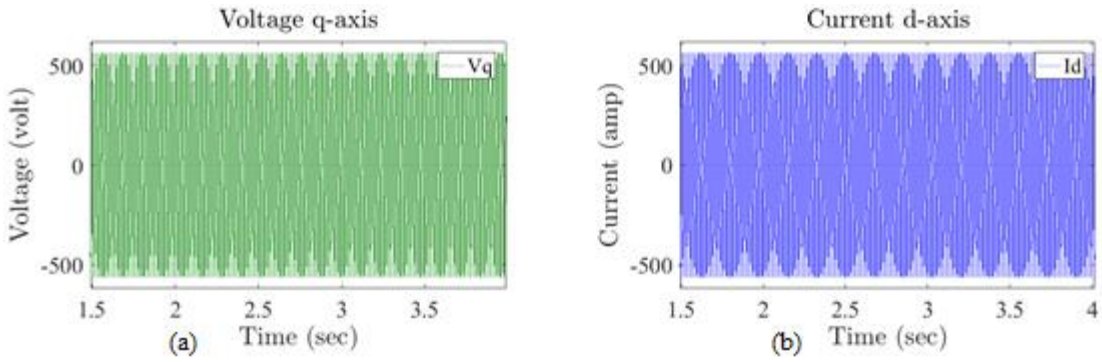

Figure 4-29 simulation result of i_d and V_q on steady state condition

From the Figure 4.29 it is clear that the current on d-component and voltage at the q-components have the same amplitude as in healthy condition and the controlled current and voltage will supply to the grid. So the controlled voltage will be integrated with the national grid without any faults.

D. Rotor Side Control of Stator Voltage

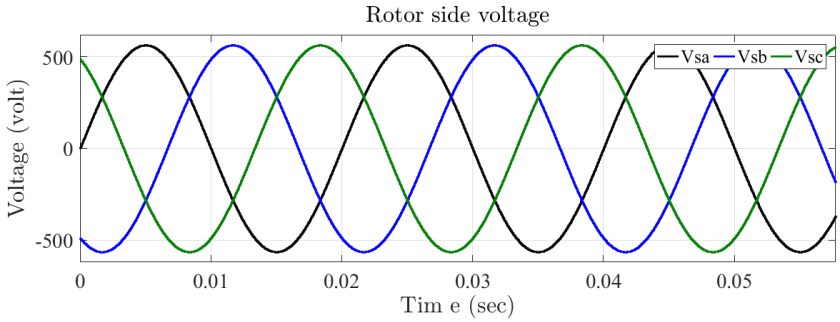

Figure 4-30 Simulation result of V_S on steady state condition

E. Stator Current and Rotor Current at GSC

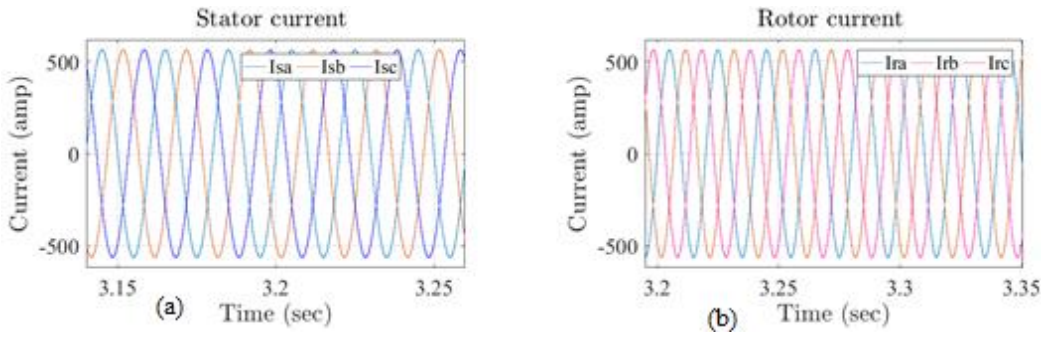

Figure 4-31 Stator and rotor current of rotor side on steady state analysis

As it is clear from the above figure the main objective of the protection system is to limit the high value of current in the rotor and the rotor voltage after the fault. It is clear that the rotor current is decreased and it doesn't flow through the converter but it flows through the crowbar protection without disconnecting the converter from the grid. The stator voltage is the same before and after the fault cleared.

4.10 Simulation Results of DFIG on GSC under Steady State Condition

Figure 4.32 showed the simulation results under steady state conditions on the grid side control (GSC). The main target of GSC is to maintain the wind turbine into the network at constant voltage and frequency, constant DC link voltage and the required reactive power with the help of the stator as the requirement of the grid code. Actually reactive power is delivered to the grid during voltage dip through the stator to compensate the grid requirement.

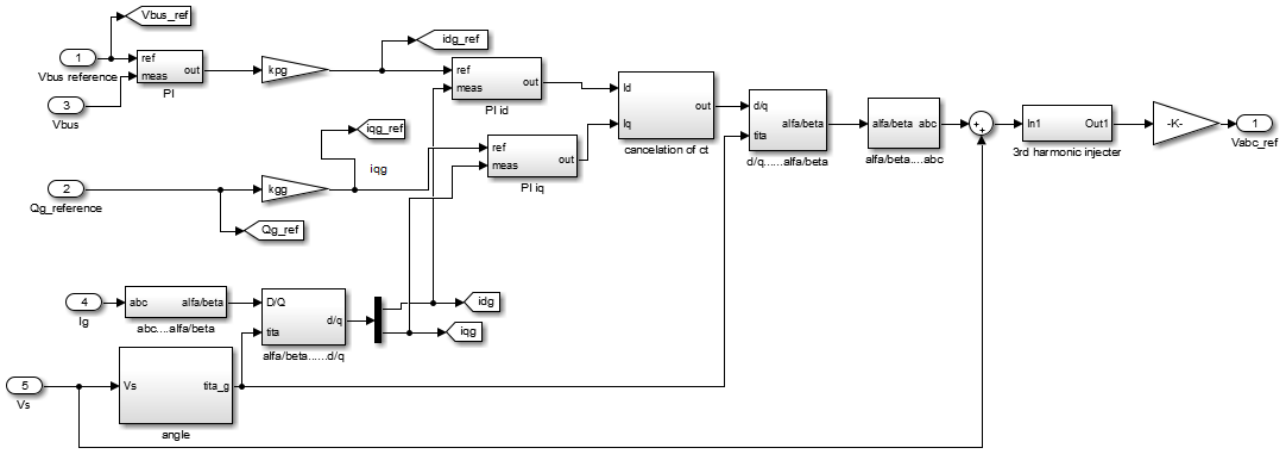

Figure 4-32 Modeling of Grid side control under steady state

A. Bus voltage and i_{dq} on Steady State Condition

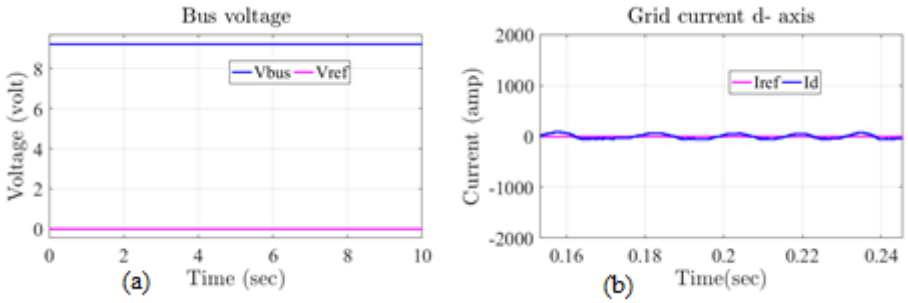

Figure 4-33 Bus voltage and I_d on steady state analysis

At the grid side control under steady state analysis, the value of startup bus voltage is overshoot but after some time it will be lower down to become stable system or it make it constant. If DC bus voltage reduced or increased, frequency will varies and power fluctuation will be occurred. Also the grid current across the d-axis is somewhat high for short period of time.

A. Grid Voltage and Reactive Power

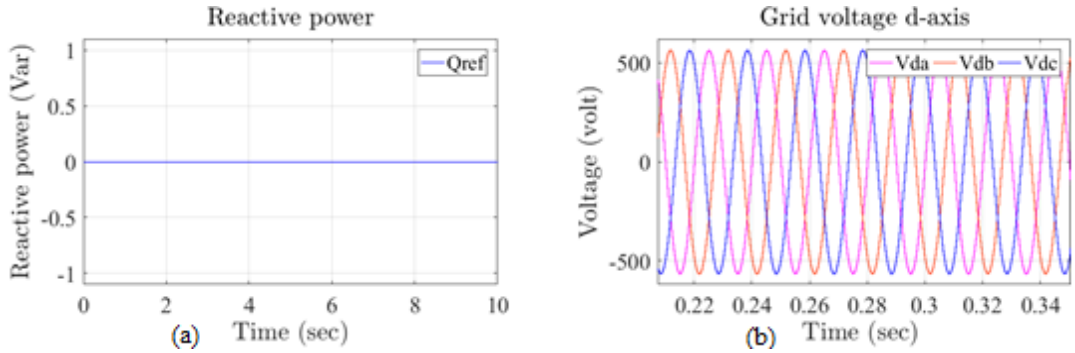

Figure 4-34 Grid voltage and grid side reference reactive power

From figure 4.34, it is clear that the output of grid side reactive power is constant i.e. under the steady state condition and the value of reactive power is constant, because there is no need of compensation. It works properly without any fault at the grid side. The grid voltage is pure sinusoidal without any disturbance. In case voltage dip is occur, the grid side control (GSC) is set to inject reactive power to the grid through the stator side whether the rotor side control is blocked or under the operation.

B. Grid Voltage And Grid Current on q-axis

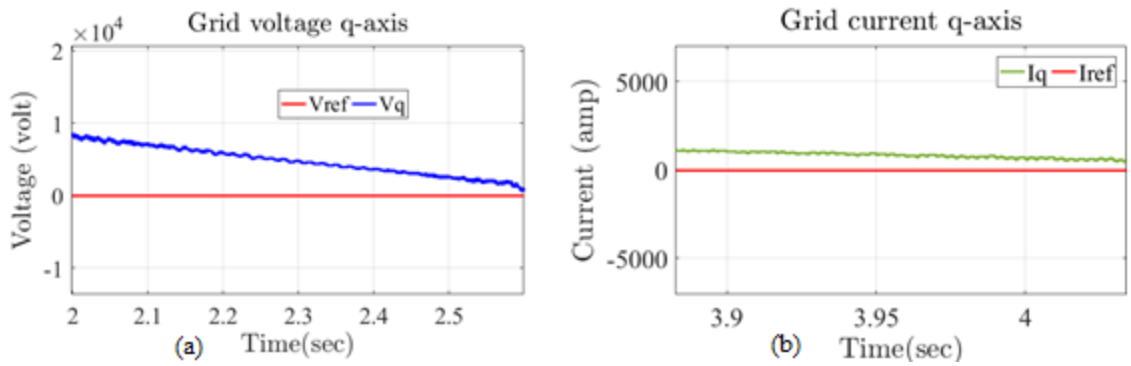

Figure 4-35 Grid voltage and current on steady state analysis

Figure 4.35 presented the value of grid current and voltage on q-axis. The q-axis reference current can be randomly adjusted to control the active power, but at the normal condition it is almost similar to reference current. During normal condition, the q-axis voltage at the grid side is zero and the d-axis voltage is constant, so the graph is almost constant.

C. Simulation Result of Stator Voltage

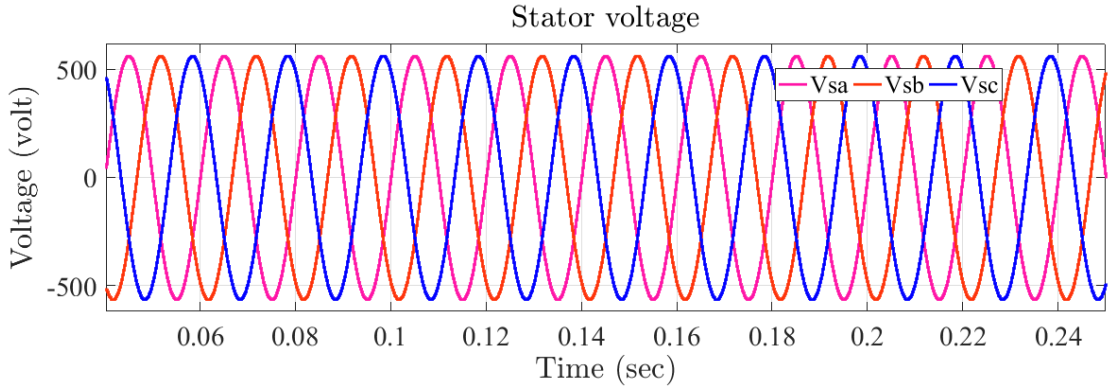

Figure 4-36 Stator voltage on steady state analysis

Figure 4.36 presented the output stator voltage, which is pure sinusoidal. During voltage dip the stator voltage is going to reach zero until it recovers and it is sinusoidal as it shown above. This indicates that the network is at healthy conditions.

D. Simulation of Grid Current and Rotor Current

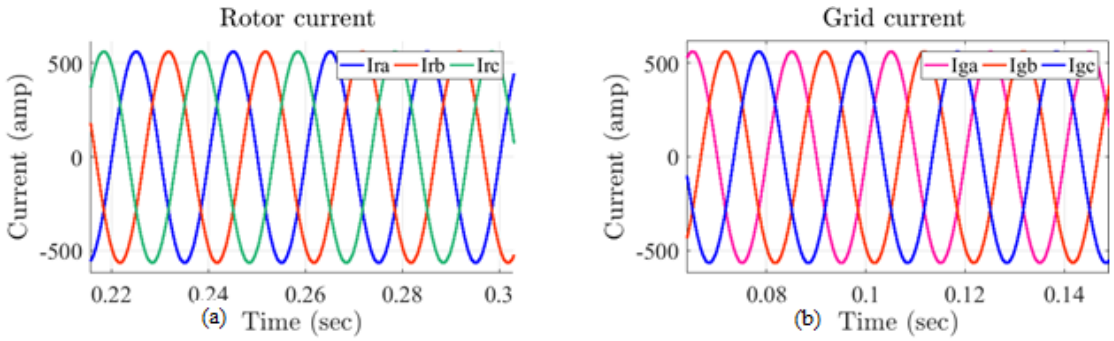

Figure 4-37 Grid current on steady state analysis

From the figure 4.37 it is clear that the simulated output grid current is controlled and balanced in order to operate the generation of wind turbine properly. Consequently, the value of active and grid voltage of national grid is also controlled. During the occurrence of voltage dip at the point common coupling (PCC), the value of rotor and DC bus voltage will be over the normal conditions. So the over current produced at the rotor side converter have ability to damage the power electronics converters and it will destruct the wind power generation system. In order to protect the wind turbine, crowbar resistor protection is used and connected parallel to the rotor side converters to dissipate the high current produced. So to overcome the above discussed problem in the current system it is recommended to use or install crowbar resistor protection at Adama-II wind farm, in order to dissipate the high current produced during the grid faults at the rotor side converter.

CHAPTER FIVE

5. CONCLUSION AND RECOMMENDATIONS

5.1 Conclusion

This paper investigates the behavior of DFIG wind farm during terminal fault in presence of crowbar protection system. The DFIG rotor current, rotor speed, active power, reactive power and DC-link voltage are monitored in steady state and fault state conditions. DFIG is one of the most popular generators in variable speed wind turbine system, but it is very sensitive to the grid faults at the time of voltage dip. Improving low voltage ride through capability of DFIG under the various operation conditions is more important in order to stay connected wind turbines to the grid. Further, during disturbance the compensation of reactive power to the grid is also important.

The simulation scenario is performed for different faults with and without crowbar resistances. So to overcome the discussed problems, phase locked loop pules width modulation, activation and deactivation of crowbar protection, grid side controller and rotor side controller along with crowbar protection resistance are designed by using MATLAB/Simulink, in order to dissipate the high current produced during the disturbance. During the absence of crowbar resistance DFIG produce high DC link voltage, and rotor current due to that reactive power is fluctuated. When crowbar protection is used, rotor current is decreased while rotor speed is increased. During the occurrence of voltage dip at time 3 second, crowbar is activated within 100 ms. and then the circulating current starts flow to the crowbar. Consequently, power electronics devices are protected. Voltage recovery time is between 3.5 to 4.17 seconds. After the disturbance is cleared, RSC is connected to the grid and DFIG is delivered reactive power to the grid for stabilizing the grid voltage.

After fault clearance and reconnection of RSC, the DFIG can provide reactive power support to the grid and thus help in stabilizing of the grid voltage. During post fault period, the absorbed reactive power by the wind farm generators is decreased when the crowbar protection is used. Finally, the rotor current, rotor speed, DC-link voltage, active power and reactive power are affected by a certain value of the crowbar resistance. Therefore, the crowbar resistance value should be chosen carefully. Several dynamic simulations are carried out for different crowbar in case of 100 ms three-phase fault occurs at wind farm terminals.

5.2 Recommendation

The results showed improvement with crowbar resistance protection system of Adama-II wind farm. Further, during the grid disturbance, wind turbine will be disconnected from the national grid, at this time power of the national grid will be reduced and customers are not satisfied. From the simulation results obtained, it has been validated that the system is fully functional. However, the following recommendations have been made as work that could be done to further improve the system. So according to the simulated results, it is clear that with the help of crowbar resistance protection, an improved low voltage ride through capability for Adama-II wind turbine can be obtained as compare to present capacitor bank switching. The wind turbine will remain connected to the grid and fully functioning with help of crowbar resistance. Therefore, based on the simulated results, crowbar resistance protection scheme can be recommended to EEP. During installation, the selection of crowbar resistance will very important and critical factor. Hear the study is done for a wind farms with DFIG which has better reactive power capability and promising result has been obtained. Therefore EEP have to consider the need of crowbar protection in order improve the system performance of wind farms.

5.3 Future Work

As a future work, crowbar protection scheme can be practically implemented and the power electronics converters are figured out in the actual simulation setup. For that purpose actual data and theoretical simulation results available in this work, can be utilized. Also it needs to integrate the initialization program with the hardware, removing of error during startup and automated. Also the DFIG will done by another controller like artificial neural network and fuzzy logic control.

REFERENCE

[1] S. Swain and P. K. Ray, "Short circuit fault analysis in a grid connected DFIG based wind energy system with active crowbar protection circuit for ridethrough capability and power quality improvement," International Journal of Electrical Power & Energy Systems, vol. 84, pp. 64-75, 2017.

[2] A. D. Hansen and G. Michalke, "Fault ride-through capability of DFIG wind turbines," Renewable energy, vol. 32, pp. 1594-1610, 2007.

[3] R. A. J. Amalorpavaraj, P. Kaliannan, S. Padmanaban, U. Subramaniam, and V. K. Ramachandaramurthy, "Improved fault ride through capability in dfig based wind turbines using dynamic voltage restorer with combined feed-forward and feed-back control," IEEE Access, vol. 5, pp. 20494-20503, 2017.

[4] A. E. Leon, J. M. Mauricio, and J. A. Solsona, "Fault ride-through enhancement of DFIG-based wind generation considering unbalanced and distorted conditions," IEEE Transactions on Energy Conversion, vol. 27, pp. 775-783, 2012.

[5] S. Mishra and J. Iyer, "Crowbar Protection of Micro-Grid with DFIG Wind Turbine," International Journal of Scientific Engineering and Research, vol. 2, 2014.

[6] G. Bekele and A. Abdela, "Investigation of Wind Farm Interaction with Ethiopian Electric Power Corporation's Grid," Energy Procedia, vol. 14, pp. 1766-1773, 2012.

[7] B. Khan and P. Singh, "The Current and Future States of Ethiopia's Energy Sector and Potential for Green Energy: A Comprehensive Study," in International Journal of Engineering Research in Africa, , pp. 115-139,2017.

[8] S. Mali, S. James, and I. Tank, "Improving low voltage ride-through capabilities for grid connected wind turbine generator," Energy Procedia, vol. 54, pp. 530-540, 2014.

[9] S. B. Naderi, M. Negnevitsky, A. Jalilian, M. T. Hagh, and K. M. Muttaqi, "Low voltage ride-through enhancement of DFIG-based wind turbine using DC link switchable resistive type fault current limiter," International Journal of Electrical Power & Energy Systems, vol. 86, pp. 104-119, 2017.

[10] R. D. Shukla and R. K. Tripathi, "Low voltage ride through (LVRT) ability of DFIG based wind energy conversion system II," in Engineering and Systems (SCES), 2012 Students Conference on, pp. 1-6, 2012.

[11] J. J. Justo, F. Mwasilu, and J.-W. Jung, "Enhanced crowbarless FRT strategy for DFIG based wind turbines under three-phase voltage dip," Electric Power Systems Research, vol. 142, pp. 215-226, 2017.

[12] Q. Huang, X. Zou, D. Zhu, and Y. Kang, "Scaled current tracking control for doubly fed induction generator to ride-through serious grid faults," IEEE Transactions on Power Electronics, vol. 31, pp. 2150-2165, 2016.

[13] J. P. Da Costa, H. Pinheiro, T. Degner, and G. Arnold, "Robust controller for DFIGs of grid-connected wind turbines," IEEE transactions on industrial electronics, vol. 58, pp. 4023-4038, 2011.

[14] P. Sebastian and U. Nair, "Improved Low Voltage Ride through Capability of a Fixed Speed Wind Generator using Dynamic Voltage Restorer," Procedia Technology, vol. 25, pp. 767-774, 2016.

[15] M. Benbouzid, B. Beltran, Y. Amirat, G. Yao, J. Han, and H. Mangel, "Second-order sliding mode control for DFIG-based wind turbines fault ride-through capability enhancement," ISA transactions, vol. 53, pp. 827-833, 2014.

[16] A. R. A. Jerin, P. Kaliannan, and U. Subramaniam, "Improved fault ride through capability of DFIG based wind turbines using synchronous reference frame control based dynamic voltage restorer," ISA transactions, vol. 70, pp. 465-474, 2017.

[17] R. Sitharthan, C. Sundarabalan, K. Devabalaji, S. K. Nataraj, and M. Karthikeyan, "Improved fault ride through capability of DFIG-wind turbines using customized dynamic voltage restorer," Sustainable Cities and Society, vol. 39, pp. 114-125, 2018.

[18] V. A. Duggirala and V. N. K. Gundavarapu, "Improved LVRT for grid connected DFIG using enhanced field oriented control technique with super capacitor as external energy storage system," Engineering Science and Technology, an International Journal, vol. 19, pp. 1742-1752, 2016.

[19] M. Gholizadeh, S. Tohidi, A. Oraee, and H. Oraee, "Appropriate crowbar protection for improvement of brushless DFIG LVRT during asymmetrical voltage dips," International Journal of Electrical Power & Energy Systems, vol. 95, pp. 1-10, 2018.

[20] S. Yang, T. Zhou, D. Sun, Z. Xie, and X. Zhang, "A SCR crowbar commutated with power converter for DFIG-based wind turbines," International Journal of Electrical Power & Energy Systems, vol. 81, pp. 87-103, 2016.

[21] S. Tohidi and M.-i. Behnam, "A comprehensive review of low voltage ride through of doubly fed induction wind generators," Renewable and Sustainable Energy Reviews, vol. 57, pp. 412-419, 2016.

[22] Y.-w. Liu, Z.-h. Chen, and J. Shen, "Application of PLL in the Generator-side Converters for Doubly-Fed Wind Power Generation Systems," Energy Procedia, vol. 16, pp. 1822-1830, 2012.

[23] A. Gomez-Exposito, A. J. Conejo, and C. Canizares, Electric energy systems: analysis and operation: CRC press, 2018.

[24] S. K. Sahoo, A. Sinha, and N. Kishore, "Low voltage ride-through of a grid-connected doubly-fed induction generator with speed sensorless vector control," in Power Systems Conference (NPSC), 2016 National, 2016, pp. 1-6.

[25] T. Tadesse, "Study of Doubly Fed Induction Generator Control Under Grid Fault Conditions," Addis Ababa University, 2016.

[26] B. Wu, Y. Lang, N. Zargari, and S. Kouro, Power conversion and control of wind energy systems vol. 76: John Wiley & Sons, 2011.

[27] S. Hu, X. Lin, Y. Kang, and X. Zou, "An improved low-voltage ride-through control strategy of doubly fed induction generator" IEEE transactions on power electronics, vol. 26, pp. 3653-3665, 2011.

[28] G. Abad, J. Lopez, M. Rodriguez, L. Marroyo, and G. Iwanski, Doubly fed induction machine: modeling and control for wind energy generation vol. 85: John Wiley & Sons, 2011.

[29] S. Sumathi, L. A. Kumar, and P. Surekha, Solar PV and wind energy conversion systems: an introduction to theory, modeling with MATLAB/SIMULINK, and the role of soft computing techniques: Springer, 2015.

[30] P. J. Satpathy and A. Sabat, "Harmonic analysis of grid connected wind farm under different fault conditions," International Journal of Computer applications, 2014.

[31] M. E. Hossain, "A non-linear controller based new bridge type fault current limiter for transient stability enhancement of DFIG based Wind Farm," Electric Power Systems Research, vol. 152, pp. 466-484, 2017.

[32] O. Anaya-Lara, D. Campos-Gaona, E. Moreno-Goytia, and G. Adam, Offshore wind energy generation: control, protection, and integration to electrical systems: John Wiley & Sons, 2014.

[33] Y.-L. Hu, Y.-K. Wu, C.-K. Chen, C.-H. Wang, W.-T. Chen, and L.-I. Cho, "A Review of the Low-Voltage Ride-Through Capability of Wind Power Generators," Energy Procedia, vol. 141, pp. 378-382, 2017.

[34] J. A. Turner, "A realizable renewable energy future," Science, vol. 285, pp. 687-689, 1999.

[35] R. Pena, R. Cárdenas, E. Escobar, J. Clare, and P. Wheeler, "Control system for unbalanced operation of stand-alone doubly fed induction generators," IEEE Transactions on Energy Conversion, vol. 22, pp. 544-545, 2007.

[36] J. Li, D. Li, L. Hong, C. Xie, and G. Chen, "A novel power-flow balance LVRT control strategy for low-speed direct-drive PMSG wind generation system," in IECon 2010-36th Annual Conference on IEEE Industrial Electronics Society, 2010, pp. 748-753.

[37] I. Erlich, J. Kretschmann, S. Mueller-Engelhardt, F. Koch, and J. Fortmann, "Modeling of wind turbines based on doubly-fed induction generators for power system stability studies," in Power and Energy Society General Meeting-Conversion and Delivery of Electrical Energy in the 21st Century, 2008 IEEE, 2008, pp. 1-8.

[38] G. Abad, J. López, M. A. Rodríguez, L. Marroyo, and G. Iwanski, "Doubly Fed Induction Machine: Modeling and Control for Wind Energy Generation.", John Wiley & Sons, 2014.

[39] V. C. Ganti, B. Singh, S. K. Aggarwal, and T. C. Kandpal, "DFIG-based wind power conversion with grid power leveling for reduced gusts," IEEE Transactions on sustainable energy, vol. 3, pp. 12-20, 2012.

[40] H. Abu-Rub, M. Malinowski, and K. Al-Haddad, Power electronics for renewable energy systems, transportation and industrial applications: John Wiley & Sons, 2014.

[41] R. Datta and V.T Ranganathan, variable speed wind power generation using doubly fed wound rotor induction machine, IEEE transactions on energy conversion, 17, and 2002.

[42] S. K. Senapati, "Modelling and simulation of a grid connected doubly fed induction generator for wind energy conversion system," 2014.

[43] J. Matevosyan, T. Ackermann, S. Bolik, and L. Söder, "Comparison of international regulations for connection of wind turbines to the network," in Nordic Wind Power Conference NWPC'04, 1.-2.3. 2004. Gothenburg, Sweden, 2004.

[44] Z. Zheng, G. Yang, and H. Geng, "Short circuit current analysis of DFIG-type WG with crowbar protection under grid faults," in Industrial Electronics (ISIE), 2012 IEEE International Symposium on, pp. 1072-1079, 2012.

[45] S. Li-ling, Y. Pu, and W. Yi, "Simulation research for LVRT of DFIG based on rotor active crowbar protection," 2012.

[46] A. Xu, L. Zhang, and C. Gu, "Crowbar circuit in wind power grid low voltage ride through," in Electricity Distribution (CICED), 2014 China International Conference on, pp. 399-402, 2012.

[47] M. G. Simoes and F. A. Farret, Alternative energy systems: design and analysis with induction generators vol. 13: CRC press, 2011.

APPENDIX A-1: ADAMA-II WPP DFIG PARAMETERS

Doubly fed induction generator (DFIG) parameters		
Rated Power	1.5 MW	1.0 pu
Rated Stator Line-to-line Voltage	690 V (rms)	
Rated Stator Phase Voltage/Base Voltage	398.4 V (rms)	1.0 pu
Rated Rotor Phase Voltage	79 V (rms)	79/398.4 =0.1983
Rated Stator Current	1110 A (rms)	$1110/I_B$=0.8844
Efficiency at rated power	>=97%	
Base Current, I_B = 1.5 MW/√3 x 690 V)	1255.11 A (rms)	1.0 pu
Rated Rotor Current	1209.852A(rms)	0.964
Rated Stator Frequency	50 Hz	1.0 pu
Rated power factor	From cosφ=0.95 inductive to cosφ=0.95 capacitive	
Rated Stator Speed, ωs	1500 rpm	1.0 pu
Rated Rotor Speed	1800 rpm	1.0 pu
Nominal Rotor Speed Range	1000-2000rpm	0.56-1.11 pu
wind turbine rotor speed range	10.6–21.1 rpm	
Rated speed of wind turbine rotor	19rpm	
Rated Slip, rated	ws-wr/ws=1500-1800/1500=-0.2	
Number of Pole Pairs	2	
Transformation Ratio, u	0.42	
Rotor/ stator connection	Delta/Star	
Rated Mechanical Torque	8.5922 kN-m	1.0
Stator Winding Resistance, R_s	0.006243 Ω	0.006243/0.3174=0.0197
Rotor Winding Resistance, R_r	*0.011074* Ω	0.0349
Stator Leakage Inductance, *Lls*	0.198822mH	Lls*ωs/Z_B=0.000198822*2*pi* 50/0.3174=0.197
Rotor Leakage Inductance, *Llr*	0.198822mH	0.197
Magnetizing Inductance, *Lm*	3.976mH	3.9354
Base Flux Linkage, $\psi_B = V_B/\omega s$	1.2681 Wb(rms)	1.0 pu
Base Impedance, $Z_B=V_B/I_B$ =398.4/1255.1	0.3174 Ω	1.0 pu
Base Inductance ,$L_B= \psi_B /I_B$	1.0103 mH	1.0 pu
Turbine inertia, Jt	85.8	
Generator inertia, Jg(kg-m2)	67	
Gear box ratio	94.7	
Base Capacitance, $C_B = \frac{1}{2\pi f Z_B}$	10028.7 µF	=1.0 pu

Air density, p	1.225kg/m3	
Converter	**Rotor side (two modules are connected in parallel)**	
	IGBT voltage level	1,700V
	Max. continuous operating voltage	1100V
	Rated continuous DC voltage	975V
	GRID SIDE(SINGLE MODULE)	
	IGBT voltage level	1,700V
	Max. continuous operating DC voltage	1100V
	Rated continuous DC voltage	975V
Cpmax.	0.4865	
Lambda opt	9	
Stator wiring	∆	
Rotor wiring	Y	
∆-winding (stator side)	220 V(L-L)	
Y-winding (stator converter)	220 V(L-L)	
Induction Generator Used In The Wind Turbine		
Nominal values	Values	
Voltage	690 V	
Frequency (electrical)	50 Hz	
Power	1.8 MW	
Machine Parameter		
Stator resistance		0.043 pu
Rotor Leakage Inductance		0.0613 pu
Stator Leakage Inductance		0.0613 pu
Mutual inductance		1.0 pu
Angular moment of inertia(J)		1.0 se
Control model parameter		
Cut in speed	1000 r/min	
Speed limit	1800 r/min	
Shutdown speed	2000 r/min	
Turbine data		
Shaft stiffness	2.5 pu/rad	
Turbine rotor speed range	9.5-21 rpm	
Rated wind speed	12 m/s	
Rotor diameter	75 m	
Gear ratio	1:86.5	
Generator data		
Rated power	2 MW	

Rated voltage	690 V	
Rated frequency	50 Hz	
Stator resistance		0.048 pu
Stator reactance		0.075 pu
Mutual reactance		3.8 pu
Rotor resistance		0.018 pu
Rotor reactance		0.12 pu
Generator rotor inertia	0.5 s	
Number of pole pairs	2	
DC- bus	C= 38µF,V_{dc}=1200 V	
RL filter	R_f=0.075Ω, L_f=0.75 mH	

APPENDIX A-2

Table procedure to derive the steady state magnitude with Q_s reference

Nº	Type	Given grid voltage $\omega_s\|$ and $\vec{V_s}\|$	Given operating point Q_s,T_{em} and ω_s		
1.	Stator Flux	$\overrightarrow{\|\psi_s\|} = \sqrt{\frac{-B \pm \sqrt{B^2 - 4AC}}{2A}}$	$C = \left[\frac{2}{3}\frac{R_s}{L_m}\right]^2 \left[(\frac{Q_s}{\omega_s})^2 + (\frac{T_{em}}{P})^2\right]$	$B = \frac{4}{3}R_s T_{em}\omega_s - \|\overrightarrow{\psi_s}\|^2$	$A = \omega_s^2$
2	Stator Current	$i_{ds} = \frac{Q_s}{\omega_s\|\vec{\psi}\|}$	$i_{qs} = \frac{T_{em}}{\frac{3}{2}P\|\overrightarrow{\psi_s}\|}$	$\|\overrightarrow{i_s}\|^2 = i_{ds}^2 + i_{qs}^2$	$\theta_{is} = \alpha tan(\frac{i_{qs}}{i_{ds}})$
3	Rotor Current	$i_{dr} = \frac{\|\overrightarrow{\psi_s}\|}{L_m}$	$i_{qr} = -\frac{L_S}{L_m}i_{qs}$	$\|\overrightarrow{i_r}\|^2 = i_{dr}^2 + i_{qr}^2$	$\theta_{is} = \alpha tan(\frac{i_{qs}}{i_{ds}})$
4	Stator Voltage	$V_{ds} = R_s i_s$	$v_{qs} = R_s i_{qs} + \omega_s\|\overrightarrow{\psi_s}\|$	$\|\overrightarrow{v_s}\|^2 = v_{ds}^2 + v_{qs}^2$	$\theta_{vs} = \alpha tan(\frac{v_{qs}}{v_{ds}})$
5	Slip	$\omega_r = \omega_s - \omega_m$		$S = \frac{\omega_r}{\omega_s}$	
6	Rotor Voltage	$V_{dr} = R_r i_{dr} - \omega_r \sigma L_r i_{qr}$	$v_{qr} = R_r i_{qr} + \omega_r \sigma L_r i_{dr} + \omega_{r\frac{L_m}{L_s}}\|\overrightarrow{\psi_s}\|$	$\|\overrightarrow{v_r}\|^2 = v_{dr}^2 + v_{qr}^2$	$\theta_{vr} = \alpha tan(\frac{v_{qr}}{v_{dr}})$
7	Rotor Flux	$\psi_{dr} = L_m i_{ds} + L_r i_{dr}$	$\psi_{qr} = L_m i_{qs} + L_r i_{qr}$	$\|\overrightarrow{\psi_r}\|^2 = \psi_{dr}^2 + \psi_{qr}^2$	$\theta_{\psi r} = \alpha tan(\frac{\psi_{qr}}{\psi_{dr}})$

8	Active Power	$P_m = T_{em}\frac{\omega_m}{p}$	$P_s = \frac{3}{2}(v_{ds}i_{ds} + v_{qs}i_{qs})$	$P_r = \frac{3}{2}(v_{dr}i_{dr} + v_{qr}iq_r)$	
9	Reactive Power	$Q_s = \frac{3}{2}(V_{qs}i_{ds} - V_{ds}i_{qs})$	$PF_s = \cos(\alpha\tan(Q_s/P_s))$	$Q_r = \frac{3}{2}(v_{qr}i_{dr} - v_{dr}i_{qr})$	$PF_R = \cos(\alpha\tan(Q_r/P_r))$
10	Efficiency	$\eta = \frac{P_m}{P_s + P_r}\ if\ Pm > 0$		$\eta = \frac{P_s + P_r}{P_m}\ if\ Pm < 0$	

APPENDIX A-3

Useful expressions

$P_s+P_r \cong P_m$	$P_r \cong -sP_s$	$P_m \cong (1-s)P_s$	$\|V_r\| \cong \|sV_s\|$
$P_m \cong T_m\frac{\omega_m}{P}$	$P_s \cong T_{em}\frac{\omega_s}{P}$		$P_r \cong T_{em}\frac{\omega_r}{P}$

APPENDIX A-4